FINAL REPORT

Minimizing Permafrost Thaw and Maximizing Thermal Heat Storage in Baker Lake, Nunavut

An Investigation on Energy Storage in Permafrost

Abra Gold[2]
Mafalda Miranda[1] Jasmin Raymond[1]
Einar Jon Asbjornsson[2]

[1]Institut national de la recherche scientifique (INRS), Centre Eau Terre Environnement
[2] Háskólinn í Reykjavík, Iceland School of Energy (HR-ISE)

Prepared for the account of:
CanmetENERGY-Ottawa

March 31st, 2023
Rapport de Recherche R2178

INRS
Institut national de la recherche scientifique

ISBN : 978-2-89146-980-7 (version électronique)

Dépôt légal - Bibliothèque et Archives nationales du Québec, 2023
Dépôt légal - Bibliothèque et Archives Canada, 2023

Table of Contents

List of Figures

List of Tables

ACKNOWLEDGEMENTS

This report was written and prepared by Abra Gold of Háskólinn í Reykjavík – Iceland School of Energy (HR-ISE), Mafalda Miranda and Jasmin Raymond of the Institut national de la recherche scientifique (INRS), and Einar Asbjornsson of HR-ISE. It was developed with support from CanmetENERGY-Ottawa (Andrew Wigston), Qulliq Energy Corporation (Don Grant), and RESPEC Consulting Inc (Matthew Minnick and Debra Shewfelt) for Natural Resources Canada. We would like to give a special mention to Dr. Zhou (RESPEC) for providing a model of a borehole thermal energy storage system to compare with the numerical model described in the report. Violaine Gascuel (INRS) is further acknowledged for donating pieces of Python-FEFLOW coupling code and providing instruction throughout the modelling process. Nicolo Giordano (Géotherma solutions Inc.) is recognized and appreciated for offering support throughout the modelling process and for providing a model of a BTES system to be built upon in this study. A word of thanks is also extended to Hubert Langevin (Géotherma solutions Inc.) for his help and support in the first stage of the project. DHI support is acknowledged for providing access to a 1-year student licence and for providing help with the modelling process.

FOREWORD

The scope of this study is to find solutions to minimize permafrost thaw while maximizing heat storage using borehole thermal energy storage (BTES) technology in an arctic climate. A FEFLOW numerical model is developed to simulate the BTES and the possible permafrost thaw mitigation techniques. The geological and environmental conditions at Baker Lake were considered in the model.

The team of INRS and HR-ISE is selected for this study to:

1) Define mitigation solution properties
2) Model Baker Lake's geological conditions
3) Model Baker Lake's permafrost and environmental conditions
4) Simulate one borehole heat exchanger (BHE) in a borehole field with seasonal energy storage
5) Test multiple mitigation solutions
6) Determine which solutions maximize energy storage
7) Determine which solutions maximize permafrost integrity
8) Determine a solution that maximizes energy storage while minimizing permafrost thaw
9) Simulate a BTES field in Baker Lake integrating possible solutions
10) Determine a solution that maximizes BTES while minimizing permafrost thaw

EXECUTIVE SUMMARY

The study describes four types of potential permafrost mitigation solutions to BHE operation:

- Insulated Grout & Cement
- Insulated Pipes
- Thermosyphons
- Empty Upper Section Providing Air Insulation

For this purpose, mitigation solutions are divided into 2 categories depending on whether the strategy functions as a heat storage, or 'passive' medium (change of grout and pipe properties or air insulation), versus a heat transfer, or 'active' medium (thermosyphon). The implementation of various mitigation strategies is tested in a FEFLOW model enclosing a single borehole with a subsurface that is representative of the geology in Baker Lake, Nunavut. These simulations were made to determine the best- and worst-case scenarios for permafrost thaw and BTES, in addition to the best combination of solutions to minimize thaw while maximizing energy storage. A BTES system with 100 boreholes was developed to test the effectiveness of solutions when the best solution is applied to every borehole vs. outer boreholes.

Model & Mitigation Scenarios

The depth to bedrock 500 m southwest from the Baker Lake BTES project site is determined to be a maximum of 4 m from exploration wells drilled for the QEC headquarters. Average monthly ground temperature data from the Baker Lake Airport is analyzed and implemented in the model to simulate seasonal freeze-thaw cycles. Available data on the porosity of the likely geological conditions at Baker Lake are also considered. Subsurface data has been translated into the single borehole model made with PiFreeze, a model plugin for FEFLOW that simulates latent heat generated by the phase changes of ice to water. A methodology is established to simulate the effect of the mitigation solutions, then compare them as a function of thermal energy storage and temperature. Four model input parameters are adjusted to simulate the effect of the solutions:

- Thermal Conductivity of Grout
- Thermal Conductivity of Pipes
- Heat Extraction of Heat Sinks (Representative of Thermosyphons)
- Reduction of thermal conductivity and volumetric heat capacity (Representative of Air)

There are 5 scenarios of solution combinations representative of Baker Lake. The resulting evaluation of mitigation solutions is shown below in **Figure A** with simulated ground temperature 0.23 m from the borehole and in **Figure B** 1.67 m from the borehole. The effectiveness as a function of energy storage is displayed in **Figure C** showing thermal power injected and extracted from the ground. The BTES system does not employ PiFreeze, and results of the application of the most successful mitigation solution from the single borehole model around both the outer edge boreholes and every borehole are presented in **Figure D**.

Determining Results
The thermal storage and subsurface temperature are evaluated from the model output, considering a 3-year of BTES operation. Thermal energy storage is quantified in the amount of heat extracted at the end of 3 years, and subsurface temperature is quantified in the temperature of points L-P, which are various observations points in the model that spread radially from the center (point L, 0.23 m from the central BHE) to the outer edge (point P, 1.67 m away from the central BHE) at the end of 3 years. For the BTES field, subsurface temperature inside and outside of the BTES field are evaluated at points L-P (L being at the center of the BTES field, N being 0 m from the edge of the BTES field, and P being 8.7 m from the edge of the BTES field) at the end of 3 years. Plots of thermal energy extracted over time, as well as temperature change through multiple points that extend radially away from the center of the models at approximately 1 m, 2 m, and 4 m depth are analyzed and compared. Evaluation of each solution considers the inlet temperature of the system (45 °C low temperature), the natural thermal gradient, the monthly ground temperature changes, and the properties assigned to the BHE(s).

Limitations & Recommendations
Limitations are addressed for methods and material properties utilized in the model simulation. Finally, recommendations for future work are also proposed to forward research on energy storage in permafrost areas, with a specific focus on Baker Lake, Nunavut.

Overall Effectiveness of Mitigation Solution Scenarios
Using the methodology outlined above and the information presently available (**Figures A – D**), the following points summarize the effectiveness of tested solutions:

- Changing grout does not have an effective impact on the temperature in the overburden above the bedrock where permafrost thaw should be minimized.
- Air insulation works slightly better than VIT casing and is inexpensive; both have a significant effect on temperature in the overburden although completely avoiding permafrost thaw in the overburden is impossible.
- A BHE with 16 m zone of air insulation improves the effectiveness of the solution and has little influence on the energy storage.
- Thermosyphons are effective in winter but less effective than VIT casing and air insulation in summer to keep overburden temperature cold.
- Air insultation in the upper section of the BHE is a solution to privilege because its cost is expected negligeable.
- If there is material contact between boundaries, heat will transfer.
- Thermal conductivity is the greatest factor in determining how much the ground temperature will increase.
- Insulating every borehole in the BTES field is slightly more effective than insulating the outside ring of boreholes at the outer edge of the BTES field.

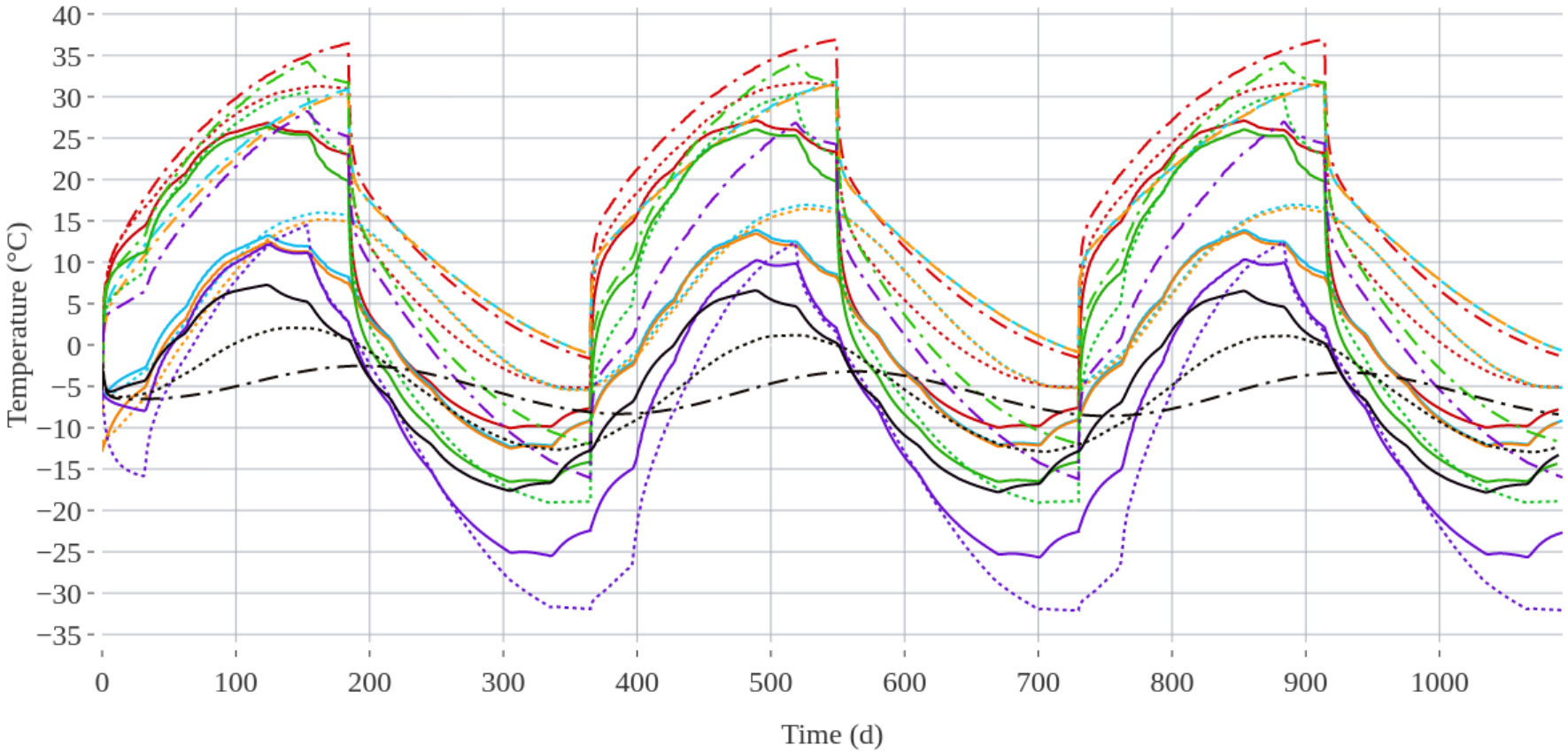

Scenario						Depth	
S1	Bentonite 10%, HDPE		S18	Bentonite 10%, HDPE, Thermosyphon		0.8 m
S3	Bentonite 10%, HDPE, VIT Casing		S19	Bentonite 10%, HDPE, Thermosyphon & VIT Casing		2 m
S16	Bentonite 10%, HDPE, Air Insulation		Natural Ground Temperature Without BHE			4 m

Figure A. Ground temperature for key scenarios 0.23 m away from the central BHE (10% bentonite grout & HDPE (S1), VIT casing around S1 (S3), air-insulation around S1 (S16), 6 thermosyphons around S1 (S18), 6 thermosyphons and VIT casing around S1 (S19)) at 0.8, 2, and 4 m depth over the course of May 2024 through May 2027.

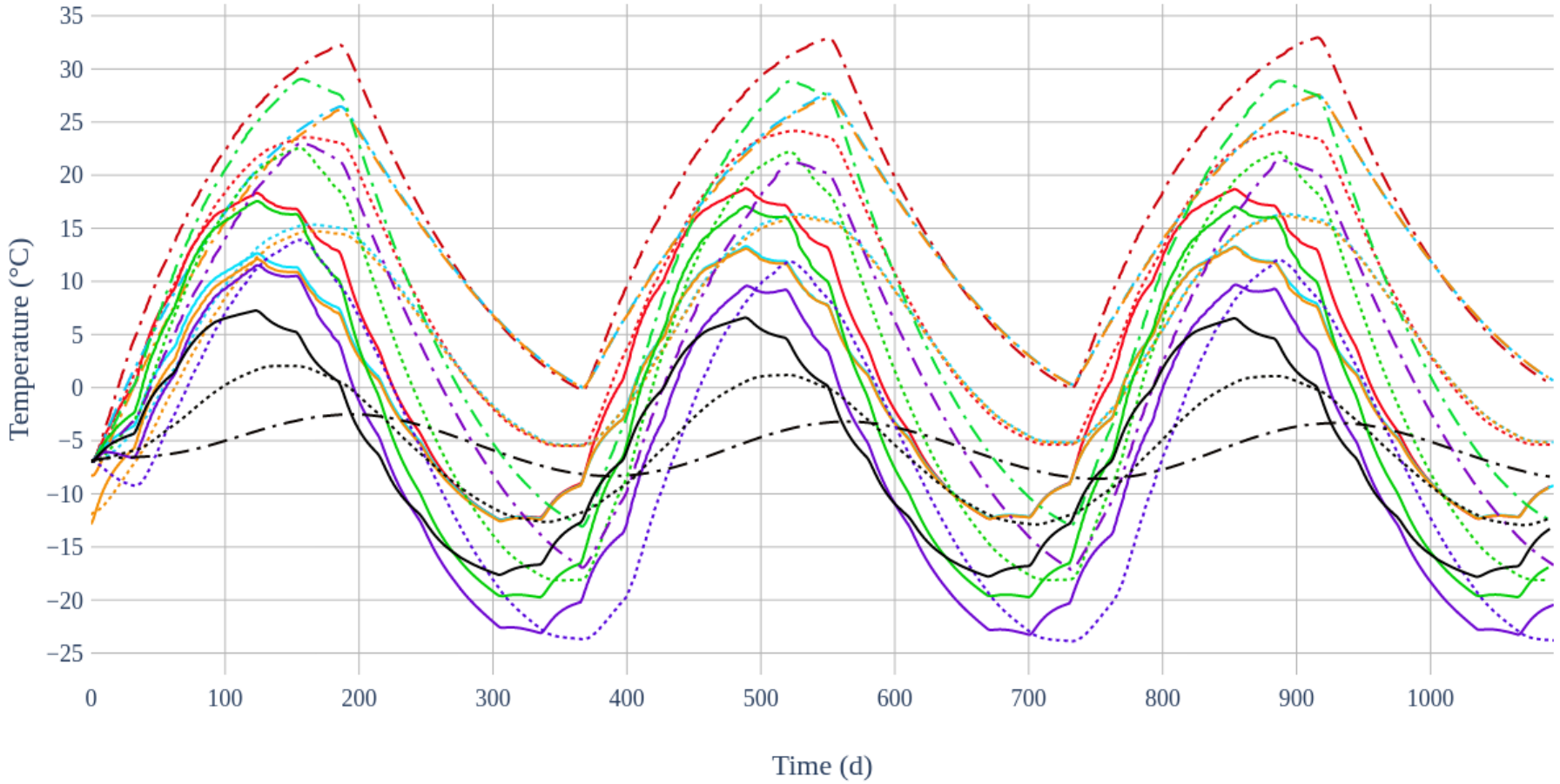

Scenario						Depth	
S1	Bentonite 10%, HDPE		S18	Bentonite 10%, HDPE, Thermosyphon		0.8 m
S3	Bentonite 10%, HDPE, VIT Casing		S19	Bentonite 10%, HDPE, Thermosyphon & VIT Casing		2 m
S16	Bentonite 10%, HDPE, Air Insulation		Natural Ground Temperature Without BHE			4 m

Figure B. Ground temperature for key scenarios 1.67 m away from the central BHE (10% bentonite grout & HDPE (S1), VIT casing around S1 (S3), air-insulation around S1 (S16), 6 thermosyphons around S1 (S18), and 6 thermosyphons and VIT casing around S1 (S19)) at 0.8, 2, and 4 m depth over the course of May 2024 through May 2027.

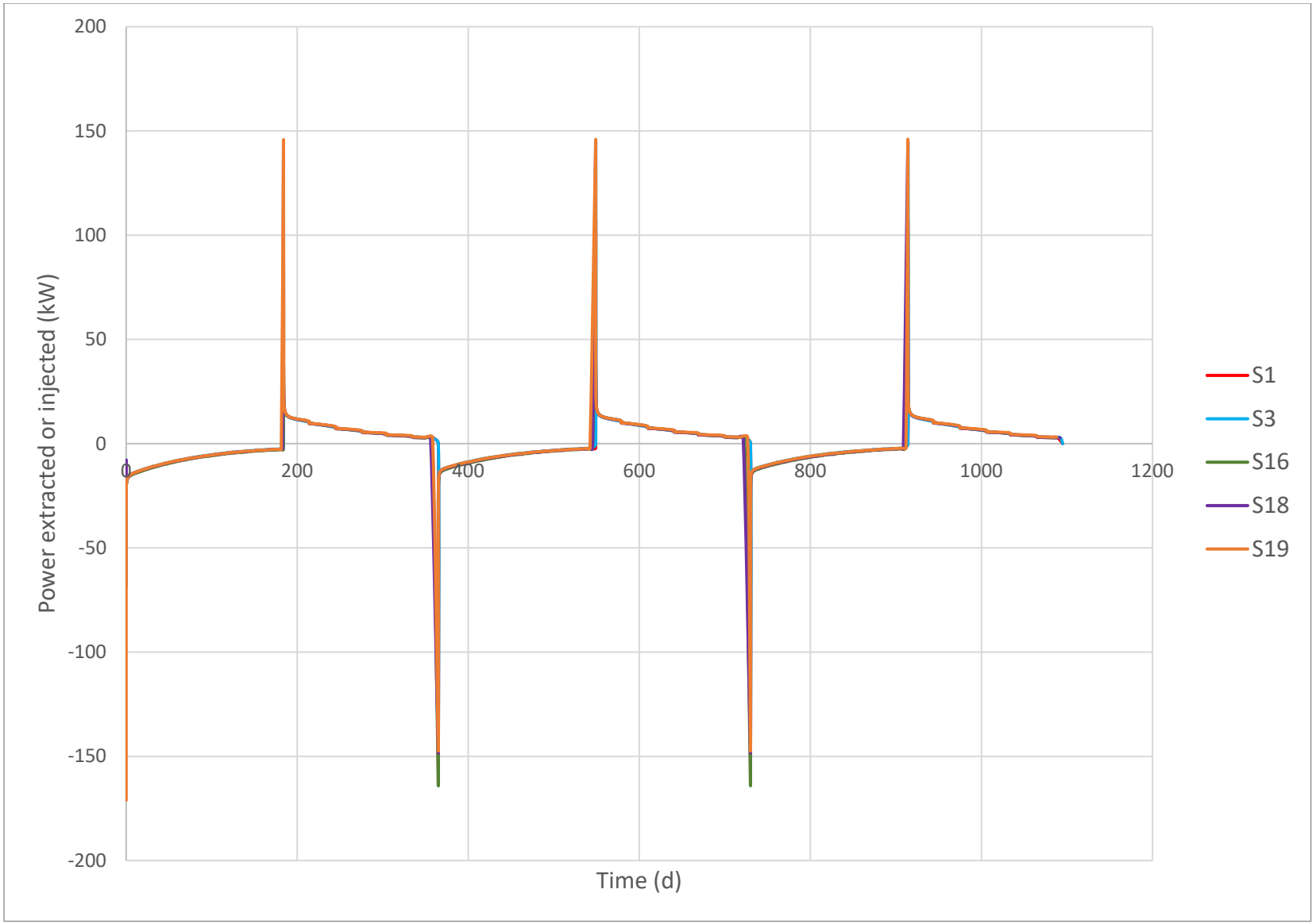

Figure C. Power injected (negative) or extracted (positive) in the ground (kW) of the key scenarios from May 2024 through May 2027.

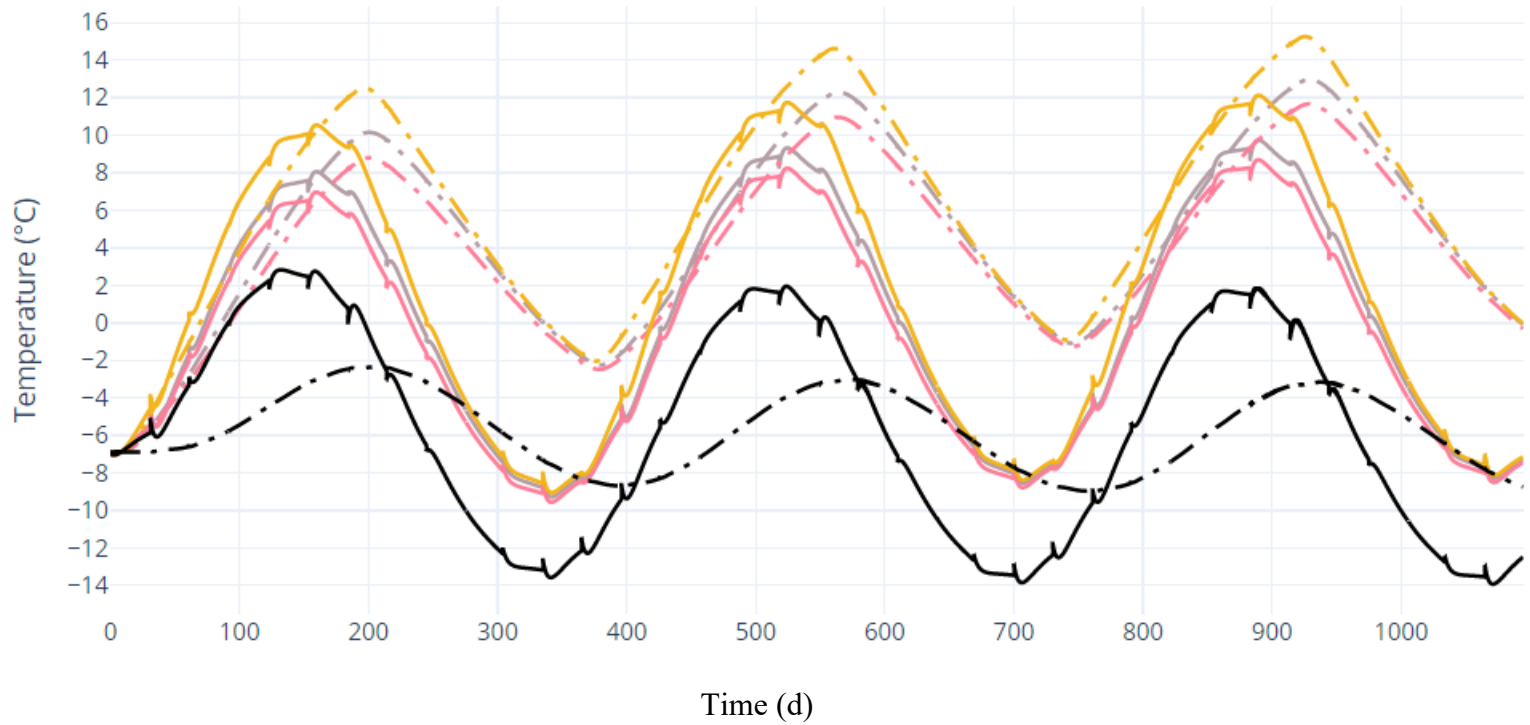

Scenario				Depth	
S21	Air Insulation (S16) outside edge of field	S22	Air Insulation (S16) every BHE in field	—	2 m
Natural Ground Temperature without BTES		S23	No Mitigation Solutions	- -	4 m

Figure D. Ground temperature at the outermost edge of the BTES field equidistant between two outer-ring BHEs (air-insulation around S1 for the outermost boreholes surrounding the field (S21), air-insulation around S1 for all boreholes (S22), and no mitigation solutions applied to the field (S23)) at 2 and 4 m depth over the course of May 2024 through May 2027. Some spikes appear in the lines at 2 m depth because of the model seasonal ground temperature changes affecting the results.

LIST OF NOMENCLATURE

Latin Symbols

A	area of the thermosyphon evaporator section	m^2
C	effective volumetric heat capacity	MJ m^{-3} K^{-1}
c	custom measurements for pipe fittings	mm or m
C_p	heat capacity of water-antifreeze mixture	J m^{-3} K
d_{in}	inlet pipe diameter	mm or m
d_{out}	outlet pipe diameter	mm or m
e	=-g/‖g‖; gravitational unit vector	1
E_s	thermal power injected or extracted	W
f_μ	viscosity relation function	1
g	the gravity vector	m s^{-2}
h	hydraulic head	m
h_{in}	inlet pipe wall thickness	mm or m
H_l	latent heat	J kg^{-1}
h_{out}	outlet pipe wall thickness	mm or m
k	porous medium permeability tensor	m^2
K	tensor of hydraulic conductivity	m s^{-1}
k_r^l	relative permeability of the liquid phase	1
L_f	latent heat of fusion	J kg^{-1}
P	material porosity	1
p^l	pressure of the liquid phase	kg m^{-1} s^{-2}
P_t	thermosyphon performance coefficient	W $^oC^{-1}$
q	Darcy velocity	m s^{-1}
Q	thermosyphon heat extraction rate	W
Q_b	bulk source/sink term for flow	m s^{-1}
q_{BHE}	flow rate of fluid inside BHE	m^3 s^{-1}
Q_{EOB}	correction sink/source term of extended Oberbeck-Boussinesq approximation	s^{-1}
$\mathbf{q}_i$	Darcy velocity vector of the fluid phase	m s^{-1}
$\mathbf{q}_j$	vector of Darcy velocity	m s^{-1}
q_l	momentum of the liquid phase	m s^{-1}
Q_t	source/sink heat function	kg m^{-1} s^{-3}
s	saturation of fluid in the void space	1
S	specfifc storage	m^{-1}
S_0	specific storage coefficient	m^{-1}
T	temperature	K
t	time	s
T_{amb}	ambient temperature	K
T_g	ground temperature	K

T_{In}	BHE inlet temperature	°C or K
T_{Out}	BHE outlet temperature	°C or K
V_q	absolute Darcy fluid flux	m s^{-1}
w	wind speed	m s^{-1}
x_i	eulerian spatial coordinate vector	m
Greek Symbols		
∇	gradient vector	m-1
α_i	inlet dispersion	m
α_L	longitudinal dispersivity	m
α_T	transverse dispersivity	m
δ_{ij}	Kronecker tensor	= 1 for i=j
ΔT	temperature difference between in and outlets	1
ε_a	air volume fraction	1
ε_i	ice volume fraction	1
ε_l	flow accessible volume fraction	1
ε_s	solid volume fraction	1
λ	effective thermal conductivity of the material	W m^{-1} K^{-1}
$\lambda^{\wedge f}$	thermal conductivity of the fluid	W m^{-1} K^{-1}
λ^a	bulk thermal conductivity of the ground	W m^{-1} K^{-1}
Λ_{ij}	tensor of hydrodynamic thermodispersion	kg m s^{-3} K^{-1}
Λ_{ij}^{cond}	conductive part of the tensor	kg m s^{-3} K^{-1}
Λ_{ij}^{disp}	dispersive part of the tensor	kg m s^{-3} K^{-1}
λ^s	thermal conductivity of the solid	W m^{-1} K^{-1}
μ^l	liquid viscosity	ML^{-1} T^{-1}
ρ	density	kg m-3
$\rho^a c^a$	volumetric heat capacity of the medium	Jm^{-3} K^{-1}
$\rho^f c^f$	volumetric heat capacity of the fluid	Jm^{-3} K^{-1}
ρ_i	density of ice	kg m^{-3}
ρ^l	density of the liquid phase	ML^{-3}
ρ_l	density of the liquid phase	kg m^{-3}
$\rho^s c^s$	volumetric heat capacity of the solid	J m^{-3} K^{-1}
φ	ice fraction	1
χ	buoyancy coefficient	1
ε	volume fraction porosity (void space)	1

1. PERMAFROST AND ENERGY STORAGE

1.1 BTES Challenges in Permafrost

In territories such as Nunavut, Canada, thawing permafrost is a major concern. Permafrost thaw in Nunavut can cause subsidence and degradation of surface soil and sediment integrity. This compromise of stability can damage infrastructure such as buildings and wells in the community of Baker Lake, and by extension the work site for this project (**Figure 1.1**; James et al. 2013 a&b; Marques et al. 2011). BTES systems are associated with a risk of ground subsidence and damage when installed in permafrost. Thaw compromises the structural integrity of the ground and may damage the BTES system upon installation, or later. In a BTES system, heat is lost from the sides and the bottom of the borehole. Permafrost which extends beyond the depth of the BHE may thaw as the mean annual ground temperature (MAGT) warms because of prolonged thermal storage. Ice acts as a cement in soils, and upon thawing compromises structural integrity (Eppelbaum & Kutasov 2019; Kleven 2018). This is also true for loose sediments, such as glacial till or marine sediments. A deep layer of thawed material unable to withstand the overbearing load may lead to consolidation and cause significant surface shifts as a result (Eppelbaum & Kutasov 2019). Unfortunately, this phenomenon can also lead to collapse of the overbearing layers when the cement properties change from a voluminous solid to a thinner, mobile liquid.

From a BTES engineering perspective, there are two main activities that cause thaw:

1. Drilling the wells.
2. Storing thermal energy.

For a location where 5 meters of till overlay frozen bedrock, significant surficial shifts may not occur. Unless a fracture or fault in the bedrock completely cemented by ice thaws, which is a unique scenario that is uncommon, damage to the system from surface shifts may not be significant. Considering a location composed of 30 m unconsolidated quaternary sediments on top of bedrock and a borehole heat exchanger that reaches 100 m depth, thawing permafrost may become an important problem.

Should 30 m continuous permafrost thaw, three scenarios (**Figure 1.2**) may occur:

A. The frozen layer underlying the 30 m of thawed sediment will act as a solid, slick surface for slip to occur, causing local mud slides and other deformation (**A**) (Kleven 2018; Hannus 2016).
B. The overbearing 30 m of thawed material may become consolidated and cause significant surface shifts and compression (**B**) (Eppelbaum & Kutasov 2019; Kleven 2018; Hannus 2016).
C. The permeability of the layers may change, changing the flow and heat transfer mechanisms evolving from conductive (**C(a)**) to unpredictable convective (**C(b)**).

These scenarios could damage the BTES system and incur costly repairs.

Figure 1.1 A. Canada, with Nunavut pictured. The red box is the area of focus for map (adapted from McMartin et al. 2021). B. Map of glaciogenic features. Work site indicated by red star (general area; adapted from McMartin et al. 2021). C. Map of infrastructure, Baker Lake. Work site indicated by red star (general area; adapted from Municipality of Baker Lake 2022) Google Earth spatial map, Baker Lake (adapted from Google Earth 2022). D. The Baker Lake Community, Nunavut, Canada (adapted from FVB Energy 2021).

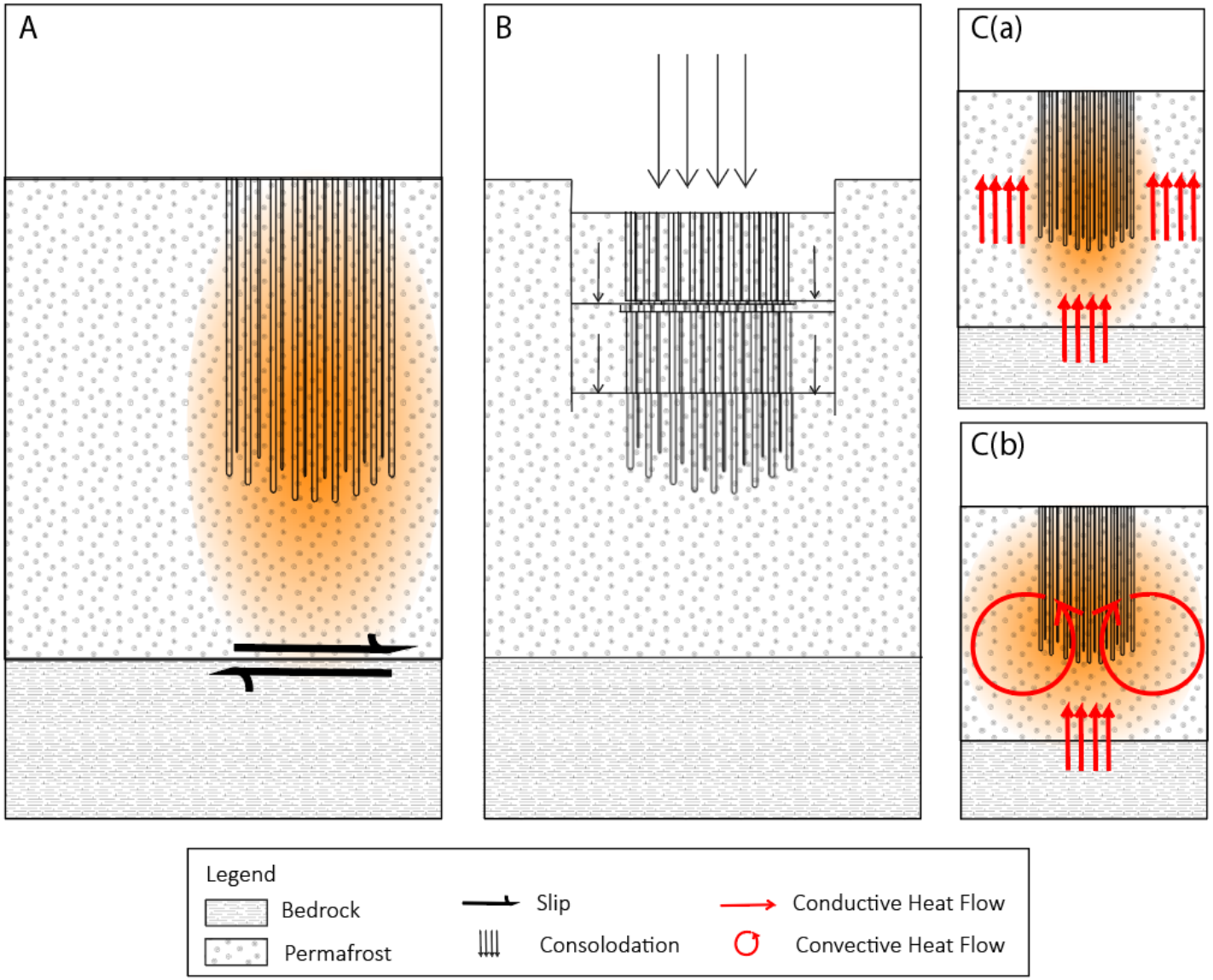

Figure 1.2 Three scenarios of thawing permafrost with a BTES system. A. Slip of a thawed permafrost layer on top of a frozen bedrock layer. B. Compaction of consolidated thawed permafrost. C(a). Conductive conditions. C(b). Convective conditions.

1.2 Project Purpose

The transition from diesel to geothermal inspires further questions, especially when envisioning underground heat storage in regions with an arctic to subarctic climate. How should energy be stored in a permafrost region, and what is the extent of permafrost thaw caused by that storage? To store energy, it is typical to install borehole heat exchangers (BHEs) and borehole thermal energy storage systems (referred to as BTES systems) in the subsurface. This installation lays the foundation for seasonal district heating. With the implementation of a district heating system, Baker Lake may be able to reduce reliance on diesel fuel (FVB Energy 2021). Qulliq Energy Corporation (QEC) and RESPEC are investigating the feasibility of the implementation of BTES in the community of Baker Lake. This system is being designed to capture waste heat from water-jackets, aftercoolers, and other exhaust of the community's power plant to be stored in the ground during seasons with low demand and extracted during seasons with high demand (FVB Energy 2021).

The purpose of this study is to evaluate solutions to minimize permafrost thaw while maximizing heat storage using BTES technology. FEFLOW is utilized to numerically simulate permafrost thaw mitigation techniques, as well as model the ground temperature fluctuations beneath the work site at Baker Lake. It is the objective of this work to explore permafrost thaw mitigation solutions that may minimize permafrost thaw while maximizing heat storage with BTES. Using permafrost thaw mitigation strategies, it may be possible to overcome engineering challenges relating to permafrost. Previous technologies developed to reduce or entirely dissuade permafrost melt have already been implemented in many subarctic communities (Fatollahzadeh Ghesari 2021; Xu & Goering 2008).

2. BACKGROUND

2.1 Borehole Heat Exchangers

BTES systems are composed of borehole heat exchangers (BHEs). BHEs are systems of pipes that are installed vertically in the ground. They are responsible for funnelling heat via heat carrier into the ground so that energy may be stored and extracted by the interactive system of BHEs, otherwise called the BTES field. The most common borehole heat exchanger in shallow boreholes, being 400 m or less, are single or double U-tubes (Silwa et al 2018). U-pipe or U-tube heat exchangers are comprised of two tubes joined at the base in a "U-shape" configuration (Bauer et al. 2011). These U-shaped pipes are grouted in boreholes with various diameters. In northern communities, it is common to see boreholes with smaller diameters, such as 75 mm, that have been drilled with diamond drills (Kanzari 2019). Modifications to BHEs can be implemented to change the thermal conductivity of the system and allow less heat from escaping the BHE to the surroundings.

2.2 Solutions to Mitigate Permafrost Thaw

Two permafrost thaw mitigation solutions are defined. 'Passive' mitigation solutions are any materials that can be used passively as an insulator, such as bentonite grout, insulated piping or an ungrouted borehole with air in the upper BHE section (**Figure 2.1**). 'Active' mitigation solutions are any devices that can be installed to actively transfer heat from a heat source to a heat sink, such as thermosyphons (**Figure 2.2**). Heat transfer mechanisms play an important role in all solutions. The main difference between 'passive' and 'active,' for the purpose of this report, is 'passive' solutions are heat-storage mediums while 'active' solutions are heat-transport mediums. Combinations of various strategies to keep permafrost cold are implemented in areas where infrastructure alters the natural thermal gradient of the surroundings.

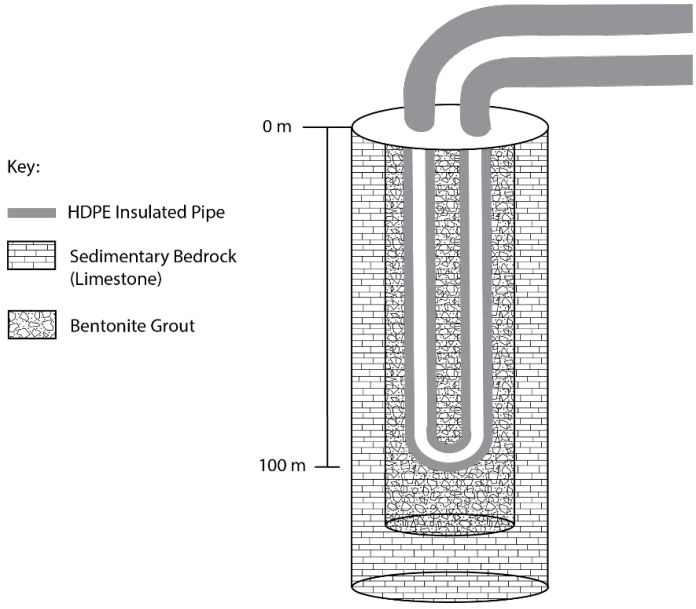

Figure 2.1. U-Tube BHE constructed with HDPE insulated pipe, grouted in bentonite.

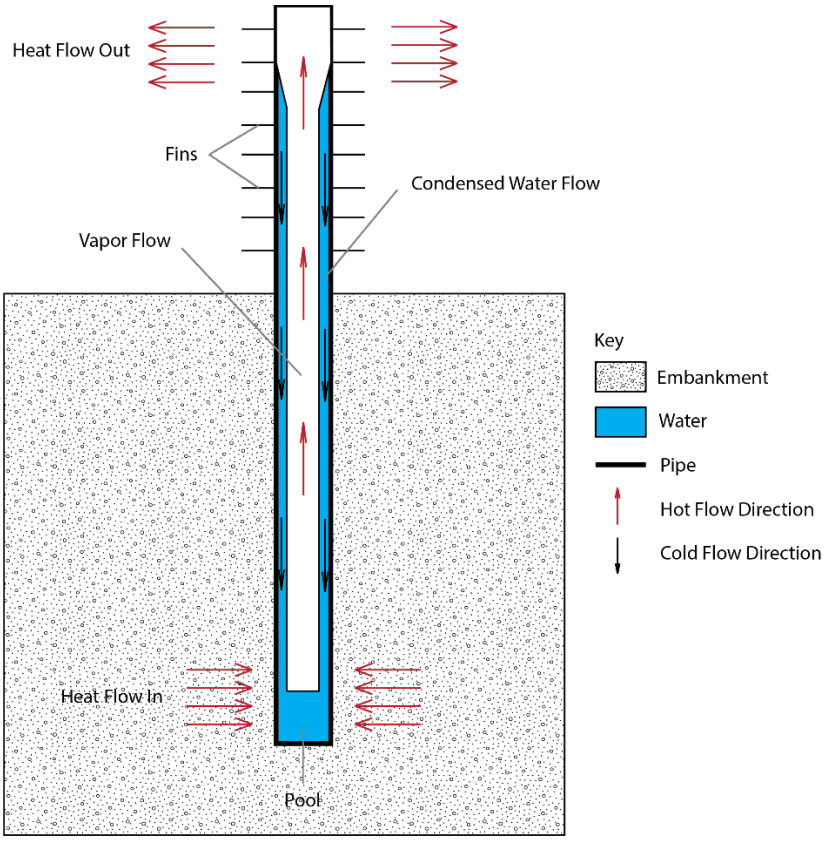

Figure 2.2. Two-Phase Closed Thermosyphon. Based on model from Pei et al. 2017.

2.2.1 Passive Solutions

2.2.1.1 Insulated Pipes

One solution to mitigate permafrost thaw is to use insulated materials in the construction of BHEs and BTES. Polyethylene is a material that serves as an insulator (Fatollahzadeh-Ghesari 2021; Saaly et al. 2020; Schulte et al. 2016). High-density polyethylene pipes (HDPE) have been used in BHEs because the material is resistant to corrosion. They operate durably with various fluids from -34 °C to 82 °C (Holmberg et al. 2016). HDPE piping may be a viable option for maximizing heat storage, but it may not preserve permafrost conditions because the thermal conductivity is not low enough to prevent heat from propagating into the permafrost. PVC pipes have a lower thermal conductivity than the previously mentioned materials (**Table 2.1**). Additionally, they also can work with fluid temperatures between -18 °C to 60 °C (Mendrinos et al. 2016). Therefore, PVC has been utilized to test mitigation solutions in the modelling process. Vacuum insulated tubing (VIT) is another material that is used to reduce the heat losses from transport of hot fluid in coaxial deep BHEs (dBHEs; Gascuel et al. 2022). VIT may also be able to maximize borehole energy storage while minimizing permafrost thaw if applied between the sediment-to-grout contact as a casing. Thermal conductivity values in conjunction with economic parameters for each material are listed in **Table 2.1**.

Table 2.1. Properties for different pipe materials. Abbreviations refer to inlet pipe diameter (d_{in}), outlet pipe diameter (d_{out}), inlet pipe thickness (h_{in}), outlet pipe thickness (h_{out}), and effective thermal conductivity of the material (λ), and custom measurements (c).

Pipe	d_{in}	d_{out}	h_{in}	h_{out}	λ	Bulk Price	Source
	mm	mm	mm	mm	W/m/K		
HDPE	32	32	3	3	0.42	1300 Euro/ton	65
PVC	32	32	2.4	2.4	0.23	800 Euro/ton	65
VIT	*c*	*c*	*c*	*c*	0.037	$150 CAD/m to 175 CAD/m	32

2.2.1.2 Grout and Cement

In the case of borehole heat exchangers (BHEs), thermally insulated grout, such as bentonite grout, prevents excessive loss of thermal energy into the surficial material at the top of the borehole (Schulte et al. 2016). When looking for viable grout solutions in permafrost zones, it is important to determine whether the grout will crack, or become unstable, after multiple freeze-thaw cycles. Mechanical shock tests are representative of the stress that occurs during a natural, seasonal freeze-thaw cycle (Xie et al. 2018). Mechanical stresses applied to cured bentonite slurry samples indicate that the slurries with 10% bentonite show a similar compressive strength to more commonly used cements (Xie et al. 2018). A list of grouts and their thermal conductivity is given in **Table 2.2**.

Table 2.2. Thermal conductivity of grout materials.

Grout	λ W/m/K
Bentonite 10%	0.7
Bentonite 10%	1.4
Bentonite/Cement/Sand 15-20%	0.7
Thermal Grout	1.47
Till	2

2.2.1.3 Empty Borehole Providing Air Insulation

The final passive scenario simulated is a borehole drilled to 100 m depth, but instead of grouting the BHE in the upper section air is used as an insulator (**Figure 2.3**). In the upper section, which is at least equivalent to the depth of the sedimentary layer, the BHE is left standing in open air inside of the borehole. Applying this air insulation removes the thermal contact between the BHE and the surrounding geological materials. Without this direct contact, it is difficult for heat to transfer from the BHE to the heat-sensitive sediments. The difficulty stems from air's naturally reduced volumetric heat capacity and thermal conductivity. In removing grout from the sediment zone of the BHE, the hope is to completely reduce heat transferred between the BHE and the sediments.

Table 2.3. Thermal conductivity of air.

Grout	λ W/m/K
Insulation with Air	0.02

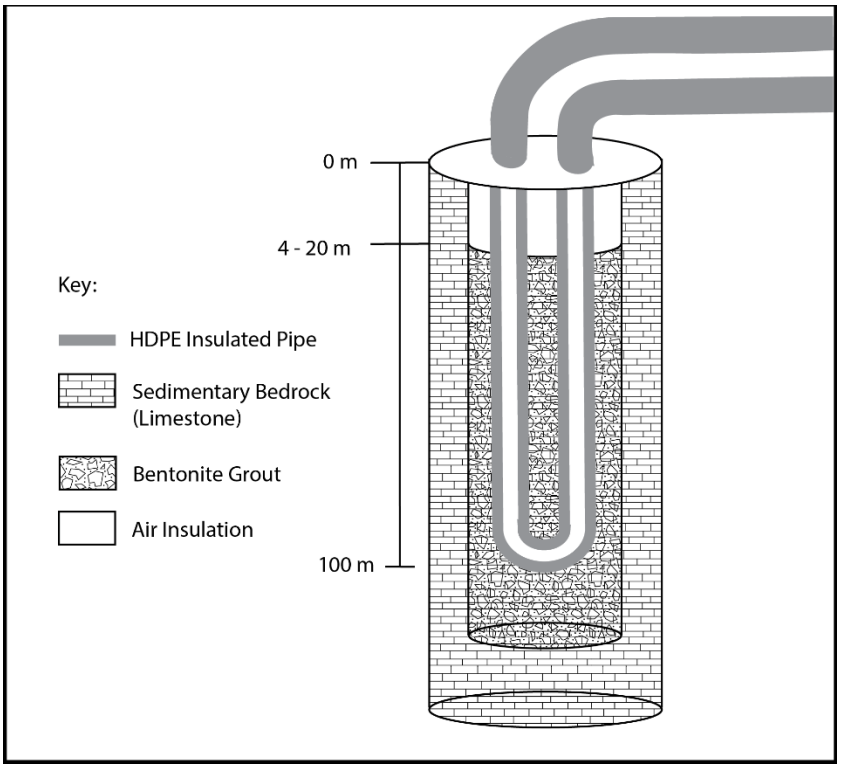

Figure 2.3. Borehole displaying air insulation inside of a borehole containing a grouted BHE.

2.2.2 Active Solutions

2.2.2.1 Thermosyphons

Thermosyphons are a technology widely used to mitigate permafrost thaw caused by seasonal temperature variations. Thermosyphons utilize air convection to inject air into the ground. They are capable of extracting heat from embankments and other ground structures in winter at a faster rate than heat can bleed into the subsurface during warmer months (Pei et al. 2017; Xu & Georing 2008; Reid et al. 1975). To achieve this heat transfer, air is pushed through the thermosyphons. The traditional thermosyphon operates by allowing cool air in winter to reach deeper areas of warmer ground. Essentially, warm air rises in the tube while frigid air sinks. "Turing thermosyphons off" in the summer is made possible by closing the tube when the temperature of the air exceeds that of the ground. Doing so prevents warm air from entering the subsurface.

2.3 Materials of the Work Area

The north-western segment of Baker Lake is the focus area for this study. The work site is situated on the edge of the town, at the tail end of the CFZ. A fault runs through the community. The most likely bedrock in the area is granite and gneiss, with thermal conductivity values that reflect that of the Canadian Shield. The surficial sediments in this area are primarily glacial deposits, ranging from 1 to 20 m in depth with upper till of 2 to 4 m thickness overlaying 10 m of lower till in some crevasses (McMartin et al. 2021; Cunningham & Shilts 1977). According to a report prepared by Canadrill Limited Geotechnical Division (2019), the site is located within a low area between two bedrock ridges. These ridges act as a valley for sediments to be deposed in. The drill logs of piles on the site location indicate that the average depth of sediments 500 m from the site was 3.2 m, and the depth at each pile ranges between 2.3 to 4 m depth. Primary materials that

can be expected are silty-gravelly till, sand and gravel, silt, clay, and exposed bedrock. The depth to bedrock is summarized in APPENDIX 1, with approximately 300 mm or more of variance. While the Canadrill Limited Geotechnical Division report (2019) is of a project in an area that was 500 m away in the southwest direction from the main site, the summary of the conditions is likely reasonable for this project's site.

2.4 Permafrost Conditions

Baker Lake is an area of continuous permafrost (Throop 2012; Smith & Burgess 2002). There is no significant drainage and therefore no water passes through, above, or near the site (Canadrill Limited Geotechnical Division 2019). The thickness of the active layer of permafrost in Baker Lake varies between locations. Near the Thelon River, the active layer of permafrost extends 0.75 m depth, while near the Kiggavik mine site permafrost extends anywhere from 0.15 to 6 m (Smith & Burgess 2002). Therefore, an active layer depth of 0.15 to 6 m is reasonable to expect.

From 1981 to 2010, the mean annual air temperature over approximately 30 years (MAAT) was determined to be -11 °C while the mean annual ground temperature (MAGT) was determined to be -7 °C at the ground surface based on reports from Tetra Tech (Smith et al. 2013), which also provided a range of past temperatures (Canadrill Limited Geotechnical Division 2019). Another study of permafrost in the Baker Lake area determined the MAGT to be -7.9 °C at the ground surface, a similar value to that recorded by Tetra Tech (Smith et al. 2013). Baker Lake has periods in the summer where the ground temperature is warmer than the freezing temperature. The overlying soils and glacial till at the site can be excavated, if the sediments are thin, and repurposed as overlying insulation.

2.5 Baker Lake's BTES

2.5.1 Heating Needs

The heating needs of Baker Lake, as provided by FVB Energy in their feasibility study on the installation of a district heating system in Baker Lake, are provided in APPENDIX (2021). A small three-row housing unit is predicted to have a maximum load of 90 kW in peak conditions and an annually energy consumption of 380 MWh. Jonah Amitnaaq High School currently has the highest maximum predicted peak load of 295 kW totalling an energy consumption of 1,220 MWh over a year. To heat all buildings in the proposed plan, a peak load of 2020 kW is required. The report also concludes that Baker Lake will experience 3,913 full load hours on yearly average (FVB Energy 2021).

2.5.2 System Parameters

This BTES system will inject heat into the middle of the field and extract from the outer end of the circular borefield (**Figure 2.4)**. For this work, the BTES system is assumed comprised of U-tube borehole heat exchangers that are 100 m in depth, with an inlet temperature of 45 °C in the summer, and -5 °C in the winter. The flow rate is 11.2 US gpm for all BHEs, and the flow reverses between heat injection and extraction seasons. The projected run time of this system is six months in the summer and six months in the winter. The system is expected to operate 24 hours a day during every day of the week. The borehole diameter is 0.15 m, the spacing is 0.04 m, and the U-tube material is HDPE. The installation of the BTES system preludes the creation of an energy transfer station for a district heating system (DHS) in Baker Lake. This system will connect clusters of customers across the community to a heating network once completed.

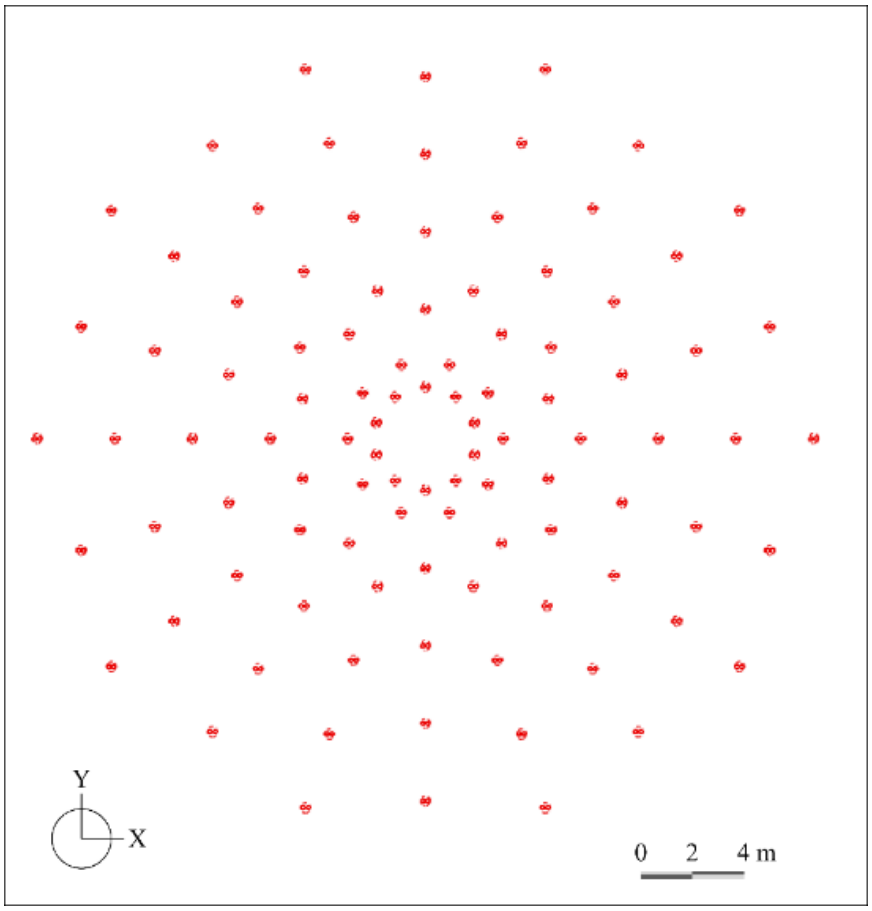

Figure 2.4 BTES System hypothetical model, where BHEs (red points) are arranged with a spacing of approximately 4 m on the outer ends, and closer towards the middle.

A single BHE model is first developed with a circular geometry to facilitate computations that can take a long time with 100 BHEs. The borehole fits the constraints of a northern system and has the appropriate diameter to reflect a diamond-drilled borehole of 75 mm that could be installed in Baker Lake (**Figure 2.5**). The flow rate is 11.2 US gpm if the BHE has HDPE pipes, and 11.3 US gpm if the BHE has PVC pipes. The single BHE runs for 6 months with an inlet of 45 °C, from the months of May to October, and then at -5 °C for 6 months from November to April. These seasons of injection and extraction are chosen to best reflect the seasonal temperatures at Baker Lake. Seasonal ground temperature changes are imposed to reflect atmospheric temperature variations, and PiFreeze is used to calculate latent heat phase changes from freezing and thawing ice.

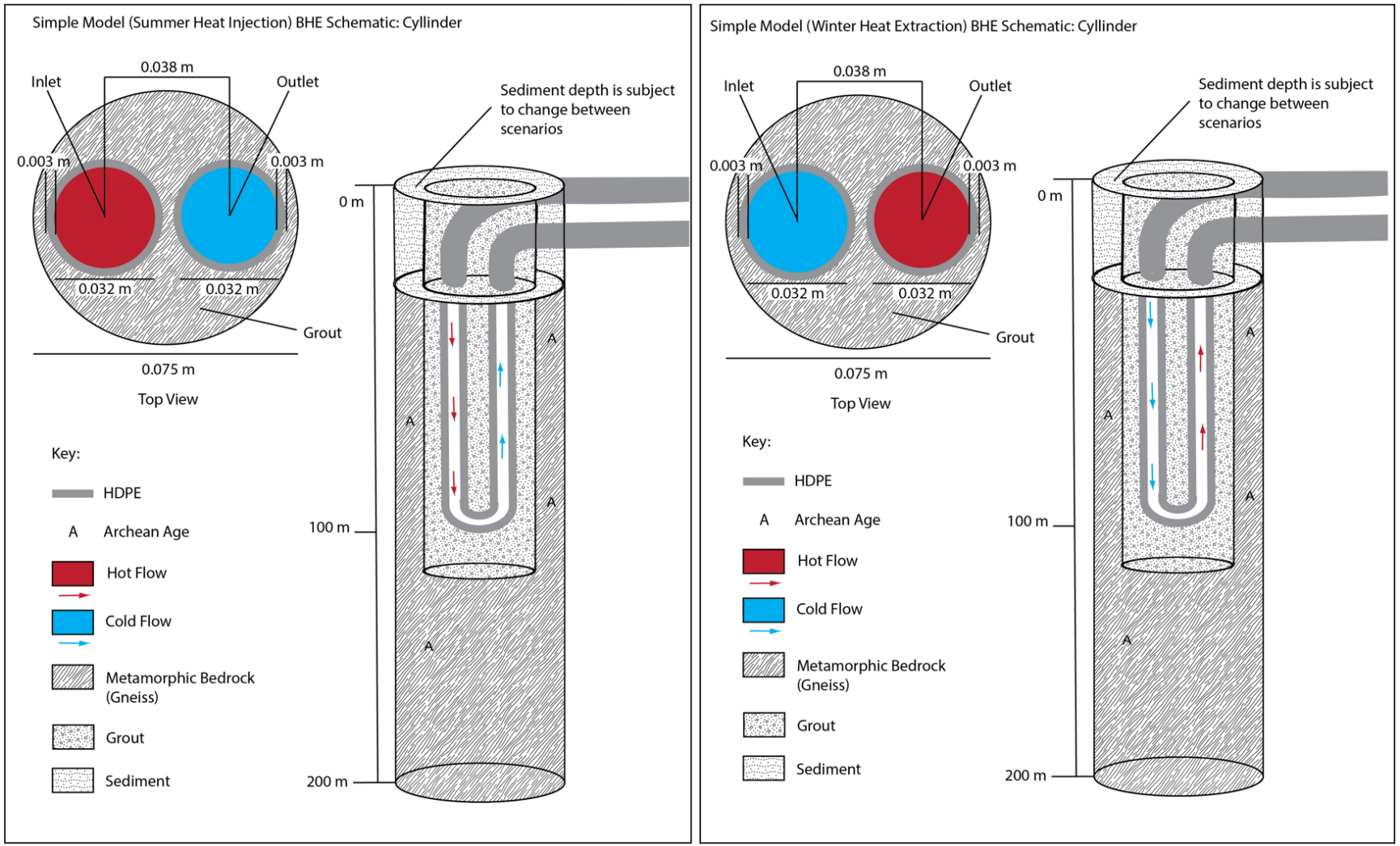

Figure 2.5. Conceptual model of the cylindrical U-Tube BHE.

3. METHODOLOGY

3.1 Single BHE & BTES Numerical Models

The BHE and BTES numerical models are developed in FEFLOW groundwater and heat transport modelling software (Diersch 2014). The PiFreeze plugin is used to simulate freezing and thawing of ice in the single BHE numerical model (MIKE 2016). PiFreeze is not utilized in the simplified model of the whole BTES field to reduce computation time. From this point on, italicized characters are input variables, non-italicized characters are non-numerical, and characters without an assigned unit are dimensionless.

3.2 Conceptual Model

3.2.1 Single BHE

A 3D cylindrical-shaped model is used for the initial simulations of the single BHE model (**Figure 3.1**). The model has a radius of 2 m and a total length of 200 m. In scenarios 1 through 19, the first 4 m of the model are defined as quaternary sediments (glacial till) and the remaining 196 m extent of the model is gneissic bedrock (**Figure 2.5**). In scenario 20, which is a scenario with 20 m of sediments and 20 m of air insulation around the central BHE in the single BHE model, sediments extend to 20 m and gneiss constitutes the remaining 180 m of the model. This model is used to mimic a single BHE located in the middle of a BTES field (**Figure 3.2**). A borehole in a BTES field spaced 4 m away from neighbouring boreholes will encounter a distance between the nearest borehole at which no heat transfer occurs. This distance is 2 m assuming the ground is homogeneous and is the equidistance between the two BHEs. To simulate this effect, the model is circular and has adiabatic boundaries. The adiabatic boundaries are imposed by FEFLOW, as no positive or negative effect is applied via boundary conditions to the model. If no boundary condition is applied to the sides, top, or bottom of the model, FEFLOW automatically assumes the boundaries are adiabatic. The initial state of the model has a constant temperature of -7 °C applied. The transient state of the model has a changing ground temperature that is applied at the surface of the model. A fluid flux of 0 is applied to the top of the model to restrict fluid flow. Applying this parameter to the top of the model sets the fluid flux to 0 in the vertical faces of the model, extending the condition from 0 – 200 m. The vertical side boundaries in the model have no fluid flux. A constant heat flux condition is applied to the bottom of the model.

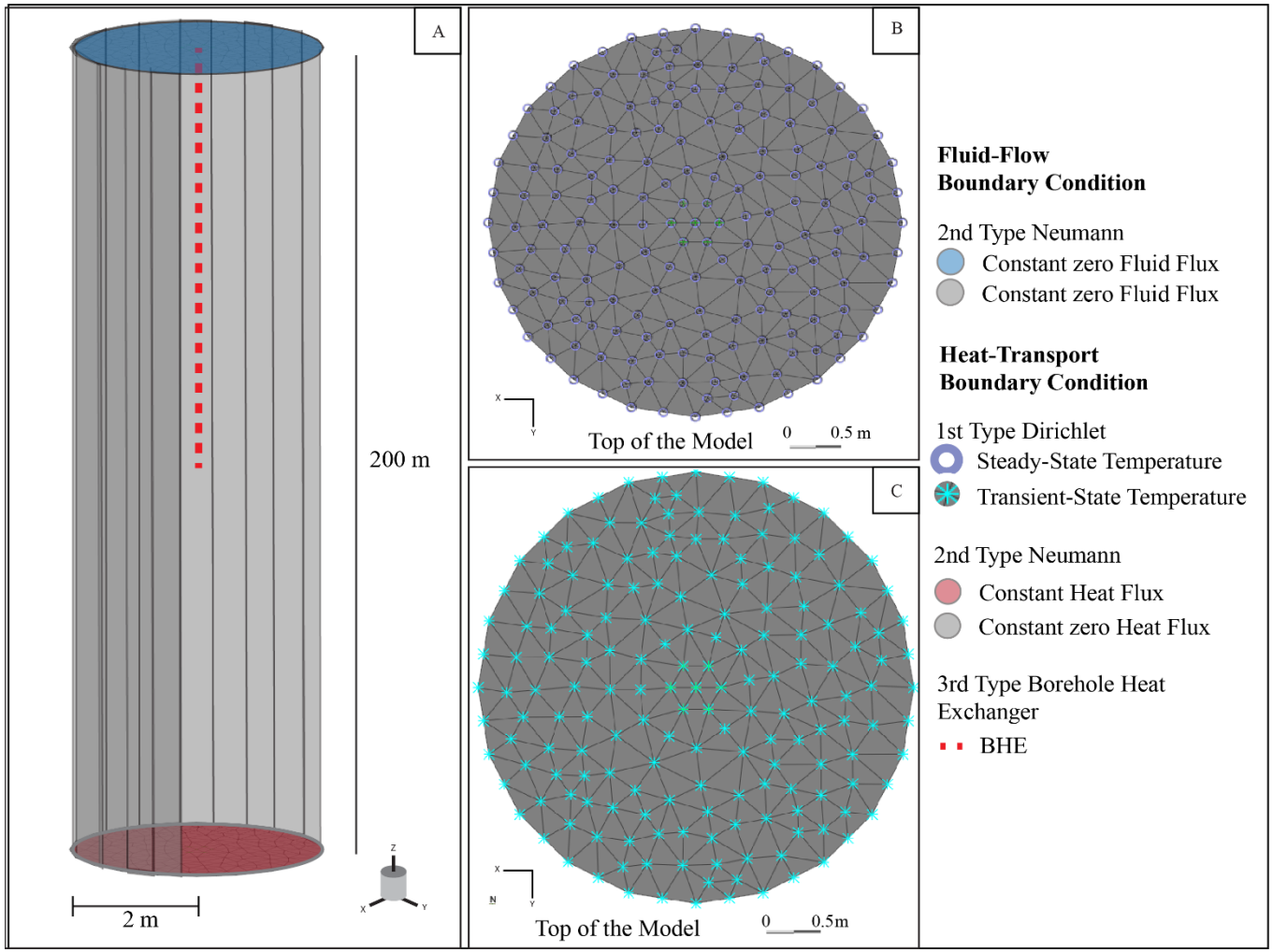

Figure 3.1. A) Boundary conditions applied to the model, with the height and radius of the model included. No flow occurs in the model because of the applied flow condition, and heat transport from the base of the model radiates to the top of the model. B) Temperature boundary condition (constant) is a first type Dirichlet condition applied to the top of the steady-state model. C) Temperature boundary condition (transient) is a first type Dirichlet condition applied to the top of the transient-state model.

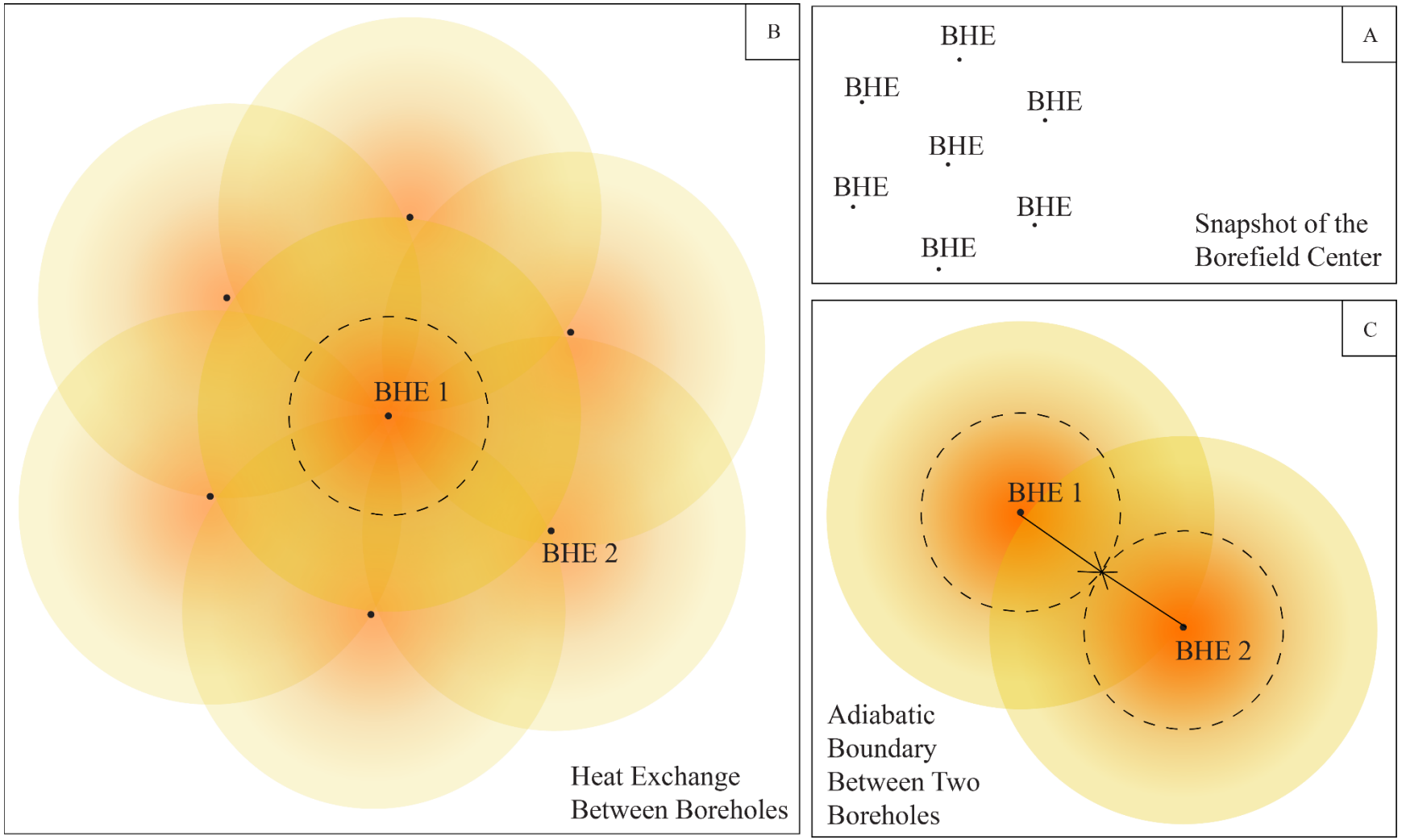

Figure 3.2 A) Center of the borehole field with 6 BHEs surrounding 1 central BHE. B) Snapshot of heat exchange between the central BHE and surrounding BHEs with a focus on the bottom right BHE. C) Diagram of the boundary at which no heat is exchanged between boreholes; the same amount of heat is radiated from each point when the BHEs are equidistant.

3.2.2 BTES

A 3-D rectangular model is used to run the BTES simulations (**Figure 3.3**). The model is 100 m wide and 50 m long. The layer spacing is refined in the BTES region and extended below the BTES field to decrease computation time. The whole model is defined as 4 m of glacial till sediment on top of 46 m of gneissic bedrock to simplify the computation demand for a large BTES field. This model proposes a hypothetical model of a BTES field in Baker Lake sedimentary and temperature conditions. The distance between each BHE is approximately 4 m until the central two rings of BHEs, where the distance becomes closer. To simulate no fluid flow, equal head boundaries have been applied to either side of the model on opposing vertical boundaries. The initial state of the model has a constant temperature of -7 °C applied. The transient state of the model has the same changing ground temperature as the single BHE model, that is applied across the entire top surface of the model.

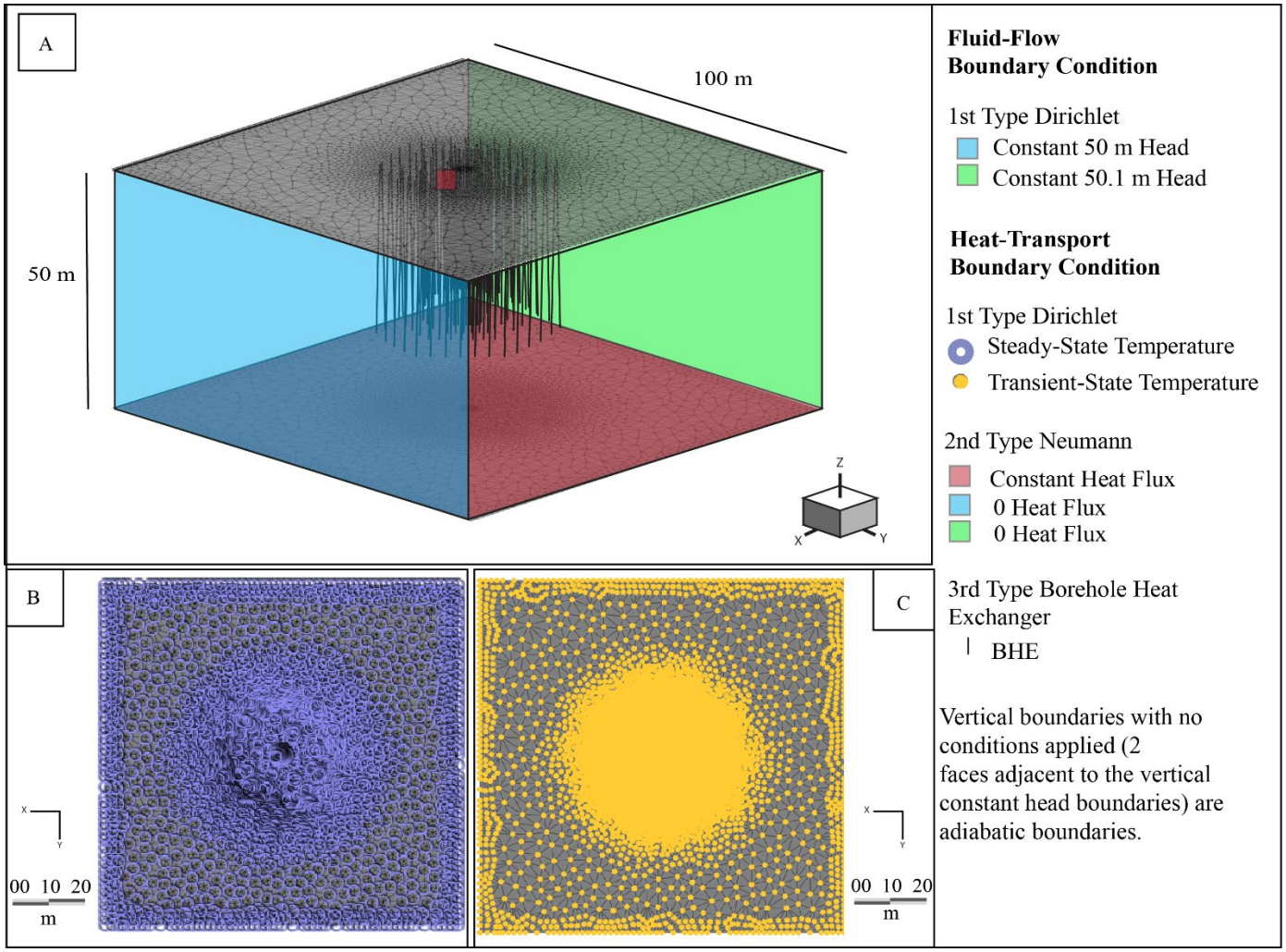

Figure 3.3 A) Boundary conditions applied to the model, with the height and length of the model included. Negligible flow occurs in the model because of the applied head condition on the vertical sides, and heat transport from the base of the model radiates to the top of the model. B) Temperature boundary condition (constant) is a first type Dirichlet condition applied to the top of the steady-state model. C) Temperature boundary condition (transient) is a first type Dirichlet condition applied to the top of the transient-state model.

3.2.3 Governing Equations – Numerical
3.2.4 Fluid Flow

The single BHE model is built employing Richard's equations to simulate flow in an unconfined aquifer. Zero fluid flux boundaries were used to minimize the impact of groundwater flow:

$$sS_0 \frac{\partial h}{\partial t} + \varepsilon \frac{\partial s}{\partial t} + \nabla \cdot q = Q_{\mathrm{b}} + Q_{\mathrm{EOB}} \tag{1}$$

$$q = -k_{\mathrm{r}} K f_{\mu} \cdot (\nabla h + \chi e) \tag{2}$$

where s is saturation of fluid in the void space, S_0 is the specific storage coefficient (m^{-1}), h is the hydraulic head (m), t is time (s), ε is the volume fraction porosity (void space), Q_b is the bulk source/sink term for flow ($m\ s^{-1}$), and Q_{EOB} is the correction sink/source term of extended Oberbeck-Boussinesq approximation (s^{-1}). In calculating q, the Darcy velocity ($m\ s^{-1}$), K is a tensor of hydraulic conductivity ($m\ s^{-1}$), f_μ is the viscosity relation function, χ is the buoyancy coefficient, and e is the gravitational vector. This is the basic form of the Richard's equation in Diersch's FEFLOW white papers (2014).

The PiFreeze module plugin operates using the Richards' equation to account for an ice phase in the porous medium. The ice phase relies on the bulk volume fraction of available pore space (MIKE 2016). As the ground is thawed or frozen, the water to ice ratio is calculated at given time steps. The two characteristics of this relationship that induce the biggest alterations to the model are the porosity of the medium, the saturation of the model, the hydraulic head, and the hydraulic conductivity of the material. Applying Richards' fluid flow in a fully saturated model allows PiFreeze to make the following modifications to the bulk porosity:

1) The Richard's equation bulk porosity:

$$\varepsilon_{\mathrm{l}} + \varepsilon_{\mathrm{s}} + \varepsilon_{\mathrm{a}} + \varepsilon_{\mathrm{i}} = 1 \tag{3}$$

where ε is the flow accessible volume fraction, ε_i is the ice volume fraction, ε_l is the liquid volume fraction, ε_s is the solid fraction and ε_a is the air fraction (Clausnitzer & Mirnyy 2016, MIKE 2016).

2) The bulk fraction of ice is treated as a fraction of the solid bulk porosity when the model is fully saturated (MIKE 2016). The ice porosity changes the equations for liquid porosity and solid porosity to:

$$\varepsilon_{\mathrm{l}} = \frac{\varphi(\varepsilon_{\mathrm{l}}+\varepsilon_{\mathrm{i}})\frac{\rho_{\mathrm{i}}}{\rho_{\mathrm{l}}}}{1-\varphi\left(1-\frac{\rho_{\mathrm{i}}}{\rho_{\mathrm{l}}}\right)} \tag{4}$$

$$\varepsilon_{\mathrm{i}} = \frac{(1-\varphi)(\varepsilon_{\mathrm{l}}+\varepsilon_{\mathrm{i}})}{1-\varphi\left(1-\frac{\rho_{\mathrm{i}}}{\rho_{\mathrm{l}}}\right)} \tag{5}$$

where ρ_i is the density of ice ($kg\ m^{-3}$), ρ_l is the density of fluid ($kg\ m^{-3}$), and φ is the ice fraction (Clausnitzer & Mirnyy 2016; MIKE 2016).

The BTES field model is run with a first-order accurate predictor-corrector scheme because it is a confined fluid flow model. For the purposes of the BTES field, the Darcy equation is used as the flow governor (**Equation 5-9**):

$$q_{\mathrm{l}} = -\frac{k_{\mathrm{r}}^{\mathrm{l}} k}{\mu^{\mathrm{l}}} \cdot \left(\nabla p^{\mathrm{l}} - \rho^{\mathrm{l}} g\right) \tag{6}$$

where q_{l} is the momentum of the liquid phase, $k_{\mathrm{r}}^{\mathrm{l}}$ is relative permeability of the liquid phase (l), k is porous medium permeability tensor (m^2), ∇ is a gradient vector (m^{-1}), p^{l} is pressure of the liquid phase (kg m^{-1} s^{-2}), ρ^{l} is density of the liquid phase (kg m^{-3}), g is the gravity vector (m s^{-2}), and μ^{l} is liquid viscosity (kg m^{-1} s^{-1}; Diersch 2014).

3.2.5 Heat Transfer

The heat transfer through both the BTES and BHE models is expressed by the following equation, which is composed of both convective and conductive parts:

$$\frac{\partial}{\partial t}\rho^{\mathrm{a}} c^{\mathrm{a}} T + \frac{\partial}{\partial x_{\mathrm{i}}}\left(\rho^{\mathrm{f}} c^{\mathrm{f}} q_{\mathrm{i}} T\right) - \frac{\partial}{\partial x_{\mathrm{i}}}\left(\Lambda_{\mathrm{ij}} \frac{\partial T}{\partial x_{\mathrm{j}}}\right) = Q_{\mathrm{t}} \tag{7}$$

where *t is* time (s), $\rho^{\mathrm{a}} c^{\mathrm{a}}$ is the volumetric heat capacity of the medium (Jm^{-3} K^{-1}), x_{i} is the eulerian spatial coordinate vector (m), $\rho^{\mathrm{f}} c^{\mathrm{f}}$ is the volumetric heat capacity of the fluid (Jm^{-3} K^{-1}), q_{i} is the Darcy velocity vector of the fluid phase (m s^{-1}), T is the temperature of the media (K), Q_{t} is the source/sink heat function (kg m^{-1} s^{-3}), and Λ_{ij} is the tensor of hydrodynamic thermodispersion (kg m s^{-3} K^{-1}), which is expressed in **Equation 8**:

$$\Lambda_{\mathrm{ij}} = {\Lambda_{\mathrm{ij}}}^{\mathrm{cond}} + {\Lambda_{\mathrm{ij}}}^{\mathrm{disp}} = \lambda^{\mathrm{a}} \delta_{\mathrm{ij}} + \rho^{\mathrm{f}} c^{\mathrm{f}} \left[\alpha_{\mathrm{i}} V_{\mathrm{q}} \delta_{\mathrm{ij}} + (\alpha_{\mathrm{L}} - \alpha_{\mathrm{T}}) \frac{q_{\mathrm{i}} q_{\mathrm{j}}}{V_{\mathrm{q}}}\right] \tag{8}$$

where ${\Lambda_{\mathrm{ij}}}^{\mathrm{cond}}$ is the conductive part of the tensor, ${\Lambda_{\mathrm{ij}}}^{\mathrm{disp}}$ is the dispersive part, λ^{a} is the bulk thermal conductivity of the ground (W m^{-1} K^{-1}), δ_{ij} is the Kronecker tensor (δ_{ij}= 1 for i=j), α_{i} is the inlet dispersion (m), V_{q} is the absolute Darcy fluid flux (m s^{-1}), α_{L} is the longitudinal dispersivity (m), α_{T} is the transverse dispersivity (m), and q_{j} a vector of Darcy velocity similar to q_{i} (m s^{-1}; Le Lous et al. 2015). The ice fraction in the single BHE model alters the original equations used to calculate the bulk thermal conductivity and heat capacity in the conductive heat transport equation:

$$\rho^{a}c^{a} = \varepsilon\rho^{f}c^{f} + (1-\varepsilon)\varepsilon\rho^{s}c^{s} \quad (9)$$

$$\lambda^{a} = \varepsilon\lambda^{f} + (1-\varepsilon)\lambda^{s} \quad (10)$$

where ε is the volume fraction, $\rho^{s}c^{s}$ is the volumetric heat capacity of the solid (J m^{-3} K^{-1}), λ^{f} is the thermal conductivity of the fluid (W m^{-1} K^{-1}), and λ^{s} is the thermal conductivity of the solid (W m^{-1} K^{-1}; Le Lous et al. 2015).

1) In the presence of ice, the effective thermal conductivity in the heat transfer equation is represented by:

$$\lambda = \varepsilon_{l}\lambda_{l} + \varepsilon_{s}\lambda_{s} + \varepsilon_{i}\lambda_{i} \quad (11)$$

$$C = \varepsilon_{l}C_{l} + \varepsilon_{s}C_{s} + \varepsilon_{i}C_{i} - \rho_{i}L_{f}\frac{\partial\varepsilon_{i}}{\partial\varphi}\frac{\partial\varphi}{\partial T} \quad (12)$$

where λ is the effective thermal conductivity of the material (W m^{-1} K^{-1}), C is the effective volumetric heat capacity (MJ m^{-3} K^{-1}), C_l is the volumetric heat capacity of the fluid, C_s is the volumetric heat capacity of the solid, C_i is the volumetric heat capacity of ice, and L_f is the latent heat of fusion (J kg^{-1}; Clausnitzer & Mirnyy 2016; MIKE 2016).

The heat equations for calculating bulk thermal conductivity and volumetric heat capacity rely on the effective porosity (heat; Diersch 2014). For the purposes of the single BHE model, the flow porosity has been set to $1 \cdot 10^{-10}$ to ensure no fluid flow through the model. Heat transport porosity is still assigned as the correct material properties. The saturation has been set to 1 to ensure full model saturation of the remaining pores available for heat transfer. The BHE is implemented in FEFLOW with 1D elements at the center of the model domain. Calculations for BHE and BTES simulations utilize the Eskilson method (Diersch 2014). Heat transfer between grout and pipes progresses as displayed in **Figure 3.4**.

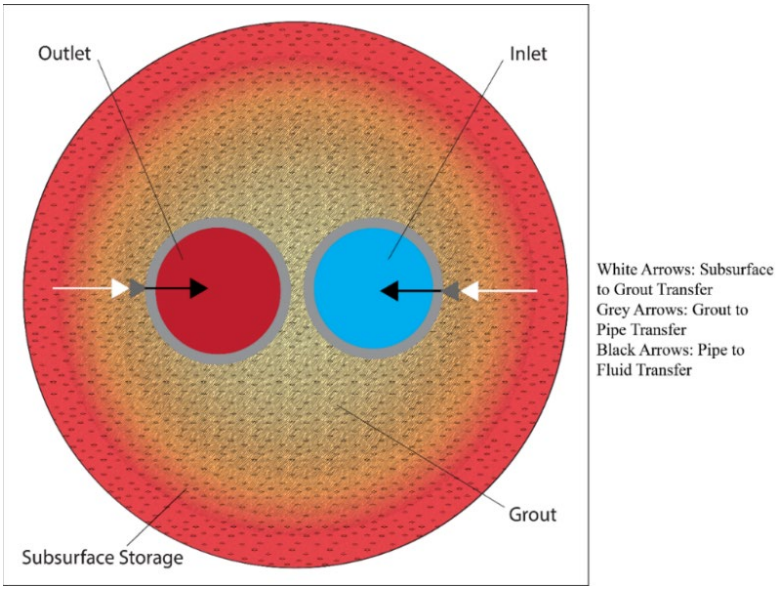

Figure 3.4 Heat flow direction of subsurface to grout, grout to pipes, and pipes to fluid in the winter heat extraction season.

3.3 Spatial and Temporal Discretion

The single BHE model is a 3D model generated from a 2D Delaunay triangular mesh. The model is configured with 0.4 m spaced 3D layers. There are approximately 156,000 elements in the model. The horizontal mesh surrounding the BHE is built in a way that ensures the borehole radius is not affected by the virtual radius by imposing a nodal distance between the BHE node and the closest surrounding nodes (Giordano et al 2019; Diersch et al. 2011). The 3D geometry is built in FEFLOW by adding slices to the model (**Figure 3.5**). A horizontal, vertical, and time step mesh independence study is then carried out to ensure that the model has the right number of layers and slices. The settings with an output that does not yield results that vary significantly (>1 °C) from the nearest refined setting is selected. For the purposes of this model, a first-order accurate predictor-corrector scheme is used.

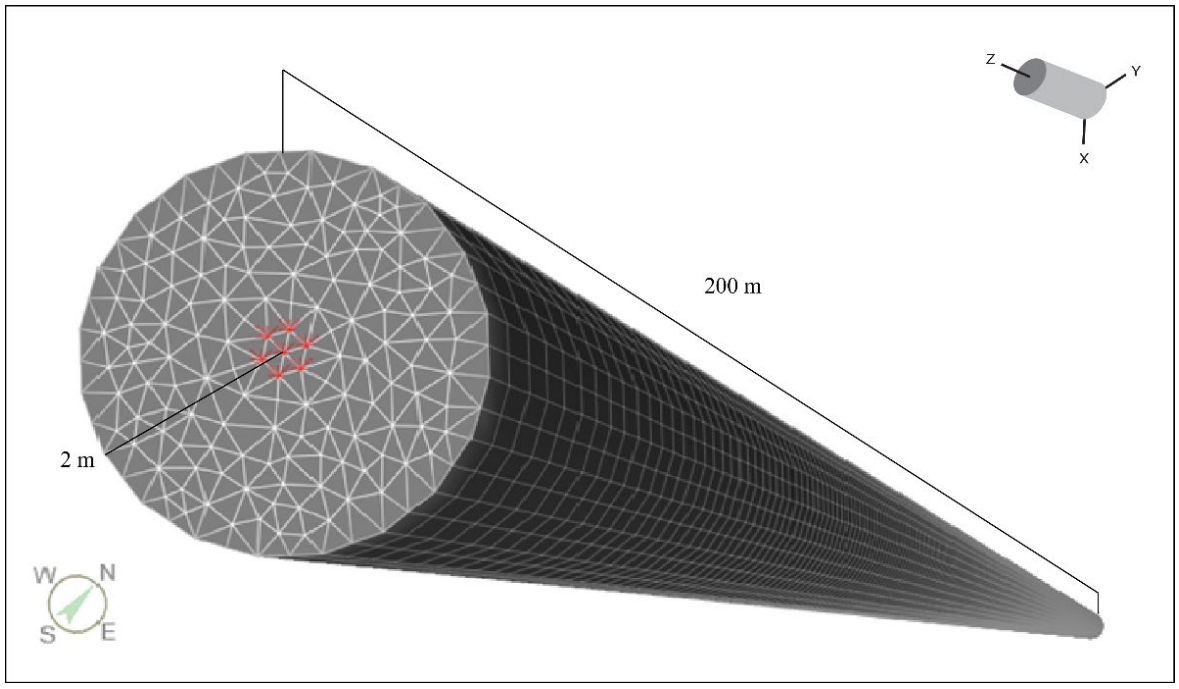

Figure 3.5 Horizontal and vertical meshes in the BHE model. Red asterisks are discretized BHE nodes.

The BTES model is a 3D model generated from a 2D Delaunay triangular mesh (**Figure 3.6**). The model is configured with 1 m spaced 3D layers for slices 50 – 32. For slices 32 – 0, the spacing between layers is 5 m. There are approximately 400,000 elements in the model. The borehole radius is not affected by the virtual radius in this mesh (Giordano et al 2019; Diersch et al. 2011). A horizontal, vertical, and time step mesh independence study is carried out to ensure that the mesh does not influence the model results. For the purposes of this model, a first-order accurate predictor-corrector scheme is used.

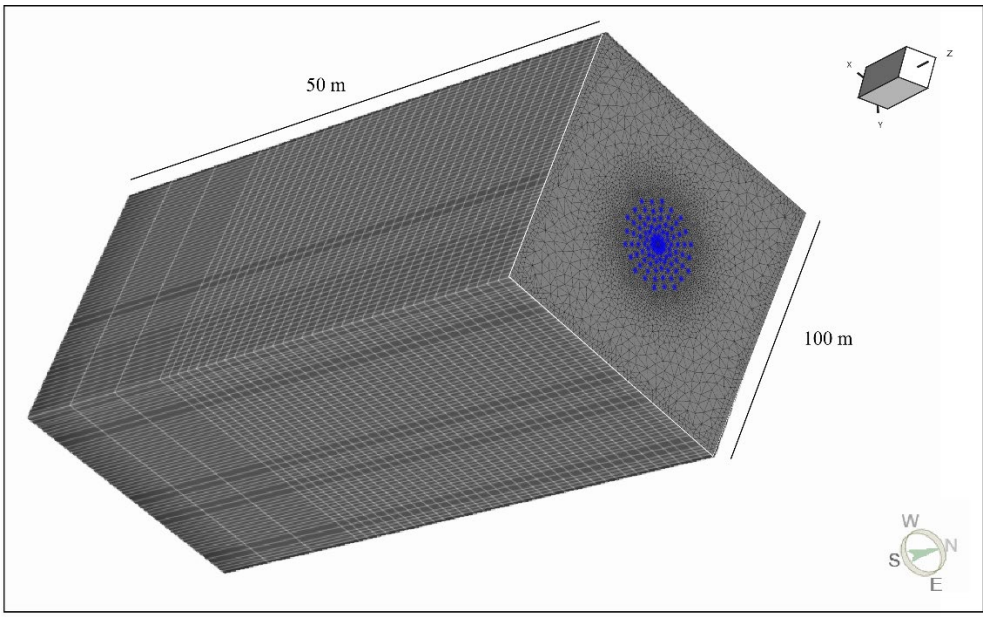

Figure 3.6 Horizontal and vertical meshes in the BTES model. Blue asterisks are discretized BHE nodes.

3.4 Properties of the Medium

The thermal properties of each material (**Table 3.1**) are based on the work of Giordano et al. (2018), Miranda et al. (2020 In progress). The heat capacity (HC), volumetric heat capacity (VHC) and thermal conductivity (TC) are the thermal properties of the solid. The FEFLOW default values for ice and water are used but only influence the heat transport portion of the model (**Table 3.2**). The values for ice and water in terms of flow are negligible because the unconfined flow porosity is reduced, and zero fluid flux is applied to the single BHE model. In the case of the BTES model a constant head boundary is applied, so fluid and solid water materials influence both parts of the model. These boundary conditions ensure minimal fluid flow in the models. The thermal properties of ice and water are the following values of ice and water in the FEFLOW PiFreeze plugin; the thermal conductivity of water has been adjusted for water at 1 °C (MIKE 2016; Diersch 2014; Ramires et al. 1995). The thermal properties of the solid are input into both models as material parameters. These properties influence the operation of heat transport in the models. The freezing function applied in PiFreeze is constant, with a linear function type. Ice freezes at 0 °C in the single BHE model, with a half of delta temperature of 1, and residual liquid fraction of 0.0001.

Table 3.1 Model material properties. Specific storage (S), porosity (P), hydraulic conductivity (K), volumetric heat capacity of the fluid (c^{f}), density (ρ) and latent heat (H_{l}).

Material	***K (x,y,z)*** md^{-1}	***S*** m^{-1}	***P*** %	$\rho^{\mathrm{a}}c^{\mathrm{a}}$ MJ m^{-3} K^{-1}	$\boldsymbol{\lambda}$ W m^{-1} K^{-1}
Gneiss	$1 \cdot 10^{-9}$	$4.6 \cdot 10^{-6}$	0.056	2.437	2.667
Glacial Till	$1 \cdot 10^{-4}$	$3.68 \cdot 10^{-4}$	0.25	2.99	1.57

Table 3.2 Model ice & water properties. Temperature of the fluid/solid that these properties apply to (Environment), density (ρ) and latent heat (H_l).

Material	Environment T	$\rho^a c^a$	λ	ρ	H_l
	°C	MJ m^{-3} K^{-1}	W m^{-1} K^{-1}	kg m^{-3}	J kg^{-1}
Water	1	4.2	0.5606	1000	-
Ice	≤ 0	1.86	2.2	917.5	334000
Air	-11	0.0013	0.0235	-	-

3.5 BHE

A U-tube BHE is selected to run the single borehole mitigation solution simulations. Various grouts and pipe materials are considered for the BHE. The spacing of the pipes remains constant (**Figure 3.7**). The borehole size, pipes, grout, heat transfer fluid, and thermal conductivity/heat capacity variables are edited with an internal BHE editor module. For the base model, the grout is an arbitrary value of 1 and the pipes are the FEFLOW default settings for high-density polyethylene (HDPE) (**Table 3.3**).

Table 3.3 Parameters for the BHE from Scenario 1.

Shape	**Single U-shape**	
Inlet Temperature Injection	45	°C
Inlet Temperature Extraction	-5	°C
Flow Rate	11.2	US gpm
Borehole Diameter	0.0754	m
Pipe Distance	0.038	m
Pipe	**HDPE**	
Inlet Pipe Diameter	0.032	m
Inlet Pipe Wall Thickness	0.003	m
Outlet Pipe Diameter	0.032	m
Outlet Pipe Wall Thickness	0.003	m
Inlet Pipe Thermal Conductivity	0.42	W m^{-1} K^{-1}
Outlet Pipe Thermal Conductivity	0.42	W m^{-1} K^{-1}
Grout	**Bentonite 10%, in water**	
Grout Thermal Conductivity	0.7	W m^{-1} K^{-1}
Refrigerant	**20% Ethyl Alcohol solution**	
Freezing Point	-10.92	°C
Saturation Properties Temperature	-5	°C
Refrigerant Volumetric Heat Capacity	4.373	MJ m^{-3} K^{-1}
Refrigerant Thermal Conductivity	0.4435	W m^{-1} K^{-1}
Refrigerant Dynamic Viscosity	0.007425	10^{-3} kg m^{-1} s^{-1}
Refrigerant Density	976.75	10^3 kg^{-1} m^{-3}
Reynold's Number	4081.1	-

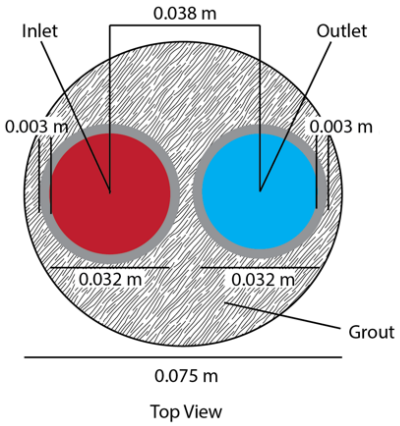

Figure 3.7 Dimensions of the BHE implemented in the single borehole model in FEFLOW (sketch showing summer injection season).

U-tube BHEs are also selected for the BTES simulation, but the borehole properties are simplified to decrease computation time and the borehole size is increased (**Figure 3.8**). For the base model, the grout is made of 10% bentonite in water and the pipes are the FEFLOW default settings for high-density polyethylene (HDPE) (**Table 3.4**). The working fluid is 20% ethanol.

Table 3.4 Parameters for the BHEs from the BTES field.

Shape	**Single U-shape**	
Inlet Temperature Injection	45	°C
Inlet Temperature Extraction	-5	°C
Flow Rate	11.2	US gpm
Borehole Diameter	0.15	m
Pipe Distance	0.04	m
Pipe	**HDPE**	
Inlet Pipe Diameter	0.032	m
Inlet Pipe Wall Thickness	0.003	m
Outlet Pipe Diameter	0.032	m
Outlet Pipe Wall Thickness	0.003	m
Inlet Pipe Thermal Conductivity	0.42	$W\ m^{-1}\ K^{-1}$
Outlet Pipe Thermal Conductivity	0.42	$W\ m^{-1}\ K^{-1}$
Grout	**Bentonite 10%, in water**	
Grout Thermal Conductivity	0.7	$W\ m^{-1}\ K^{-1}$
Refrigerant	**20% Ethyl Alcohol solution**	
Freezing Point	-10.92	°C
Saturation Properties Temperature	-5	°C
Refrigerant Volumetric Heat Capacity	4.373	$MJ\ m^{-3}\ K^{-1}$
Refrigerant Thermal Conductivity	0.4435	$W\ m^{-1}\ K^{-1}$
Refrigerant Dynamic Viscosity	0.007425	$10^{-3}\ kg\ m^{-1}\ s^{-1}$
Refrigerant Density	976.75	$10^{3}\ kg^{-1}\ m^{-3}$
Reynold's Number	4081.1	-

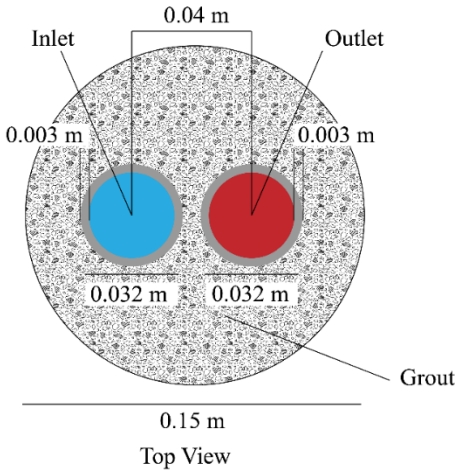

Figure 3.8 Dimensions of the BHE implemented in the BTES field in FEFLOW (sketch showing winter extraction season).

For modelling the operation of the BHE and BTES field, two periods are simulated that span six months each. The charge period is during which heat is injected in the ground. The discharge period is the period during which heat is extracted from the ground. Charge and discharge periods are imposed according to seasons. 'Summer' is the charge period and 'winter' is the discharge period. The 'summer' season starts at the beginning of the first day in May and ends at the end of the last day in October. Conversely the 'winter' season begins at the start of the first day of November and ends on the end of the last day in April (**Table 3.5**).

Table 3.5 Heat injection and Extraction periods over 3 years.

Years		Season	Day	Period	1st day of mo.
	2024	summer	0	Inject	May
	2024	winter	184	Extract	Nov.
1	2026	summer	365	Inject	May
	2026	winter	549	Extract	Nov.
2	2027	summer	730	Inject	May
	2027	winter	914	Extract	Nov.
3	2027	summer	1095	Inject	May

3.5.1 Boundary and Initial Conditions

3.5.1.1 Single BHE

A surface zero fluid flux is imposed to the top of the model to avoid water infiltration. Lateral boundaries are zero fluid flux boundaries to eliminate lateral groundwater flow and simulate a similar effect of equal head boundaries. By applying this condition laterally, FEFLOW automatically assumes 0 fluid flux along the vertical sides of the model, eliminating fluid flow. A constant heat flow value of 45 mW m^{-2} (Minnick et al. 2018) is imposed as a lower boundary condition and a constant surface temperature (-7 °C), based on the most recent measurement from

TetraTech, is imposed as upper boundary condition to obtain the initial conditions for steady state simulation (Canadrill Limited Geotechnical Division 2019). The initial condition (i.e., the geothermal gradient) used for subsequent transient simulations of ground surface temperature changes is obtained by doing a steady state simulation. Afterwards, a time-dependent surface temperature is imposed as upper boundary condition to simulate the seasonal surface temperature variations (**Figure 3.9**). These seasonal variations can have an impact on the BTES and therefore must be considered. The transient heat conduction model is then run for 1 year and the results obtained at the end becomes the initial condition for transient BHE simulations. The seasonal ground temperatures based on average monthly air temperatures are used to create the time series for the time-dependent surface temperature. These temperatures are recorded by the Baker Lake A station, spanning a period of 29 years from 1981 to 2010, and can be found in the directory of Canadian Climate Normals (Government of Canada 2022). The average monthly ground temperatures are calculated with Equation 12:

$$T_{\mathrm{g}} = 17.898 + 0.951 T_{\mathrm{amb}} \tag{13}$$

where Tg is the ground temperature (K) and T_{amb} is the ambient temperature (K; Miranda et al. 2021, Ouzzane et al. 2015).

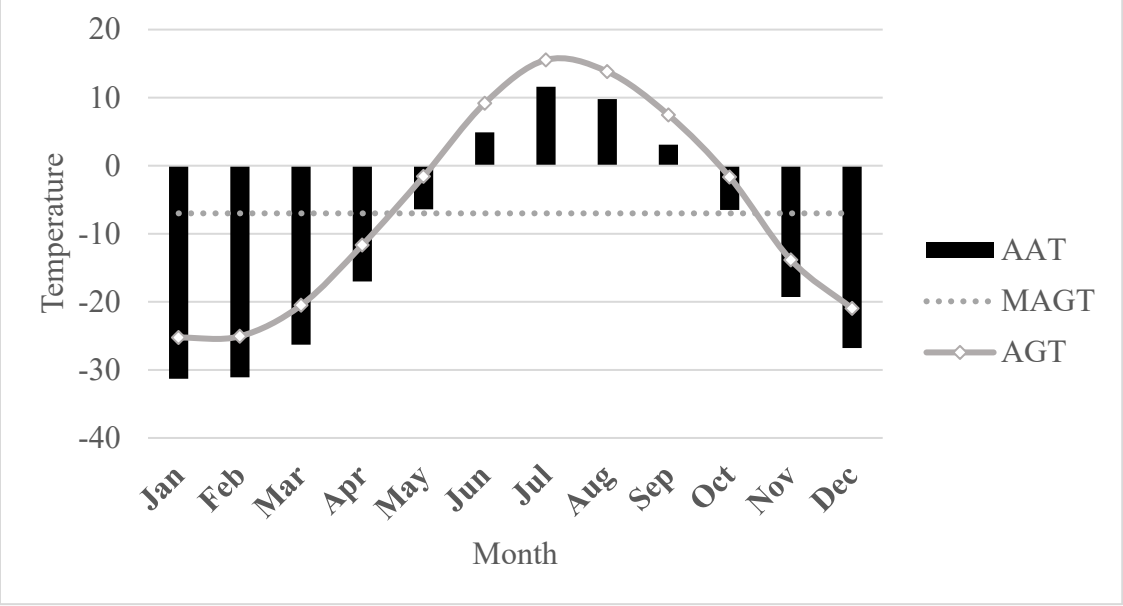

Figure 3.9 MAGT (mean annual ground temperature), AAT (ambient annual temperature) and AGT (average ground temperature) in Baker Lake.

3.5.1.2 BTES Field

The same heat flux and temperature initial and boundary conditions are applied in the same way to the entire BTES field. The only difference between the BTES field and single BHE model boundary conditions is that a hydraulic head is applied instead of a fluid flux boundary condition to both the steady state and transient simulations. The hydraulic head boundary condition on the left side of the model is 50.1 m, while on the right side of the model it is 50 m. Simulating non-equal head boundaries creates a small amount of fluid flow that may be typical of natural ground. Applying the condition in this way creates negligible fluid flow in the model throughout the

simulation, as the Darcy Flux is restricted to a maximum order of $1 \cdot 10^{-6}$ md^{-1}. For the system to remain conduction-ruled, $q < 8.7 \cdot 10^{-8}$ m/s (Ferguson 2015).

3.6 Mitigation solutions

3.6.1 Grout and pipes

The grout and pipes properties are specified in FEFLOW's BHE dataset editor. The diameter, thickness, and thermal conductivity of the pipes is varied with the BHE editor. The thermal conductivity of the grout is also varied. The volume of grout added as insulation is equivalent to the volume and depth of the borehole specified in the BHE dataset editor (**Table 3.5**). The thermal conductivities of grout and pipes of given materials are taken from the Earth Energy Designer database (Sanner & Hellstroem 1997).

Table 3.6 Scenarios defined by combinations of mitigation solutions.

Scenario #	Grout	Pipe	Grout λ W m^{-1} K^{-1}	Pipe λ W m^{-1} K^{-1}
1	Bentonite 10%, in Water	HDPE	0.7	0.42
2	Bentonite 10%, in Water	PVC	0.7	0.23
4	Bentonite 20%, in Water	HDPE	0.6	0.42
5	Bentonite 20%, in Water	PVC	0.6	0.23
7	Bentonite/Sand	HDPE	1.5	0.42
8	Bentonite/Sand	PVC	1.5	0.23
10	Thermal Grout	HDPE	1.47	0.42
11	Thermal Grout	PVC	1.47	0.23
13	Till	HDPE	2	0.42
14	Till	PVC	2	0.23

3.6.2 VIT Casing & Air Insulation

VIT is assumed as a casing of the BHE for a mitigation solution of the following scenarios because of its very low thermal conductivity. The casing is simulated by assigning VIT thermal conductivity (**Table 3.6**) around the borehole (**Figure 3.10**). The size of the central hexagon where the VIT thermal conductivity is assigned is a hexagon with endpoints that are 0.23 m from the BHE node to each outer node. The depth to which the VIT thermal conductivity is assigned is 4 m, which corresponds to the depth of the overburden.

Table 3.7 Thermal conductivity of VIT casing and grout in VIT casing scenarios.

Scenario #	Grout	Pipe	Casing	Grout λ W m^{-1} K^{-1}	Casing λ W m^{-1} K^{-1}
3	Bentonite 10%, in Water	HDPE	VIT	0.7	0.037
6	Bentonite 20%, In Water	HDPE	VIT	0.6	0.037
9	Bentonite/Sand	HDPE	VIT	1.5	0.037
12	Thermal Grout	HDPE	VIT	1.47	0.037
15	Till	HDPE	VIT	2	0.037

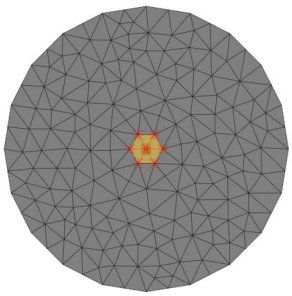

Figure 3.10 Area in the model where the VIT casing is assigned (yellow shading). The red asterisks are the BHE discretized nodes.

To create a model that simulates air between the grout and sediment contact, model properties for air are assigned to the elements spanning a radial distance of 0.23 m in approximate length from the BHE central node (**Table 3.8**). This strategy is also used to assign VIT properties to the BHE as described previously. A second scenario is run to determine the effect of air insulation that extends to a greater depth; instead of 4 m of vertical air insulation, 16 m of vertical air insulation is assigned to the single BHE model in scenario 17.

Table 3.8 Thermal conductivity of air insulation and grout in the air scenario for the single BHE model.

Scenario #	Grout	Pipe	Insulation	Grout λ W m^{-1} K^{-1}	Insulation λ W m^{-1} K^{-1}
16	Bentonite 10%	HDPE	Air (4 m)	0.7	0.0235
17	Bentonite 10%	HDPE	Air (16 m)	0.7	0.0235

Air insulation is also assigned to the first 4 m of the BHEs in the BTES field to test the effectiveness of using the solution on the outer edge of the borefield versus the center of the field (**Table 3.9**).

Table 3.9 Thermal conductivity of air insulation and grout in the air scenario.

Scenario #	Grout	Pipe	Insulation	BHEs #	Grout λ W m^{-1} K^{-1}	Insulation λ W m^{-1} K^{-1}
21	Bentonite 10%	HDPE	Air	20/100	0.07	0.0235
22	Bentonite 10%	HDPE	Air	100/100	0.07	0.0235

3.6.3 Thermosyphons

Thermosyphons surrounding the BHE are considered as a mitigation solution in the next simulation scenarios. The full physical phenomenon involved with a thermosyphon are not simulated in FEFLOW. Instead, a representation of the thermosyphon is simulated by nodal heat drains. Six nodes in the model are selected and an internal heat drain condition is applied (**Figure 3.11**). The nodes are horizontally spaced within the appropriate less than 2.5 m working distance of a thermosyphon (Mu et al. 2015). Four heat drains are emplaced at slice 2, slice 7, slice 10, and

slice 14. Spacing the thermosyphons in this manner prevents the area of heat extraction from overlapping. The heat drain assignments extend to 5.2 m depth in the model. This length represents a thermosyphon which is anchored in bedrock.

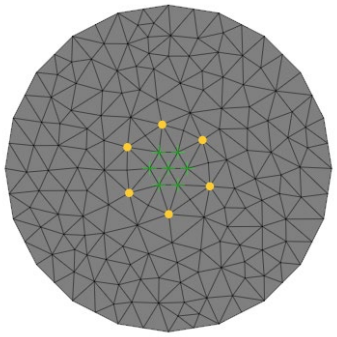

Figure 3.11 Area in the model where the thermosyphon-representative nodal heat sink is applied. The thermosyphon nodes are represented by yellow circles. The green crosses are the BHE discretized nodes.

The calculated heat extraction rates from the following rate equation are applied as the nodal heat sink extraction rate (W) in FEFLOW. The monthly ground temperature and air temperature of the environment are utilized to calculate the heat extraction rate, along with the performance coefficient.

$$Q = P(T_g - T_a) \tag{13}$$

where Q is the heat extraction rate (W) and P is the performance coefficient of a thermosyphon (Aftret & Daleng 2022; Geo Slope 2014). During the summer months when $0 \leq T_g$, an extraction rate of 0 W is assumed, representing a perfect closed thermosyphon. The performance coefficient of a thermosyphon is calculated according to the average wind speeds in Baker Lake and the surface area of a thermosyphon with a 7 m evaporator section and a condenser section that is less than 6 m, which is 1.67 m (Baker Lake, Canada—Climate & Monthly weather forecast; Mu et al. 2015).

$$P = (2.54 + 4w^{0.62})A \tag{14}$$

where w is the wind speed (m s^{-1}) and A is the area of the evaporator section of the thermosyphon (m^2; Geo Slope 2014).

The equation for the heat extraction of a thermosyphon is only valid for thermosyphons that are inclined greater than 5 degrees (Geo Slope 2014). Additionally, the rate equation gives the maximum heat extraction capability of the thermosyphon over its entire length and states that this value must be divided by the actual constructed length of pipe in the field (Geo Slope 2014). Heat extraction rates for the quasi-thermosyphon are presented in **Table 3.10** with a time series of the thermosyphon. The extraction rate was not divided by the actual constructed length of pipe in the field before being assigned to sink nodes. The thermosyphon scenarios are listed in **Table 3.11**.

Table 3.10 Wind speed, ground temperature, air temperature, performance coefficient and extraction rates of the modelled representation of a thermosyphon.

Month	**Wind Speed**	T_g	T_a	P	Q
	km/h	°C	°C		W
Jan	17.3	-25.3	-31.3	4.249	25.7
Feb	16.6	-25.1	-31.1	4.248	25.7
Mar	16.4	-20.5	-26.3	4.248	24.7
Apr	17.4	-11.7	-17	4.249	22.7
May	16.1	-1.6	-6.4	4.248	20.5
Jun	16.4	9.8	4.9	4.248	0.0
Jul	16.7	15.5	11.6	4.248	0.0
Aug	17.7	13.8	9.8	4.249	0.0
Sep	19.5	7.5	3.1	4.249	0.0
Oct	19.1	-1.7	-6.5	4.249	20.5
Nov	17.8	-13.8	-19.3	4.249	23.2
Dec	17.3	-21.0	-26.8	4.249	24.8

Table 3.11 Properties of material for thermosyphon scenarios.

Scenario #	**Grout**	**Casing/Pipe**	**Thermosyphons** #	**Grout λ** W m^{-1} K^{-1}	**Casing λ** W m^{-1} K^{-1}
17	Bentonite 10%	HDPE	6	0.7	-
18	Bentonite 10%	HDPE+VIT	6	0.7	0.037

3.7 Scenarios

The permafrost thaw mitigations strategies are specified in **Table 3.12**, which houses a comprehensive list of scenario names and their corresponding combination of mitigation solutions. Working fluid and flow rates are also specified. “S” stands for scenario in these cases, where 1, 2…, n stands for the nth scenario number. The BTES scenarios are specified in **Table 3.13**.

Table 3.12 Scenarios defined by combinations of mitigation solutions. EA represents Ethyl Alcohol; PG stands for Propylene Glycol.

Scenario #	Grout	Pipe	Flow US gpm	Applications	Fluid
Base	Generic (λ = 1)	HDPE	6.2	-	20% PG
1	Bentonite 10%, in Water	HDPE	11.2	-	20% EA
2	Bentonite 10%, in Water	PVC	11.3	-	20% EA
3	Bentonite 10%, in Water	VIT	11.2	Casing	20% EA
4	Bentonite 20%, in Water	HDPE	11.2	-	20% EA
5	Bentonite 20%, in Water	PVC	11.3	-	20% EA
6	Bentonite 20%, in Water	VIT	11.2	Casing	20% EA
7	Bentonite/Sand	HDPE	11.2	-	20% EA
8	Bentonite/Sand	PVC	11.3	-	20% EA
9	Bentonite/Sand	VIT	11.2	Casing	20% EA
10	Thermal Grout	HDPE	11.2	-	20% EA
11	Thermal Grout	PVC	11.3	-	20% EA
12	Thermal Grout	VIT	11.2	Casing	20% EA
13	Till	HDPE	11.2	-	20% EA
14	Till	PVC	11.3	-	20% EA
15	Till	VIT	11.2	Casing	20% EA
16	Bentonite 10%, in Water	HDPE	11.2	Air (4m)	20% EA
17	Bentonite 10%, in Water	HDPE	11.2	Air (16m)	20% EA
18	Bentonite 10%, in Water	HDPE	11.2	Thermosyphon	20% EA
19	Bentonite 10%, in Water	VIT	11.2	Thermosyphon	20% EA
20	Bentonite 10%, in Water	HDPE	11.2	Air (20m) + 20 m Sediment	20% EA

Table 3.13 Scenarios defined by combinations of mitigation solutions. EA represents Ethyl Alcohol.

Scenario #	Grout	Pipe	Flow US gpm	Applications	BHEs #	Fluid
21	Bentonite 10%, in Water	HDPE	11.2	Air (4m)	20/100	20% EA
22	Bentonite 10%, in Water	HDPE	11.2	Air (4m)	100/100	20% EA
23	Bentonite 10%, in Water	HDPE	11.3	NONE	100/100	20% EA

Inlet temperatures are tested to determine the most efficient, most productive scenario for storing heat in the subsurface and are held constant throughout trials of mitigation solutions. It is important to choose an inlet temperature that allows the BHEs to operate properly. The system's functionality is dependent on the minimum operating temperature of the working fluid (Wang 2014). The flow rates are fixed. The Reynold's number for HDPE pipe and a flow rate of 11.2 US gpm is 4081.1, and for PVC pipe with a flow rate of 11.3 US gpm it is 4034.08. Properties for water are derived from Earth Energy Design recommendations (Sanner & Hellstroem 1997). Propylene Glycol

values are from MOKON (2022), and the Reynold's number for the base case scenario is 4629. Ethyl Alcohol is represented by properties from a study of thermophysical properties of working fluids (Melinder 2007). The base model is run with 20% propylene glycol, but because the freezing point of the model is -7 °C, propylene glycol does not provide a large enough buffer to safely use it in this system. Ethyl alcohol (20%) is the final fluid that is used with the scenarios because it provides a buffer of freezing of approximately -5 °C. The volumetric heat capacity of the fluids are hand-calculated with 0.001 kg substance. Based on operating parameters, a fixed inlet temperature of 45 °C in the summer and -5 °C in the winter has been determined for the model based on the fluid operation parameters and efficiency of energy storage.

3.7.1 Analysis of Results

To analyze the effect of the mitigation solutions on the ground temperature in the single BHE model, five points extending radially away from the borehole are analyzed. The points are assigned throughout vertical layer slices in the following configuration as observation points (**Figure 3.12**). The radial points extend to 6 m depth in the model and are emplaced every 0.4 m, creating 450 observation points total. The depth and temperature data are compiled via python at the end of every injection and extraction season simulated.

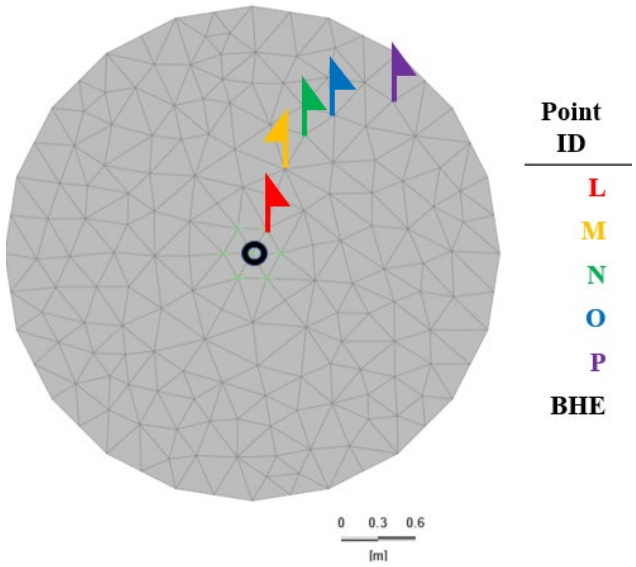

Figure 3.12 Assignment of radial observation points in the model to evaluate the ground temperature.

To analyze the BTES system, a similar array of points is assigned in the model (as points L through P), and the focus is on the points that are in the center of the BTES field, 0 m from the edge of the BTES system, 4.3 m from the edge of the system, and 8.7 m from the edge of the system.

To calculate the energy stored, the following temperature differential is considered from the model's resultant inlet and outlet temperatures:

$$\Delta T = T_{\text{Out}} - T_{\text{In}} \tag{15}$$

where ΔT is the temperature difference, T_{Out} is the BHE outlet temperature (°C or K), and T_{In} is the BHE inlet temperature (°C or K).

The thermal power injected or extracted is then considered by:

$$E_{\mathrm{S}} = C_{\mathrm{p}} \cdot q_{\mathrm{BHE}} \cdot \Delta T \tag{16}$$

where E_{S} is the power injected or extracted (W), C_{p} is the heat capacity of the water-antifreeze mixture (J m^{-3} K), and q_{BHE} is the flow rate of fluid in the BHE (m^3 s^{-1}). For the purposes of this study, energy storage is provided in terms of instantaneous power (kW) illustrated over the charge or discharge season time (days).

4. RESULTS

4.1 Mesh and Time-Step Independence

4.1.1 Single BHE model

The resultant Delaunay Triangular mesh independence of the single BHE model is recorded below. All models are adjusted for Delaunay and Aspect Ratio errors before completing each test. The transient state simulation runs from time 0.001 through 200 days to encapsulate 1 period of heat injection at 45 °C for each mesh test (horizontal, vertical, and time-step). The outlet temperatures at the end of 200 days are the point of comparison for each model. The tests produce outlets on day 200 that do not vary by more than 1 °C. The flow rate varies between mitigation scenario tests and the base model. Variation of the flow is caused by differences in pipe inlet and outlet tube sizes between the HDPE and PVC pipes. The results of the horizontal, vertical, and time-step mesh independence are shown in **Figure 4.1**.

The following 2-D meshes are used to test the mesh with an arbitrary growth factor between time steps of 2, and the 2-D element count provided:

- Mesh 1: 188 elements
- Mesh 2: 312 elements
- Mesh 3: 470 elements

Mesh 2 is chosen as the appropriate mesh to run the simulations. After the horizontal meshes are tested, different models of mean slice widths are built and tested with an arbitrary growth factor between time steps of 2. The results are compared to select a model that is independent of the vertical 3-D mesh configuration with the lowest computation time:

- Mesh A: 0.45 m
- Mesh B: 0.4 m
- Mesh C: 0.25 m
- Mesh D: 0.2 m

A slice width of 0.4 m is chosen as the vertical layer width for the model (Mesh B) because this slice width requires the smallest computation time for the model out of the 4 meshes. After the 0.4 m slice 3-D model is developed, an arbitrary BHE is simulated with constant properties. The only variation in the model are the automatic timestep control settings, where the growth factor (TS) between subsequent timesteps is adjusted:

- TS1: 4
- TS2: 2
- TS3: 1.5

The growth factor of 2 between any 2 timesteps is chosen as the appropriate factor to keep computation time reasonable while the results are unaffected. An unrestricted minimum timestep and maximum timestep of 10 days is also employed.

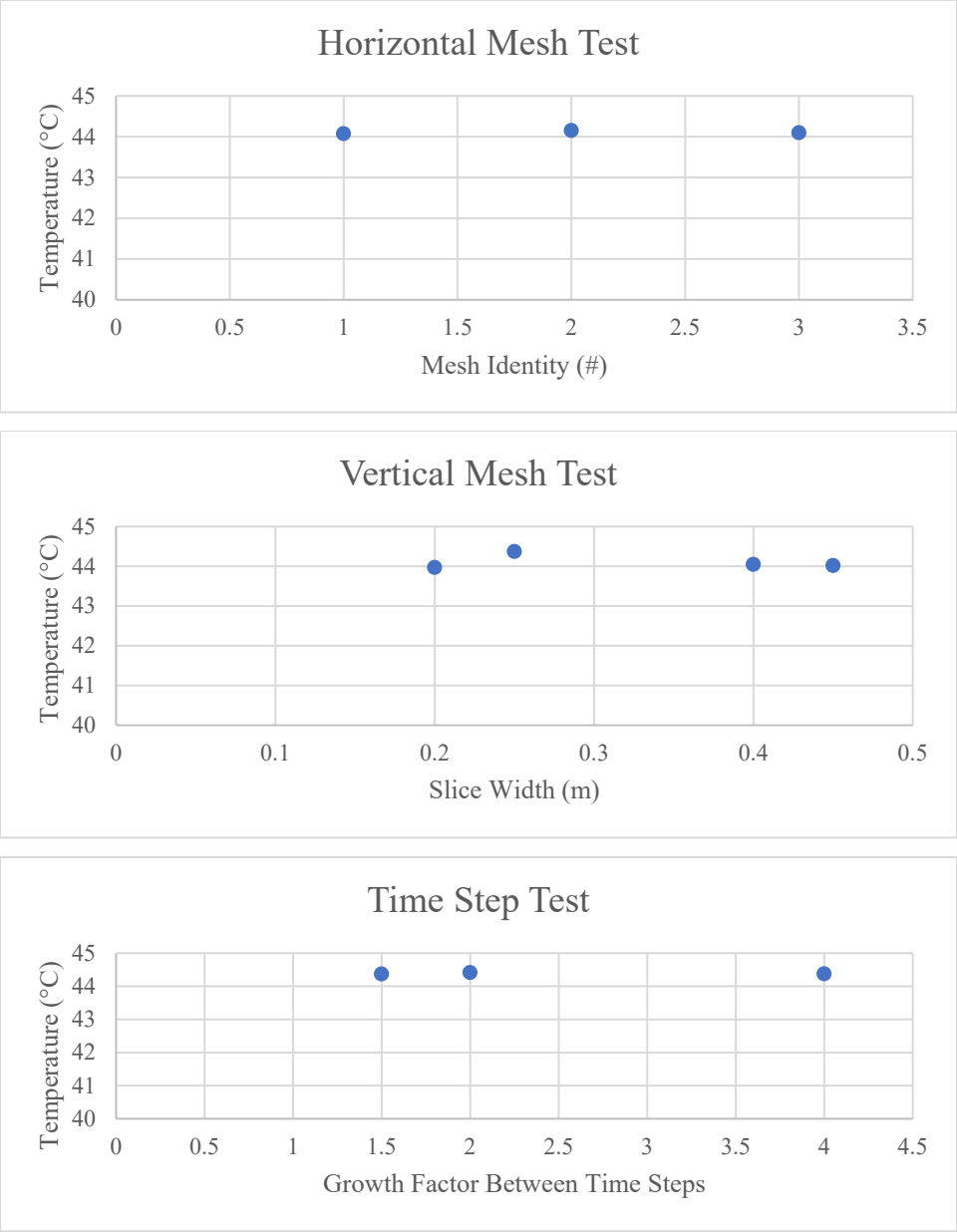

Figure 4.1 Visual results of the mesh tests after 200 d injection period compared at the outlet of the BHE.

4.1.2 BTES Field model

The resultant Delaunay Triangular mesh independence of the BTES is recorded below. All models are adjusted for Delaunay and Aspect Ratio errors before completing each test. The transient state simulation runs from time 0.001 through 200 days to encapsulate 1 period of heat injection at 45 °C for each mesh test (horizontal, vertical, and time-step). The outlet temperatures at the end of 200 days are the point of comparison for each model. The tests produce outlets on day 200 that do not vary by more than 1 °C. Results for these tests are shown in **Table 4.1**.

The following 2-D meshes are used to test the mesh with an arbitrary growth factor between time steps of 2, and the 2-D element count provided:

- Mesh 1: 12653
- Mesh 2: 10516
- Mesh 3: 5340

Mesh 2 is chosen as the appropriate mesh to run the simulations. After the horizontal meshes are tested, different models of mean slice widths are built and tested with an arbitrary growth factor between time steps that is unrestricted. The results are compared to select a model that is independent of the vertical 3-D mesh configuration with the lowest computation time:

- Mesh A: Slice 50 to 32, 1 m; slice 31 to 0, 5 m
- Mesh B: Slice 50 to 32, 0.5 m; slice 31 to 0, 5 m
- Mesh C: Slice 50 to 32, 1.5 m; slice 31 to 0, 5 m

A slice width of 1 m is chosen as the vertical layer width for the portion of the model with the BTES system (Mesh A) because this slice width requires the smallest computation time for the model out of the 4 meshes and is fine enough to produce reasonable results. At slice 32, the distance between slices is increased to 5 m to decrease computation time. This extension does not affect the results of the simulation. After the vertical 3-D model is developed, an arbitrary array of 5 BHEs is simulated with constant properties. The only variation in the model are the automatic time step control settings, where the growth factor (TS) between subsequent time steps is adjusted:

- TS1: Unrestricted
- TS2: 2
- TS3 : 4

The unrestricted growth factor between any 2 time steps is chosen as the appropriate factor to keep computation time minimized while the results are unaffected. An unrestricted minimum time step and unrestricted maximum time step is also employed.

Table 4.1 Scenarios defined by combinations of mitigation solutions. EA represents Ethyl Alcohol; PG stands for Propylene Glycol.

Mesh Tested	Outlet Temperature
1	41.97265
2	41.88842
3	41.95948
A	41.98317
B	41.97865
C	41.97265
TS1	41.97528
TS2	42.00752
TS3	41.98317

4.2 Permafrost Active Layer

The active layer above the permafrost in the single BHE model is determined from the seasonal ground temperature variations modelled in FEFLOW and is represented in **Figure 4.2** The gradient is shown by temperature slices pulled directly from the FEFLOW modelling software. According to the numerical data, the active layer is 3.2 m depth, which is comparable to the active layer for the Baker Lake area (0.15 m to 6 m active freeze-thaw zone; Smith & Burgess 2002). When the BHE is added, the active layer is no longer present in the model and the temperature is always above 0 °C over the entire BHE depth.

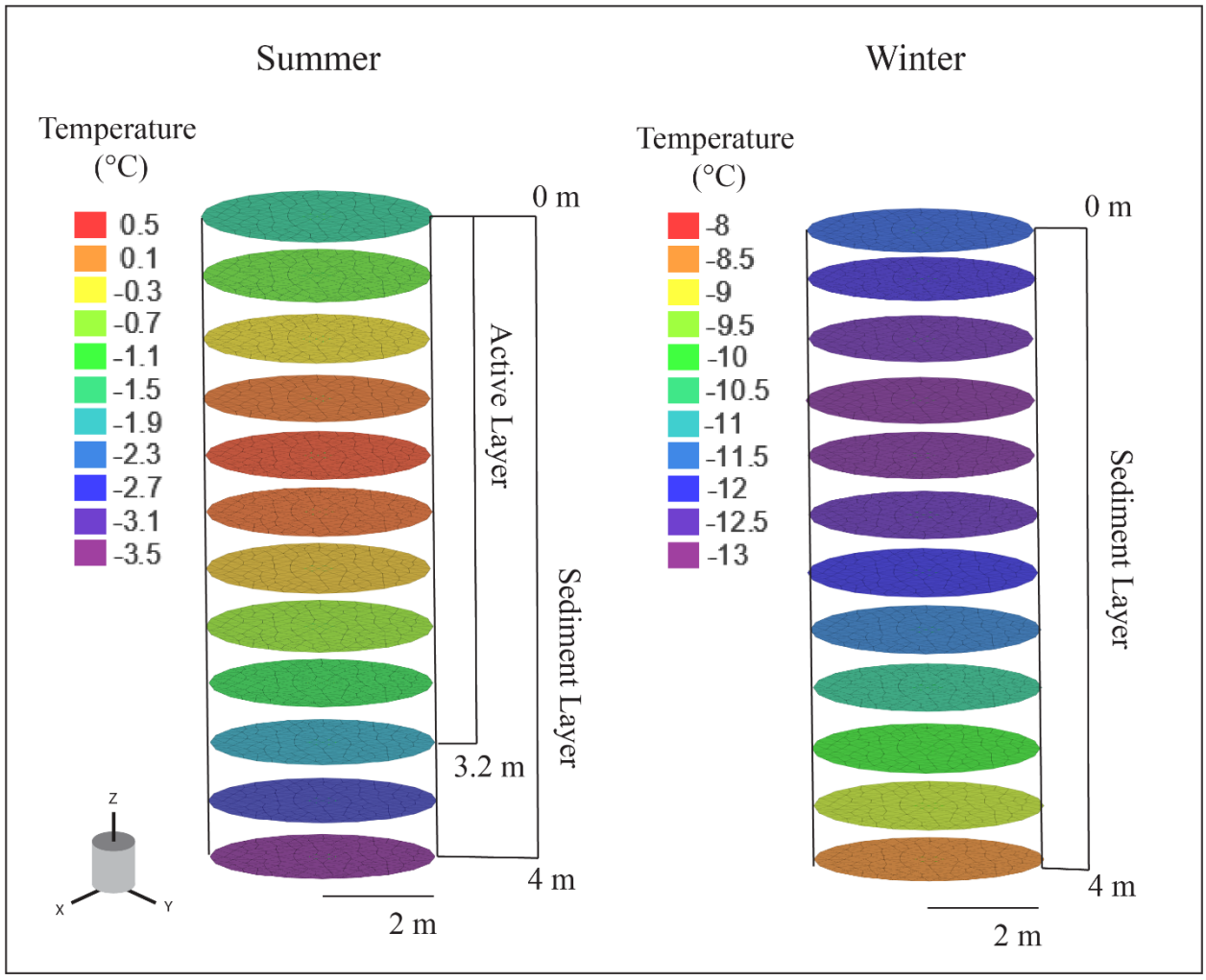

Figure 4.2 Right) Last day of injection period from year 3 simulation with no BHE added to the model. Left) Last day of extraction period from year 3 simulation. The summer simulation shows the greatest depth in the active layer of permafrost in the FEFLOW model (3.2 m).

4.3 Single BHE Permafrost Mitigation Results

4.3.1 Grouts & Pipes

The scenario that keeps the overburden coldest is S5, which has the lowest thermal conductivity grout and pipe material (Bentonite 20%, in water & PVC pipe). The scenario that keeps the overburden cool while maximizing borehole energy storage is S1, with 10% bentonite grout, in

water and HDPE pipe. The scenario that keeps the overburden warmest is S13, which contains materials with the highest thermal conductivity grout and pipe (Till & HDPE). No solutions succeed in keeping the permafrost in the overburden from thawing (**Figure 4.3**).

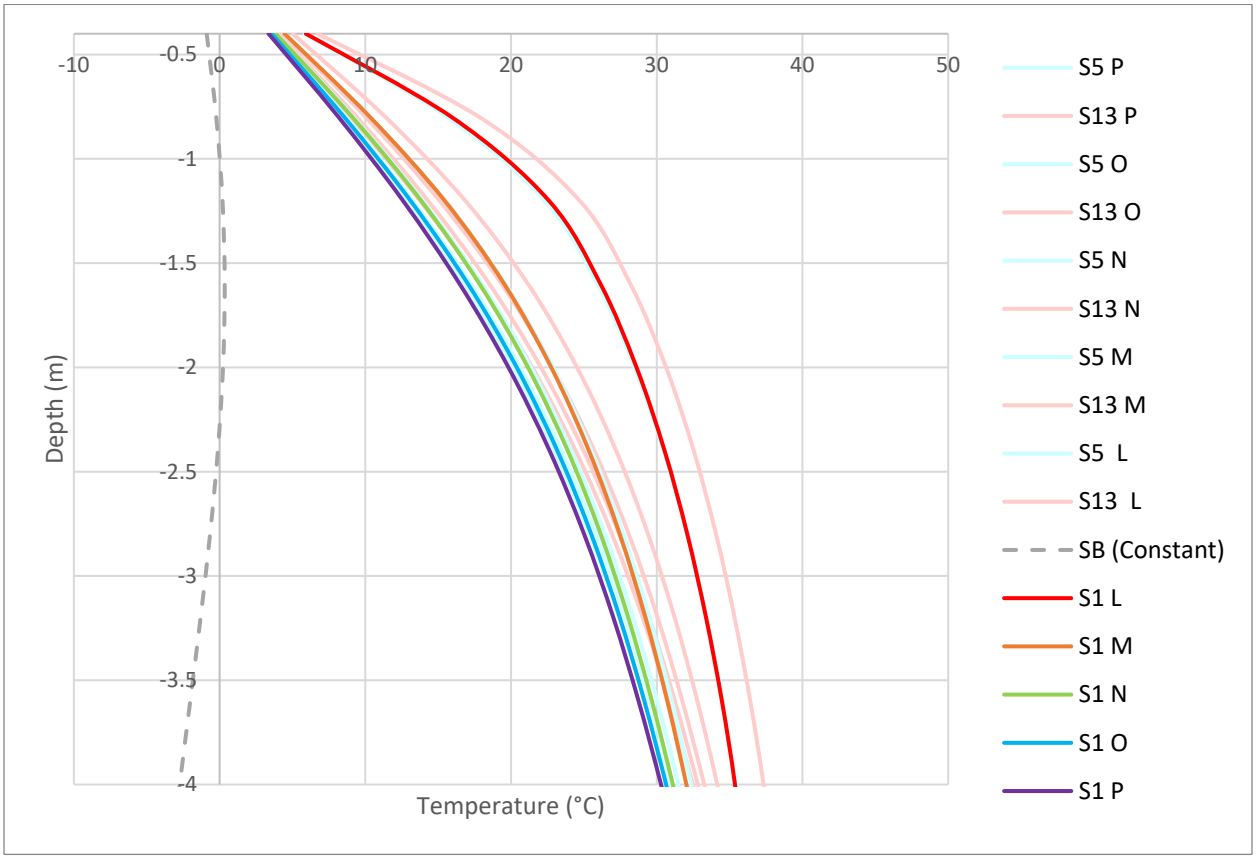

Figure 4.3 Temperature for Grout & Pipe mitigation solutions S1, S5, and S13 with regular seasonal thermal gradient on the last day of October (SB) at the end of the injection season in the third year (summer).

4.3.2 Vacuum Insulated Tube (VIT) Casing & Air Insulation

Previous pipe and grout data comparisons determine that 10% bentonite grout, in water and HDPE pipe (S1) maximizes energy storage while keeping the overburden cool. Therefore, the focus test of VIT Casings is S1 encased in VIT (S3). The permafrost temperature data at the end of the third year's summer (last day in October) is compared graphically (**Figure 4.4**). Largest percent differences between S1 and S3 are at point L at 0.8 m depth (near the surface of the model). Smallest percent differences between the same scenarios are at point P at 4 m depth. Point L having the greatest difference and P having the smallest difference is a consistent trend at every depth (0.8, 2 and 4 m). Ground temperature for the air-insulated scenario is simulated for the last day of the injection season and compared to the VIT scenario (**Figure 4.5**). These results differ only slightly from VIT results.

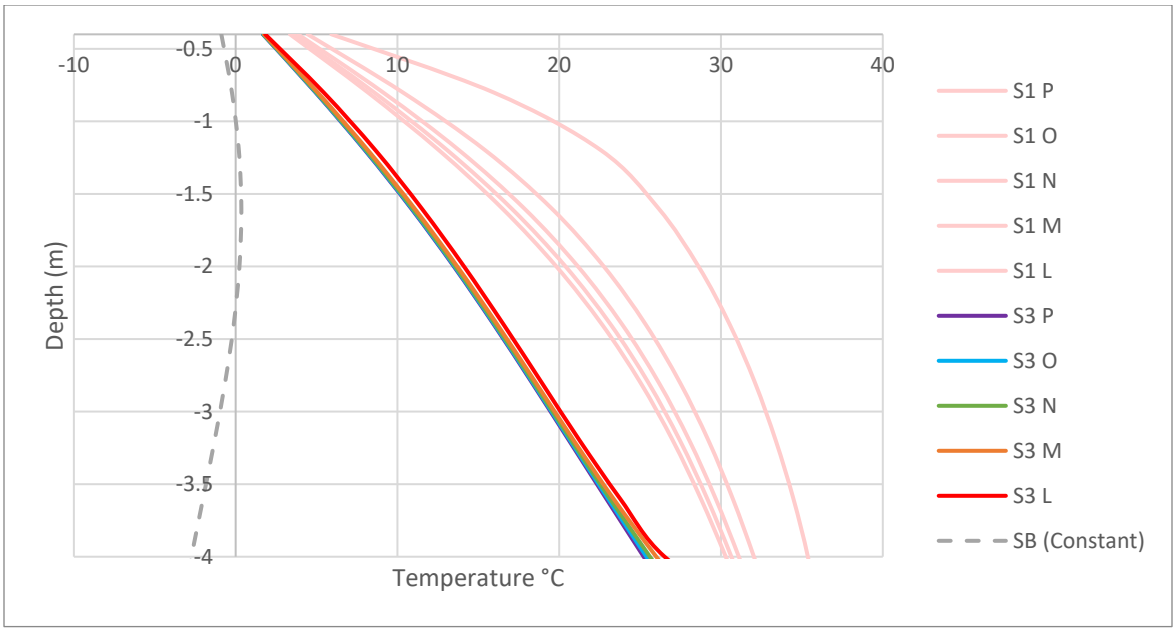

Figure 4.4 Temperature for VIT scenario 3 with S1 Pipe & Grout scenario and the regular seasonal thermal gradient on the last day of October (SB) pictured for comparison. The data refers to the final day at the end of the injection season in the third year (summer).

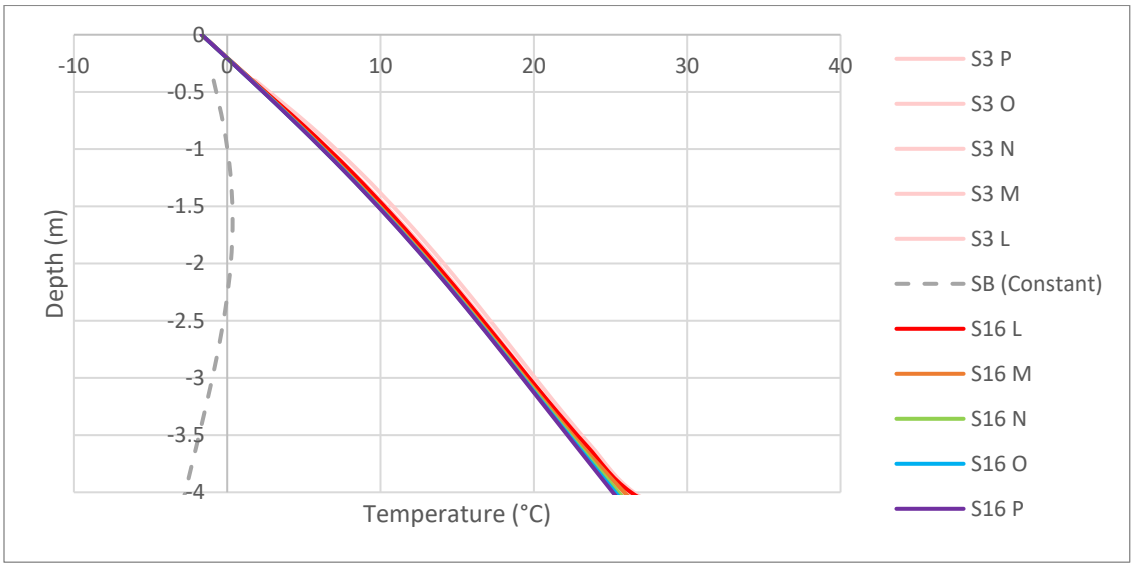

Figure 4.5 Temperature for the air insulated scenario 16 (S16) with VIT scenario 3 (S3) and the regular seasonal thermal gradient on the last day of October (SB) pictured for comparison. The data refers to the final day at the end of the injection season in the third year (summer).

4.3.3 Thermosyphon

Ground temperature simulated for the last day of the injection season is compared for two thermosyphon scenarios: a thermosyphon scenario with no VIT (S18) and a scenario with VIT (S19; **Figure 4.6**).

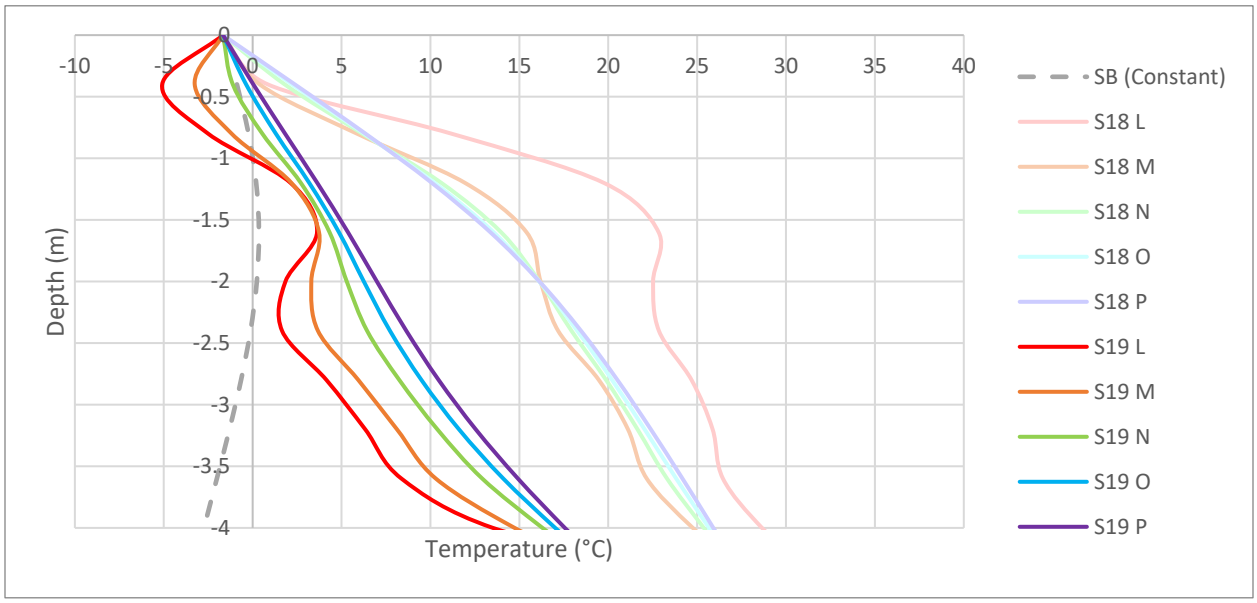

Figure 4.6 Temperature for thermosyphon + VIT scenario 17 (S19) with thermosyphon scenario 16 (S18) and the regular seasonal thermal gradient on the last day of October (SB) pictured for comparison. The data refers to the final day at the end of the injection season in the third year (summer).

4.3.4 Temperature Profiles

The mitigation solutions are compared against each other, and the following ground temperature at 0.8, 2 and 4 m depth in the model at 0.23 m from the central BHE is analysed from May 2024 to May 2027 (**Figure 4.7**). The key scenarios from the simulations are as follows, all of which include 10% bentonite grout, in water, around the HDPE U-Tube BHE:

- S1: No added solutions
- S3: VIT casing around grouted BHE
- S16: Air insulation around the grouted BHE
- S18: 6 Thermosyphons surrounding BHE
- S19: 6 Thermosyphons surrounding a VIT-cased grouted BHE

VIT and air insulation trends exhibit an elevated consolidation from thermosyphons and appear to reflect the natural thermal gradient more closely. At a distance of 1.67 m from the central BHE, the trends become most consolidated and exhibit no difference in the order of effectiveness in which the scenarios better keeps the ground cold (**Figure 4.8**). The trends for VIT, air insulation, and thermosyphons also become closer in relative effectiveness from the 0.23 m distance. Additionally, the VIT and air insulation scenario exhibit similar resulting trends. A comparison of the air insulation scenarios with insulation to 4 m depth (S16) and 16 m depth (S17) is also provided in **Figure 4.9**. A comparison of air insulation in 4 m sediments versus 20 m sediments is offered in **Figure 4.10**.

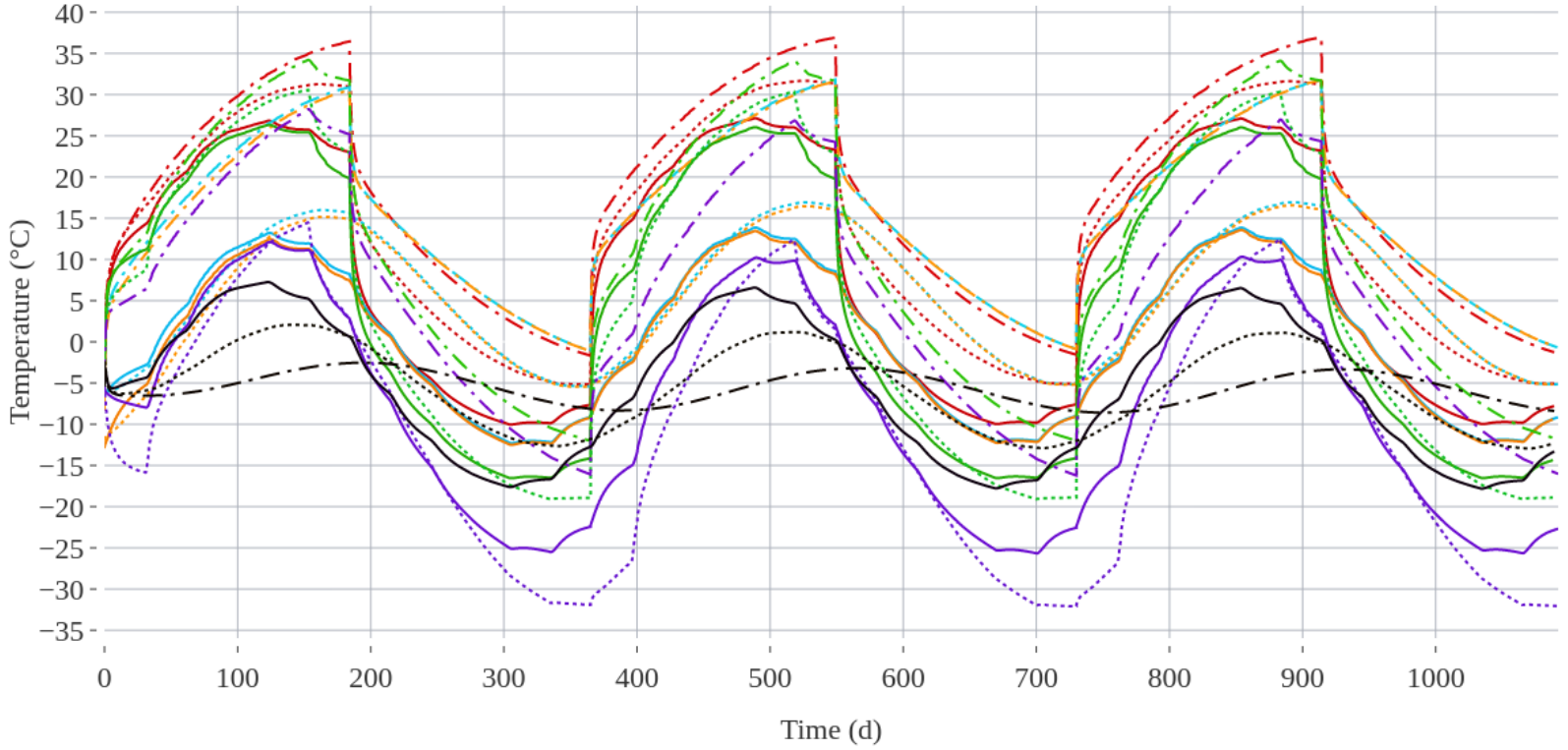

Scenario						Depth	
S1	Bentonite 10%, HDPE		S18	Bentonite 10%, HDPE, Thermosyphon		0.8 m
S3	Bentonite 10%, HDPE, VIT Casing		S19	Bentonite 10%, HDPE, Thermosyphon & VIT Casing		2 m
S16	Bentonite 10%, HDPE, Air Insulation		Natural Ground Temperature Without BHE			4 m

Figure 4.7 Ground temperature for key scenarios 0.23 m away from the central BHE (10% bentonite grout & HDPE (S1), VIT casing around S1 (S3), air-insulation around S1 (S16), 6 thermosyphons around S1 (S18), 6 thermosyphons and VIT casing around S1 (S19)) at 0.8, 2, and 4 m depth over the course of May 2024 through May 2027.

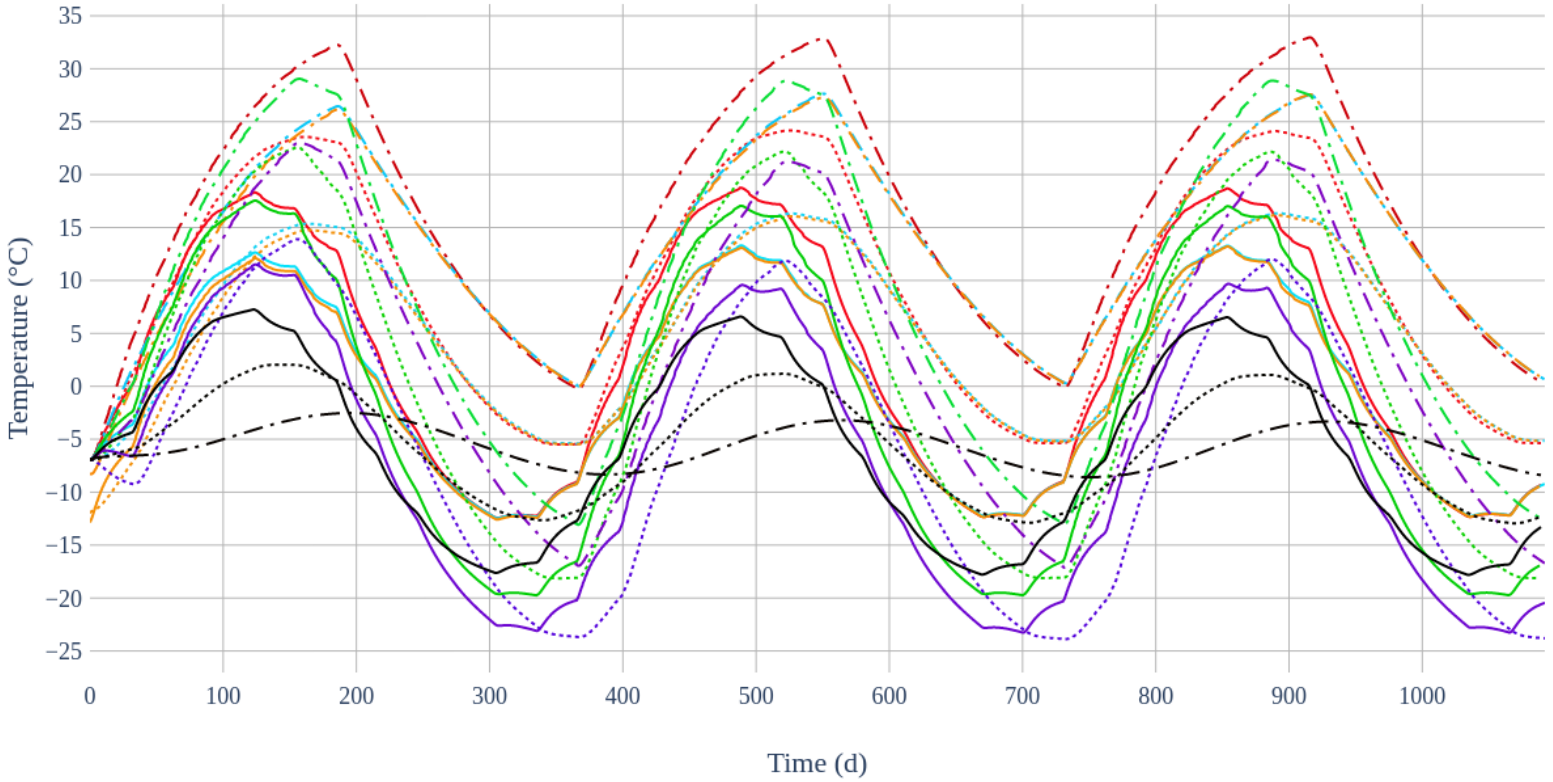

Scenario						Depth	
S1	Bentonite 10%, HDPE		S18	Bentonite 10%, HDPE, Thermosyphon		0.8 m
S3	Bentonite 10%, HDPE, VIT Casing		S19	Bentonite 10%, HDPE, Thermosyphon & VIT Casing		2 m
S16	Bentonite 10%, HDPE, Air Insulation			Natural Ground Temperature Without BHE		4 m

Figure 4.8 Ground temperature for key scenarios 1.67 m away from the central BHE (10% bentonite grout & HDPE (S1), VIT casing around S1 (S3), air-insulation around S1 (S16), 6 thermosyphons around S1 (S18), and 6 thermosyphons and VIT casing around S1 (S19)) at 0.8, 2, and 4 m depth over the course of May 2024 through May 2027.

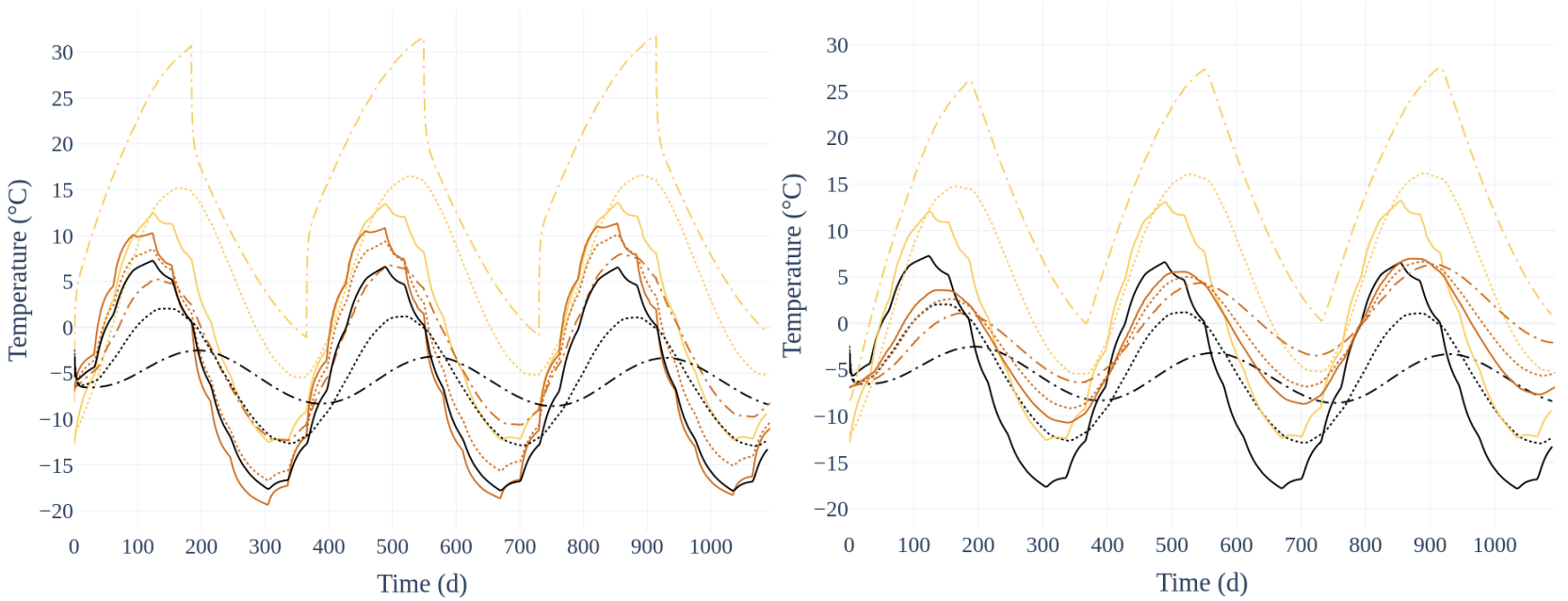

Figure 4.9 Ground temperature for air insulation scenarios 0.23 & 1.67 m away from the central BHE (air-insulation around S1 for 4 m (S16), air-insulation around S1 for 16 m (S17)) at 0.8, 2, and 4 m depth over the course of May 2024 through May 2027. The natural ground temperature is the same at 0.23 and 1.67 m.

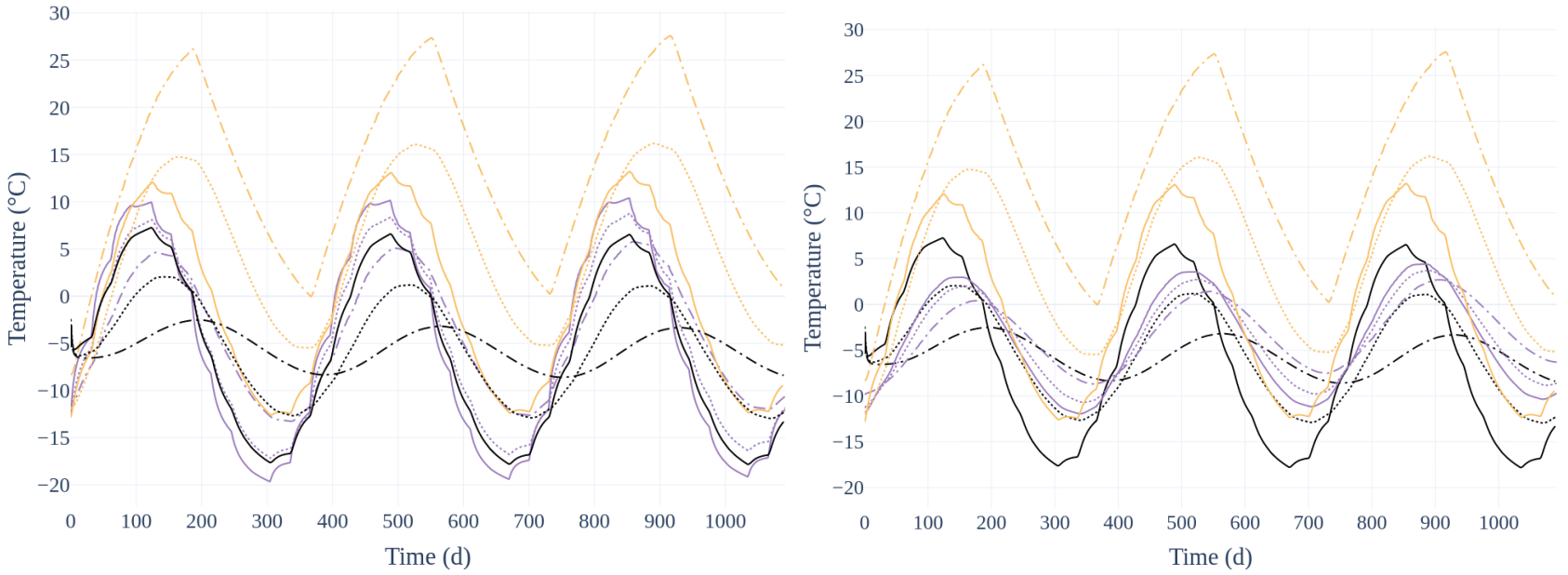

Scenario			Depth
S16 Air Insulation (4 m), 4 m sediments	S20 Air Insulation (20 m), 20 m sediments		0.8 m
Natural Ground Temperature Without BHE			2 m
			4 m

Figure 4.10 Ground temperature for air insulation scenarios 0.23 & 1.67 m away from the central BHE (air-insulation around S1 for 4 m in 4 m sediments (S16), air-insulation around S1 for 20 m in 20 m of sediments (S20)) at 0.8, 2, and 4 m depth over the course of May 2024 through May 2027.

4.4 BTES Field Permafrost Mitigation Results

The BTES Field has been simulated for the main purpose of observing whether the mitigation solutions are effective when emplaced around the outer edge of the field (S21) versus around every borehole in the field (S22). For comparison to a BTES field with no mitigation solutions employed, S23 represents such a case. Results regarding the effectiveness of the two scenarios from the BTES field are presented in **Figures 11 through 15**. Insulating every borehole in the field yields a cooler ground temperature in the center of the BTES field than insulating only the outer ring of BHEs. Outside of the BTES field, both scenarios produce similar ground temperature cooling capabilities.

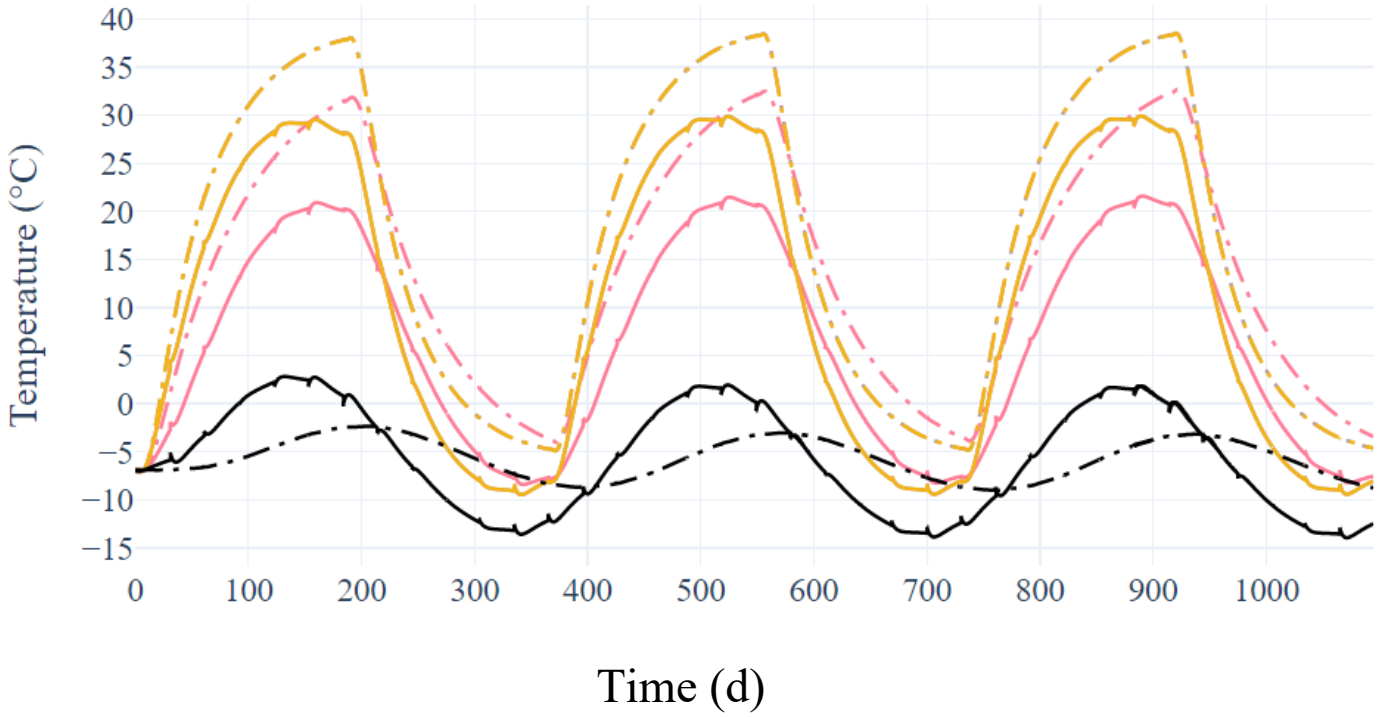

Figure 4.11 Ground temperature in the center of the BTES field (air-insulation around S1 for the outermost boreholes surrounding the field (S21), air-insulation around S1 for all boreholes (S22), and no mitigation solutions applied to the field (S23)) at 2 and 4 m depth over the course of May 2024 through May 2027. Some spikes appear in the lines at 2 m depth because of the model seasonal ground temperature changes affecting the results.

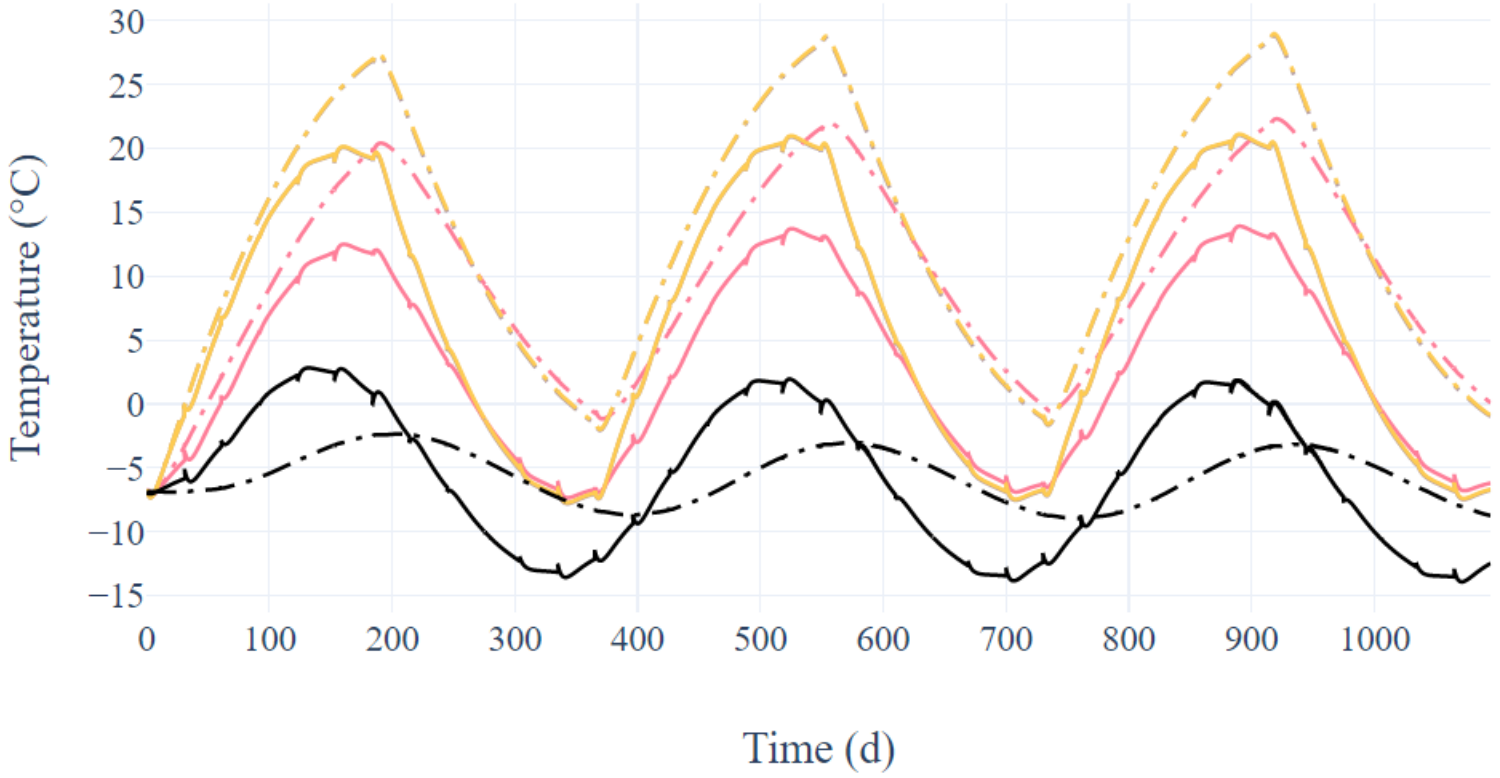

Scenario				Depth	
S21	Air Insulation (S16) outside edge of field	S22	Air Insulation (S16) every BHE in field	—	2 m
Natural Ground Temperature without BTES		S23	No Mitigation Solutions	-·-	4 m

Figure 4.12 Ground temperature a quarter distance from the edge of the BTES field (air-insulation around S1 for the outermost boreholes surrounding the field (S21), air-insulation around S1 for all boreholes (S22), and no mitigation solutions applied to the field (S23)) at 2 and 4 m depth over the course of May 2024 through May 2027. Some spikes appear in the lines at 2 m depth because of the model seasonal ground temperature changes affecting the results.

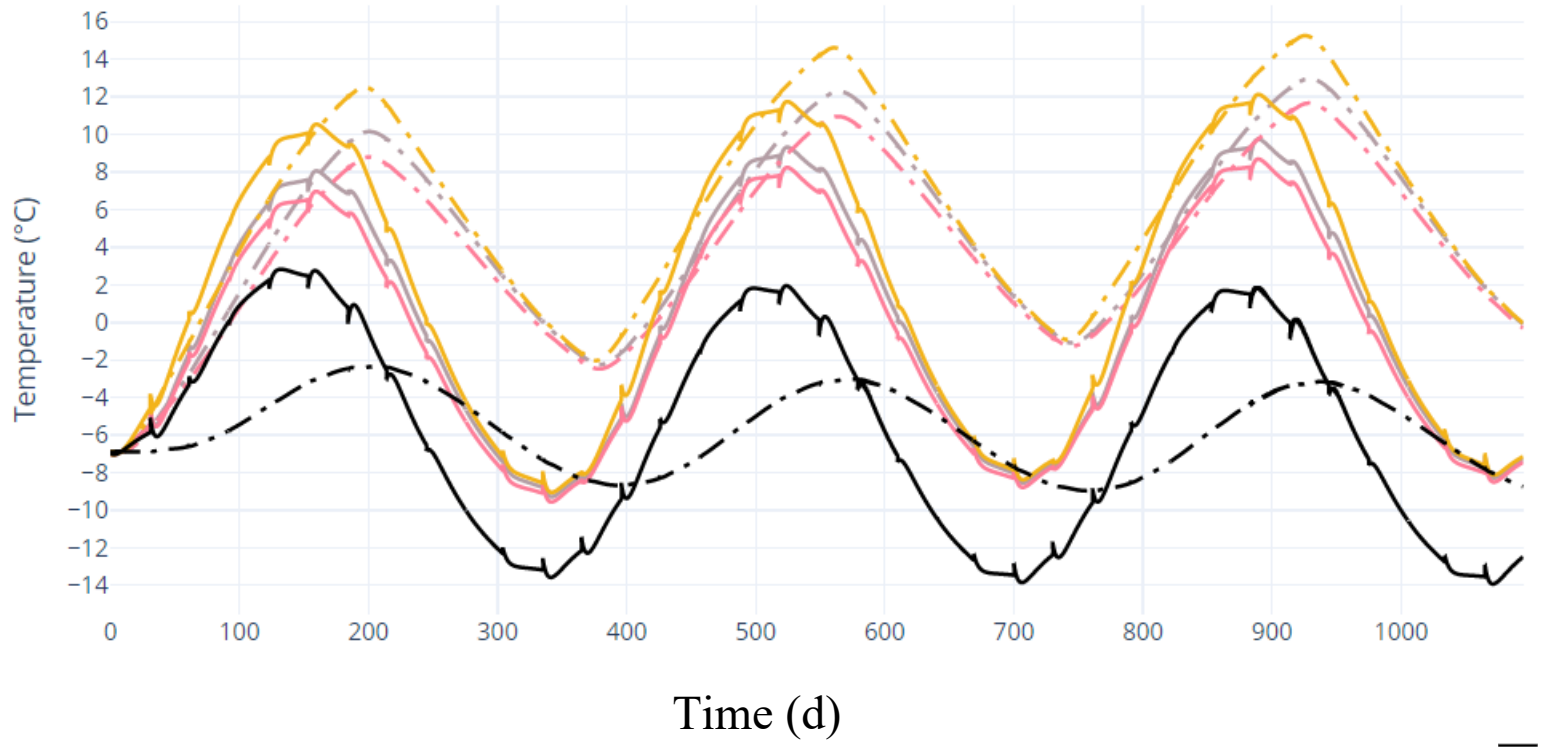

Scenario				Dep
S21	Air Insulation (S16) outside edge of field	S22	Air Insulation (S16) every BHE in field	2 m
Natural Ground Temperature without BTES		S23	No Mitigation Solutions	4 m

Figure 4.13 Ground temperature at the outermost edge of the BTES field equidistant between two outer-ring BHEs (air-insulation around S1 for the outermost boreholes surrounding the field (S21), air-insulation around S1 for all boreholes (S22), and no mitigation solutions applied to the field (S23)) at 2 and 4 m depth over the course of May 2024 through May 2027. Some spikes appear in the lines at 2 m depth because of the model seasonal ground temperature changes affecting the results.

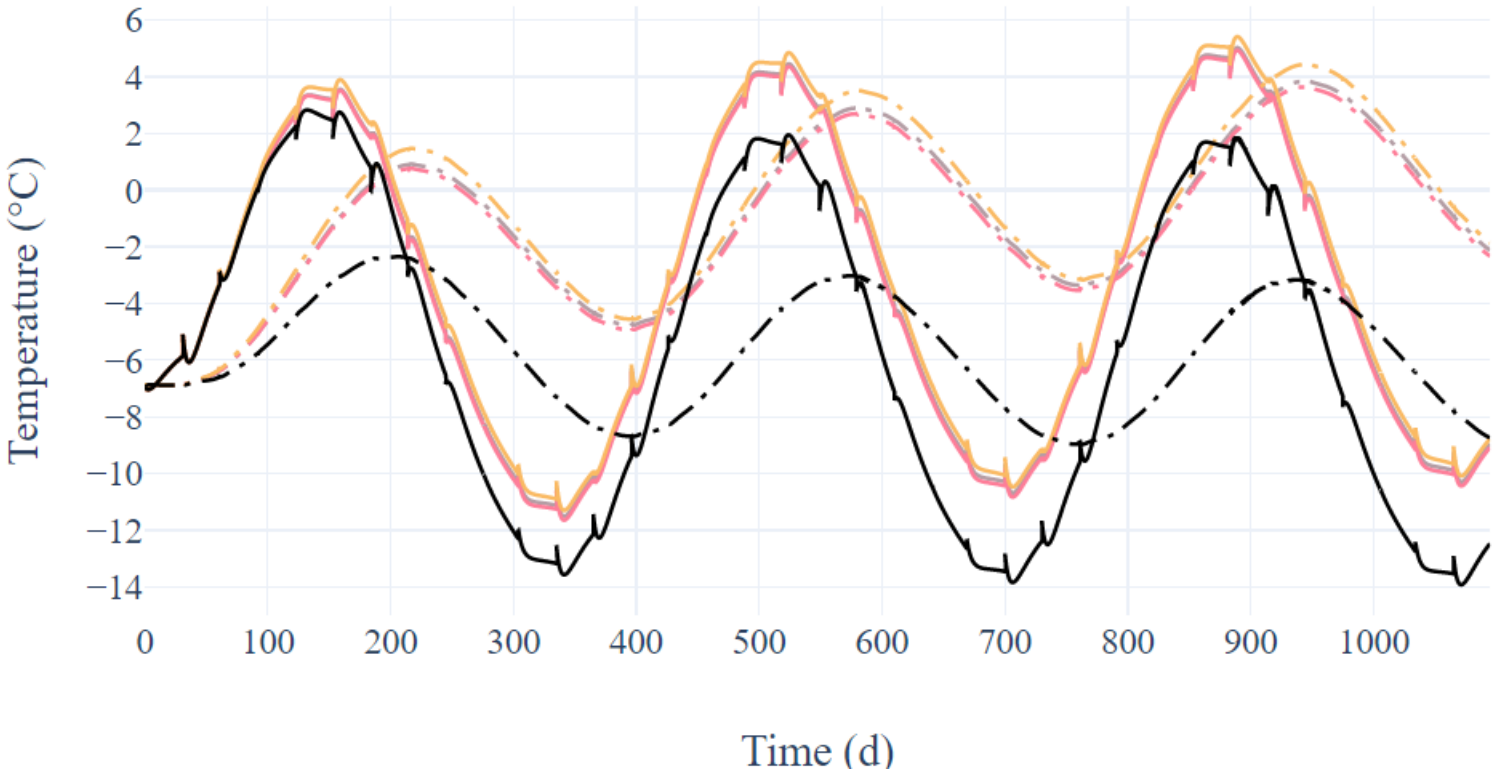

Scenario				Depth	
S21	Air Insulation (S16) outside edge of field	S22	Air Insulation (S16) every BHE in field	—	2 m
	Natural Ground Temperature without BTES	S23	No Mitigation Solutions	- -	4 m

Figure 4.14 Ground temperature 4.3 m outside of the outermost edge of the BTES field (air-insulation around S1 for the outermost boreholes surrounding the field (S21), air-insulation around S1 for all boreholes (S22), and no mitigation solutions applied to the field (S23)) at 2 and 4 m depth over the course of May 2024 through May 2027. Some spikes appear in the lines at 2 m depth because of the model seasonal ground temperature changes affecting the results.

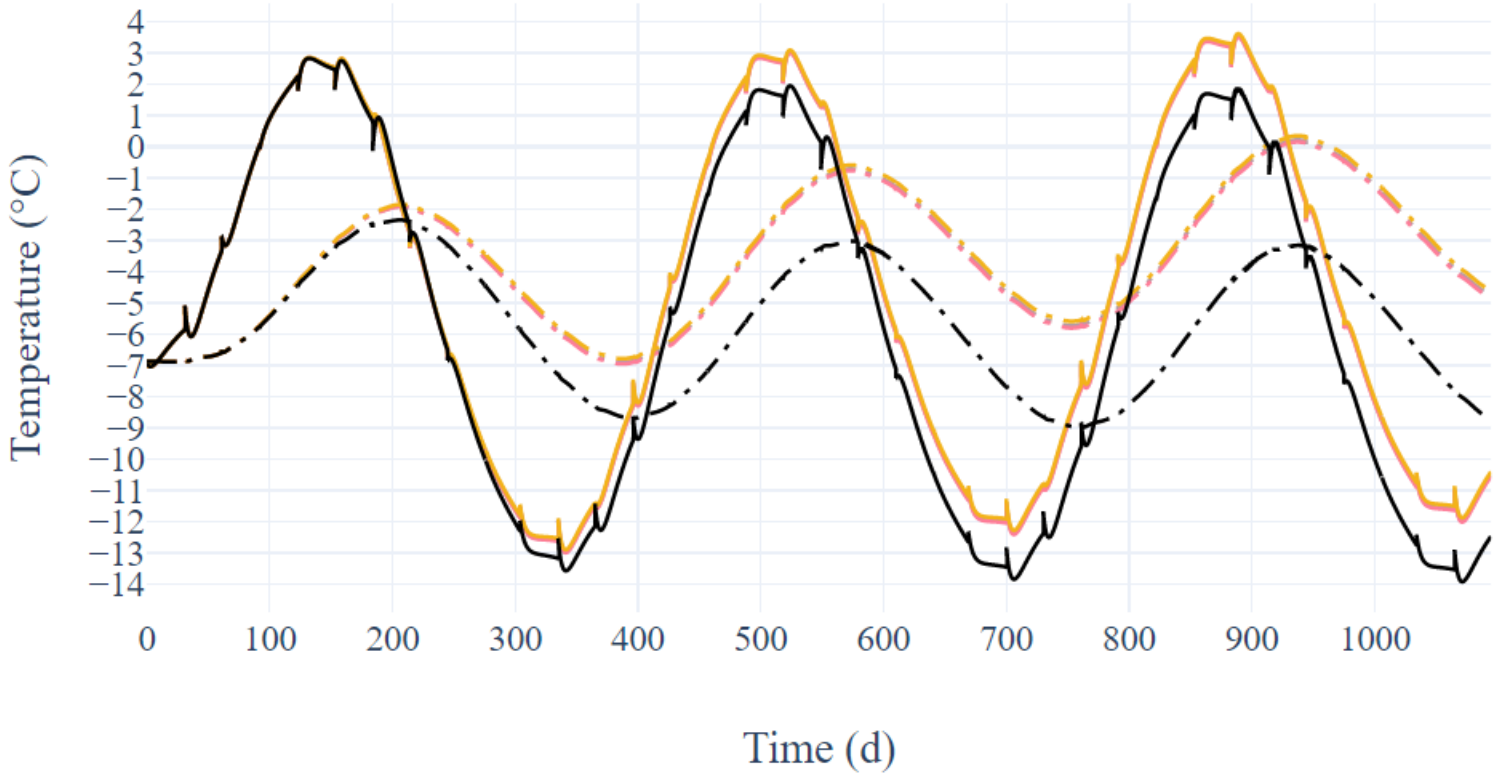

Scenario				Depth	
S21	Air Insulation (S16) outside edge of field	S22	Air Insulation (S16) every BHE in field	—	2 m
Natural Ground Temperature without BTES		S23	No Mitigation Solutions	- · -	4 m

Figure 4.15 Ground temperature 8.7 m outside of the outermost edge of the BTES field (air-insulation around S1 for the outermost boreholes surrounding the field (S21), air-insulation around S1 for all boreholes (S22), and no mitigation solutions applied to the field (S23)) at 2 and 4 m depth over the course of May 2024 through May 2027. Some spikes appear in the lines at 2 m depth because of the model seasonal ground temperature changes affecting the results.

4.5 Single BHE Energy Storage

The energy storage of the scenarios is analysed and contrasted with permafrost temperature data to determine the most efficient solution. The key scenarios (S1, S3, S16, S17, S18, & S19) are all compared to determine which scenarios maximize energy storage while reducing permafrost thaw (**Figures 4.16 & 4.17**). Between all scenarios, the differences in energy storage are negligible. Therefore, the best-case scenario for maximizing energy storage and minimizing permafrost thaw is determined primarily by the ground temperature trends. Even the thermosyphons do not provide an energy storage that differs significantly from the other scenarios. The energy storage between 4 m of air insulation and 16 m of air insulation also shows negligible differences.

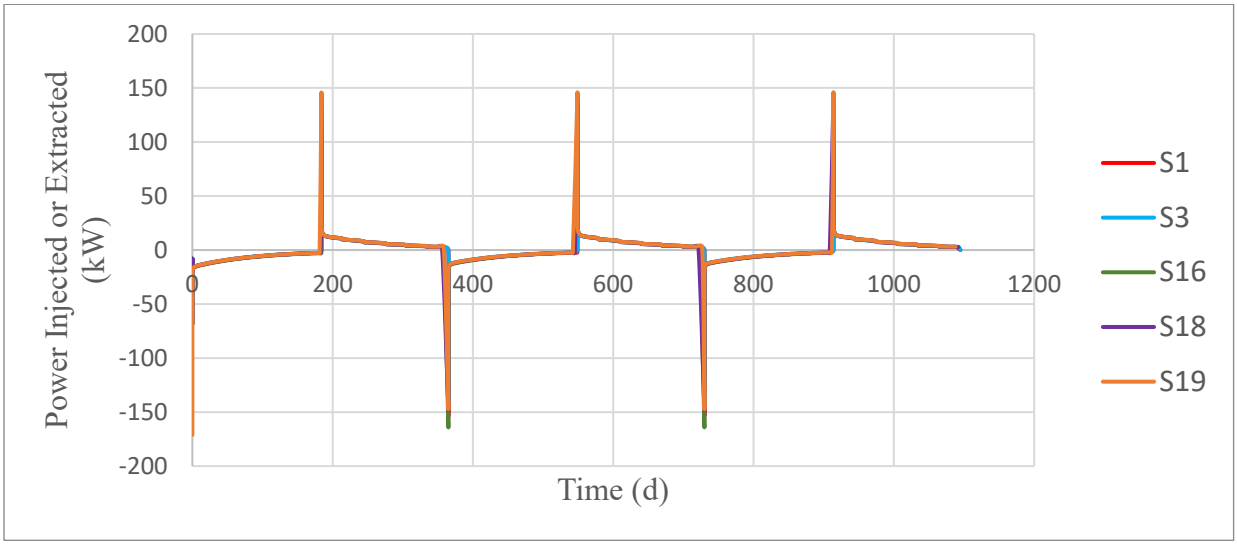

Figure 4.16 Power injected (negative) or extracted (positive) in the ground (kW) for the key scenarios from May 2024 through May 2027.

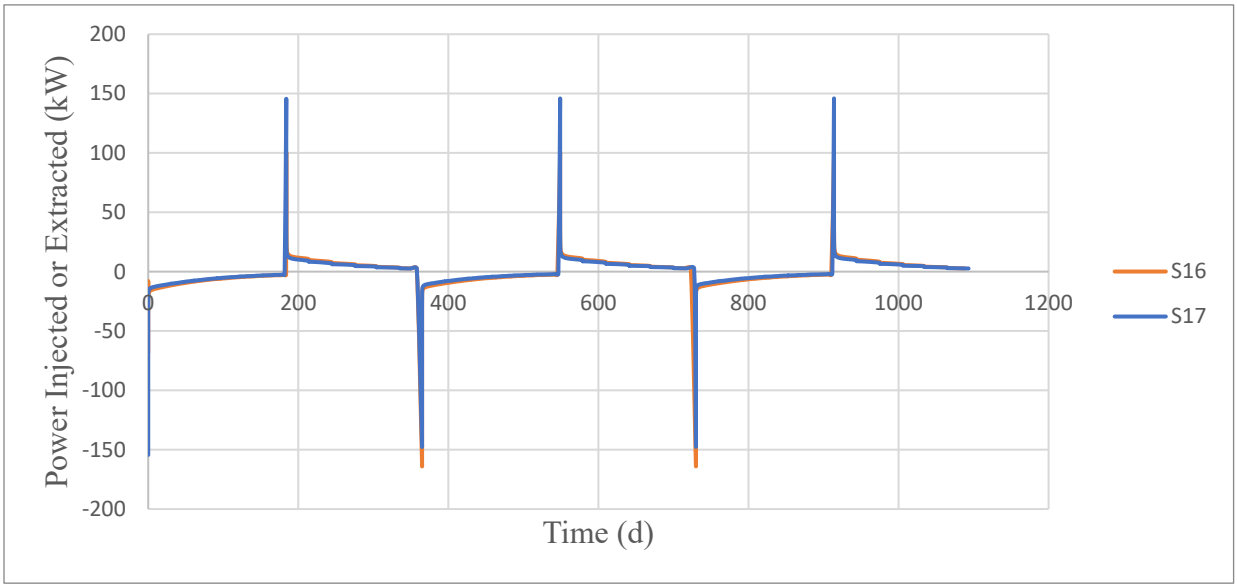

Figure 4.17 Power injected (negative) or extracted (positive) in the ground (kW) of the 4 m air insulation (S16) and the 16 m air insulation (S17) scenarios from May 2024 through May 2027.

4.6 BTES Energy Storage

The two scenarios for BTES energy storage are compared in **Figure 4.18**. Energy storage differences between the two scenarios are negligible. Therefore, the ground temperature will be the determining factor in recommending a solution for mitigation of permafrost thaw and maximization of energy storage.

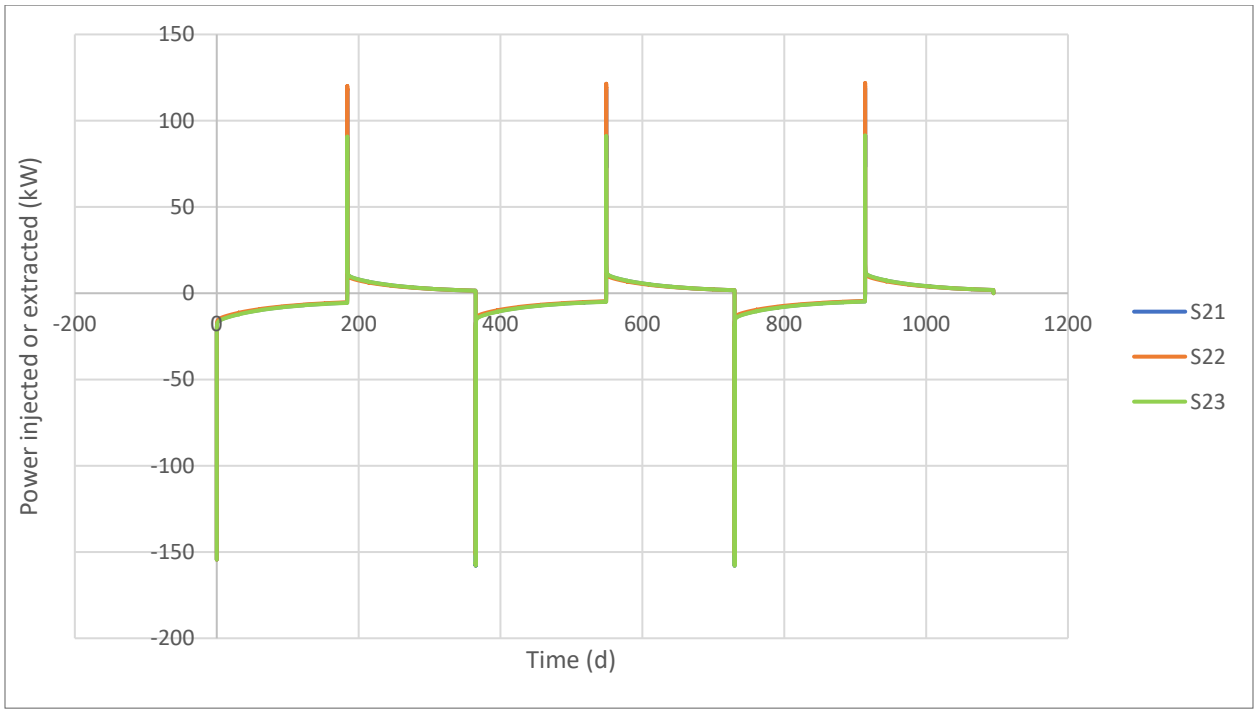

Figure 4.18 Power injected (negative) or extracted (positive) in the ground (kW) of the outside edge scenario (S21), the entire field scenario (S22), and for no mitigation solutions applied (S23) for the BTES field from May 2024 through May 2027.

5. DISCUSSION

5.1 Scenarios

To determine the most effective energy storage and permafrost mitigation solutions in the single borehole model, 20 solutions are compared among each other. The tested thaw mitigation solutions vary in their success at keeping the ground cold. The solutions that are most efficient at keeping the ground temperature cold in the overburden are VIT casing, air insulation, and thermosyphons. Changing the grout and pipe has a very small effect on keeping the ground temperature cold. The solutions each store a similar amount of energy. The most effective materials for energy storage have high thermal conductivities.

The BTES field has been simulated for the main purpose of evaluating whether the mitigation solutions are effective when emplaced around the outer edge of the field versus around every single borehole in the field. To test this hypothesis, although computation time was very long (12 h per 3-year simulation), three scenarios have been developed: the first is air insulation of the BHEs around the outer edge of the field, the second is air insulation around every BHE in the field (100 BHEs air insulated), and the third is a scenario with no mitigation solutions applied. The ground temperatures inside of the BTES field display increases in both scenarios, while the ground temperature extending radially beyond the edge of the BTES field is better regulated. The differences in energy storage between the two scenarios is negligible. Applying a mitigation solution to every borehole inside of the borefield shows small differences from applying the same solution to every borehole around the outside edge of the field.

5.2 Modified Design Elements

To increase the effectiveness of the simulations, the borehole in the single BHE model parameters has been chosen considering those of a BHE made with a diamond drill that is more common to northern communities in Canada (Kanzari 2019). A 20% ethyl alcohol working fluid has been adjusted to reflect the appropriate freezing temperature. This working fluid is acceptable for use by humans as determined by government regulations and is injected into the system at a flow rate of 11.2 gpm for HDPE pipes and 11.3 gpm for PVC pipes. This flow rate keeps the Reynold's number greater than 4000 in both cases to ensure turbulent flow in both types of pipes (4081.1 for HDPE and 4034.1 for PVC). The physical properties of the materials are from prior studies in Kuujjuaq (Nunavik, northern Quebec), which is another northern community that is located on the Canadian Shield, and therefore the sediments and bedrock are expected to have a similar likeness to that of Baker Lake, Nunavut. The base case runs with HDPE pipe and an arbitrary grout thermal conductivity of 1. To improve the base case, seasonal ground temperature variations are added to reflect monthly ground temperature changes from Baker Lake. To further improve the model, PiFreeze is used to simulate cyclical freezing and thawing.

Multiple mitigation solutions are tested and compared. First, a parametric study by changing grout and pipe types is carried out. These simulations rely on thermal conductivities and dimensions obtained from literature review. Then, VIT casings, air insulation and thermosyphons are introduced to the model. The thermal conductivity of VIT determined in prior research is utilized (Gascuel et al. 2022). The unconfined flow porosity and hydraulic conductivity are reduced to a very small value in the unconfined flow simulation to reflect the impenetrability of the VIT material. VIT naturally has a very low thermal conductivity and heat capacity. For the air insulated scenarios, the hydraulic conductivity and unconfined flow porosity are reduced to a very small

value in the unconfined flow simulation to reflect the properties of the air. The thermal conductivity and volumetric heat capacity of air is determined for a temperature of -11 °C to reflect the mean annual air temperature at Baker Lake. Thermosyphons have been adjusted to reflect the extraction of a model thermosyphon from literature (Aftret & Daleng 2022) and are applied to the model with specific spacing between nodal heat sinks. Providing this spacing ensures that the numerical extraction radius does not overlap, as overlapping these areas provides falsely elevated extraction effects.

To compute results for the BTES field in a reasonable amount of time without incurring error, 100 BHEs of 30 m depth have been simulated in glacial till that resembles the sedimentary material at Baker Lake. The use of a 50 m sediment model allows for a better understanding of mitigation solutions on the thermal gradient produced by the BTES field, and on energy storage. Additionally, use of FEFLOW default borehole parameters simplifies the creation of the mesh, as the boreholes are not as small as the single BHE model, and therefore the vertical spacing between the layers does not need to be as refined. All modifications have been emplaced primarily to reduce the computational complexity of the model, as adding 100 BHEs with 20 flow arrays requires extensive computation time in FEFLOW.

5.3 Comparison of Scenarios

A graphic comparison of all mitigation solution MAGT to the natural ground's MAGT is provided in **Figure 5.1**. The difference between scenarios concerning energy stored remained negligible.

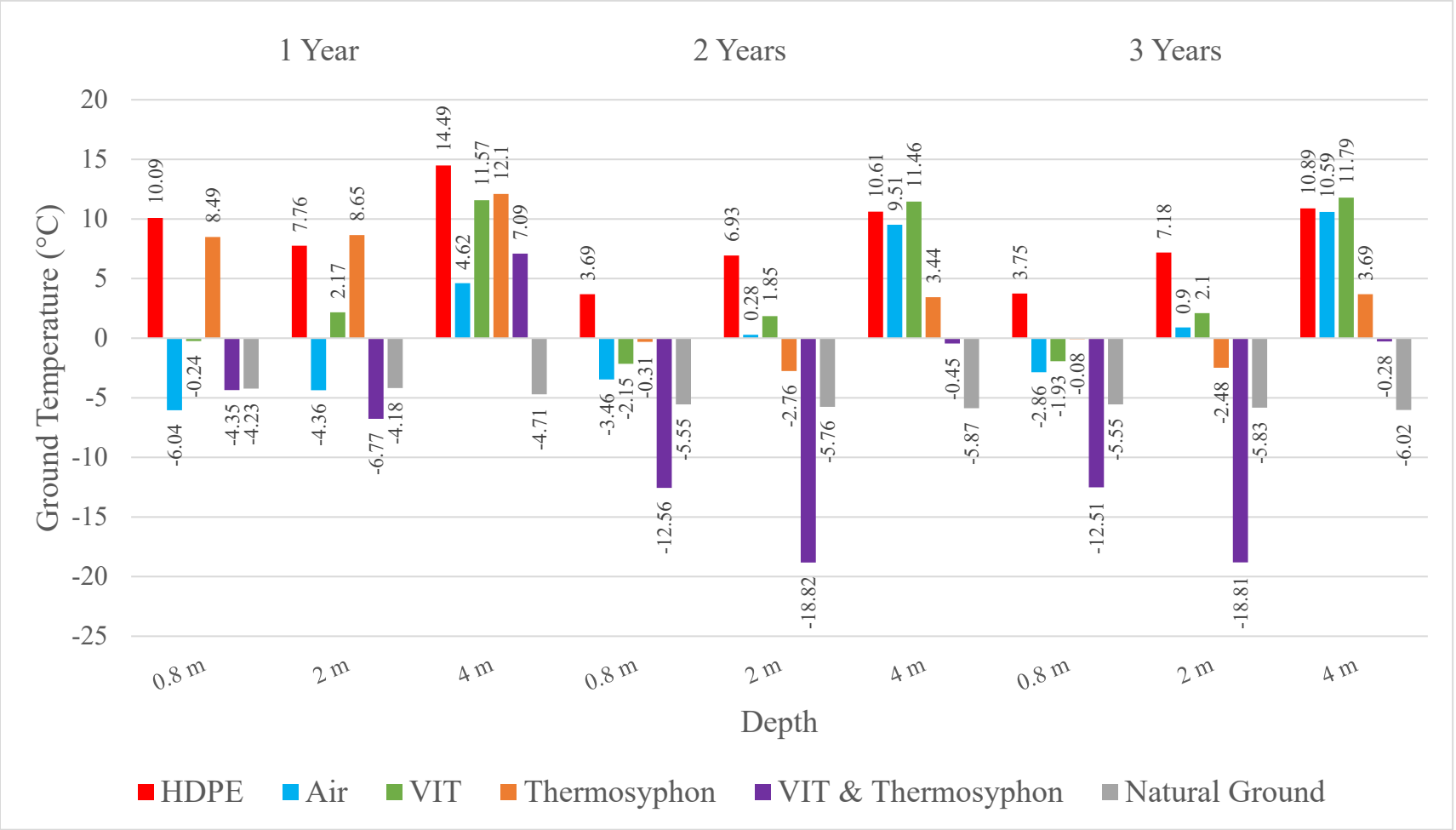

Figure 5.1 Mean annual ground temperatures in key scenarios 0.23 m away from the central BHE at 0.8, 2 and 4 m depth during years 1, 2, and 3 for each mitigation solution.

5.4 Effective Solutions for Ground Cooling

In summer, the best solutions are a combination of thermosyphons and VIT or air insulation. The thermosyphon representations alone are unable to keep the ground cooler even with a perfect 0 heat exchange rate applied to the thermosyphon representation. In winter, the most effective solution is the thermosyphon representation, as this solution can inject cold air into the ground directly. The differences in energy storage between solutions are negligible for the single borehole model.

The ground temperature inside of the BTES field shows increases that are independent of whether the mitigation solution is applied to every borehole vs. the outside edge boreholes. Outside of the BTES, the ground temperature is kept below 0 °C at 8.7 m in both scenarios. The scenarios do not show large differences from each other 4.3 and 8.7 m from the edge of the borefield. At the edge of the field, applying the mitigation solution to every borehole in the field shows a smaller increase in temperature from the natural ground temperature than applying the solution to outer edge boreholes.

5.5 Potential cost of mitigation solutions

The best solution for permafrost thaw mitigation appears to be a combination of solutions – i.e., a thermosyphon and VIT or air insulation. However, thermosyphons are associated with a high cost. It may not be advantageous to install a thermosyphon to an air-insulated borehole; instead, it may be more efficient to drill deeper into the ground and extend the air insulation. This would arguably cost less than grouting the borehole, as expenses are limited to the size of the hole drilled to encase the top portion of the well in air, and then the cost of drilling a smaller hole into bedrock.

The probable cost of mitigation solution materials is ranked from least to most expensive as follows (**Table 5.1**). VIT and HDPE pipe costs are for the material and do not include the cost of installation (Gascuel et al. 2022). The total cost of a 4 m VIT casing per borehole is likely $660 CAD. The cost of thermosyphons have been determined from the length, diameter, and the bulk price of carbon steel. The cost of a screen to enable smooth fluid, use of Therminol VP-1 working, and the cost of welding the end shut in the summer are considered for a thermosyphon 24 mm in diameter with a length of 6 m (Robak et al 2011). If every borehole requires 6 thermosyphons, the most likely cost of thermosyphons per borehole will total $384 CAD. Operation, maintenance, and installation costs are not included in thermosyphon costs. Grout expenses have not been included in this approximation due to a lack of information on cost in literature.

Table 5.1 Average likely cost of mitigation solution materials in different currencies, ranked from least expensive to most expensive. Current exchange rate as of March 2023 for CAD to USD is -3.91%, CAD to Euro is -10.49%, USD to CAD is 4.07%, and USD to Euro is -6.85%.

Solution	CAD	USD	Euro	Source
Air Insulation	0 m^{-3}	0 m^{-3}	0 m^{-3}	
HDPE pipe	14.45 m^{-1}	10.56 m^{-1}	9.84 m^{-1}	32; CAD
Thermosyphon	64 $Unit^{-1}$	47 $Unit^{-1}$	44 $Unit^{-1}$	107; USD
VIT Casing	165 m^{-1}	120 m^{-1}	112 m^{-1}	32; CAD

5.6 Air Insulation & Natural Ground Temperature Comparison

In the single borehole model, equilibrium is reached after year 1, and the simulations are extended to year 3 to review trends. The best solution, which is most cost-effective and capable of keeping the ground cool in both summer and winter, is the air-insulation scenario. The largest differences between the natural thermal gradient and the adjusted thermal gradient when air insulation is applied occur at 4 m depth, which is the sediment-bedrock contact. The smallest differences remain in the upper 2 and 0.8 m of sediments, where the maximum difference is 273% at 2 m depth during the third year of thermal energy storage.

In the BTES field, equilibrium is reached after year 1 and the simulations are extended to year 3 for the review of trends, similar to the single borehole model. The best solution based on the data is to insulate every borehole in the field. The largest differences in the middle of the field occur at 4 m depth, which is the sediment-bedrock contact and where the air insulation terminates. Drilling a deeper zone of air insulation may significantly decrease the effect of energy storage on the ground temperature.

The main findings of the research are as follows:

- Changing pipe and grout properties does not have large impact. Compared to the capabilities of air insulation, VIT casing, and thermosyphons changing the pipes and ground only influences the ground temperature within 5 °C.
- Air insulation works slightly better than VIT casing and is not as expensive as other solutions. This is likely because the thermal conductivity of air is lower than that of the VIT scenario.
- Drilling a deeper zone of air insulation (for instance, 16 m instead of 4 m) improves the effectiveness of the solution and does not influence energy storage in the single-borehole scenario.
- Thermosyphons are effective in winter but less effective in summer, even when the exchange rate of warm air to the ground is a perfect scenario. This could be a result of being unable to extract heat in summer.
- If there is a material contact between boundaries, heat will transfer no matter what preventative steps have been taken.

- Thermal conductivity is the greatest factor in determining how heat will transfer in the model, as other parameters have been altered and not had an elevated effect when compared to altering thermal conductivity.
- Insulating every borehole in the BTES field is slightly more effective than insulating the outside ring of boreholes at the outer edge of the BTES field.

To summarize the study, the most effective additions to the model and the solutions are recalled. The application of realistic grout and pipe thermal conductivity values, as well as the application of a model thermosyphon extraction rate are useful in creating more effective models. Other worthwhile additions are the thermosyphon representation with appropriate in-model spacing, the reduced heat transfer materials (VIT, air), and the inlet temperature of -5 °C in the model with the usage of an assumed heat pump. The most effective solutions are air insulation and thermosyphons; air insulation for the low cost and slightly better mitigation of ground temperature than VIT casing, and the thermosyphon for its ability to extract heat in winter. The testing of a BTES field determines that insulating every BHE in the field with air is slightly more effective than insulating the outermost BHEs in the field. The results of this study can be considered valid for communities in similar permafrost regions.

5.7 Limitations

Limitations of the single BHE mesh include the reduction of a large model to a 2 m radial model so that heat could be conserved. Without restricting the model boundaries, no heat could be stored in a larger square model. This is because heat would escape to the outer boundaries too quickly, as the ground temperature at depth is -7 °C through the entire model (excluding the surficial area of the model, which is affected by the ground temperature gradient). For the model run in a reasonable amount of time with the most consistent results, a coarse mesh is chosen to test the solutions.

Additionally, porosity is reduced to $1 \bullet 10^{-10}$ for both the sediment and bedrock material unconfined fluid flow properties. This reduction allows the application of PiFreeze to run in a fully saturated, non-flow model without requiring an unreasonable run time and without distorting BHE outlet results. This small 2 m radial model cannot be fully saturated and contain both PiFreeze and a BHE. PiFreeze requires a finer mesh to operate, but refining the mesh further around the central BHE induces falsely elevated outlet temperatures. The model cannot be fully saturated without producing a large courant error and high-magnitude Darcy Flux inside the discretized BHE elements. Therefore, the fluid flow in the model is restricted to avoid computational error caused by employing PiFreeze. The effect of latent heat on the model is still considered, and the model is ruled by conduction, as a large difference in energy storage results is visible between a confined, non-PiFreeze model and PiFreeze model (**Figure 5.2**).

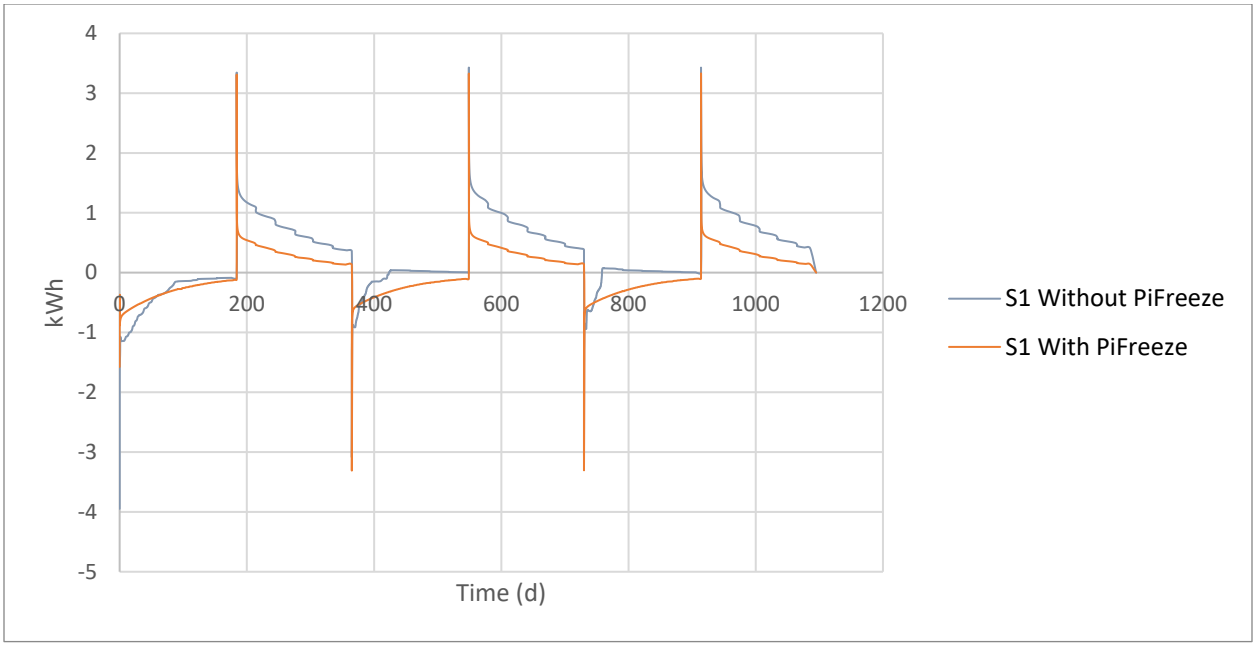

Figure 5.2 Comparison of S1 with and without PiFreeze applied showing latent heat differences.

To create a material in FEFLOW that is a solid material such as VIT, with no chance of fluid seepage or other incorrect behaviors, the porosity and hydraulic conductivity of VIT is restricted to negligible values. The same restrictions are employed for air. The thermosyphon is applied as a nodal sink at 4 points in the simulation to ensure no overlap of thermal extraction in the model. Overlapping the radius of extraction causes the extraction to compound and significantly distort the ground temperature. The thermosyphon tested in FEFLOW is a representation of a thermosyphon because there is no model application for a thermosyphon in FEFLOW.

It is worth mentioning that the research portion of the project is limited to 6 months, and computational requirements of PiFreeze are heavier than the available computers' processing power. Therefore, concessions are made to ensure stable results and adherence to the project timeline.

Limitations of the BTES field are the inability to produce a field with PiFreeze and 100 m deep boreholes. With these parameters applied, the computation time of the simulations increased dramatically. Refining the mesh to improve the quality of any of the previously mentioned variables increases the computation time for each simulation. These limitations stem from the time constraints on the project, and the lack of computational power required to run the desired applications.

6. CONCLUSIONS

After completing research on the single borehole model, the following conclusions have been made.

1. Changing grout does not have an effective impact on the temperature in the overburden above the bedrock where permafrost thaw should be minimized.
2. Air insulation works slightly better than VIT casing and is inexpensive; both have a significant effect on temperature in the overburden although completely avoiding permafrost thaw in the overburden is impossible.
3. A BHE with 16 m zone of air insulation improves the effectiveness of the solution and has little influence on the energy storage.
4. Thermosyphons are effective in winter but less effective than VIT casing and air insulation in summer to keep overburden temperature cold.
5. Air insultation in the upper section of the BHE is a solution to privilege because its cost is expected negligeable.
6. If there is material contact between boundaries, heat will transfer.
7. Thermal conductivity is the greatest factor in determining how much the ground temperature will increase.
8. Insulating every borehole in the BTES field is slightly more effective than insulating the outside ring of boreholes at the outer edge of the BTES field.

6.1 Future areas of exploration

Future studies may commit to studying one mitigation solution in depth, such as thermosyphons, in a model built specifically for testing the solution. Using a modelling program that has proper applications for thermosyphons, air, and casings may be beneficial. Or, adapting existing analytical models to the simulation of BHEs with latent heat effects incorporated in the ground to simulate the effect of mitigation solutions more rapidly. Additionally, further research on areas with elevated sediment overburdens may be useful for determining the effectiveness of mitigation solutions on different parts of the world. Creating a BTES system that analyses the effectiveness of mitigation solutions further is also necessary; for instance, a scenario should be developed to evaluate whether insulating the all BHEs in a large borefield with 16 m of air effects energy storage capabilities. Finally, it would be beneficial to create a discretized model with a non-grouted borehole in the overburden section, and to create a simulated circulation of cold air in the winter in the air-insulated portion of the model.

7. REFERENCES

7.1 References - Introduction

1 Benge, M., Reyes, J., & Xiao, E. (2016). Lightweight Cement Systems Help Prevent Permafrost Melt. Public report. *SPE Thermal Well Integrity and Design Symposium - Lightweight Cement Systems Help Prevent Permafrost Melt.* Society of Petroleum Engineers, Banff, Alberta, Canada, 1-10. DOI: https://doi.org/10.2118/182524-MS

2 Briquetti, S. (12 May 2021). Security implications of climate change: The case of permafrost thaw. Independent article. Observer Research Foundation, New Delhi, India, n.p. URL: https://www.orfonline.org/expert-speak/security-implications-climate-change-case-permafrost-thaw/

3 Fatollahzadeh Gheisari, A. (2021). *Long-term efficiency of horizontal closed-loop geothermal heat exchangers for stabilization of permafrost beneath a Subarctic lagoon* (25522). [Master's Thesis, The University of Manitoba]. FGS - Electronic Theses and Practica. URL : https://mspace.lib.umanitoba.ca/xmlui/handle/1993/35668

4 FVB Energy Inc. (1 Feb. 2021). Municipality of Baker Lake District Heat System Business Case study: Baker Lake, Nunavut. Internal report. FVB Energy Inc, Edmonton, Alberta, 1-72.

5 Ghoreishi-Madiseh, S. A., Fahrettin Kuyuk, A., Rodrigues de Brito, M. A., Baidya, D., Torabigoodarzi, Z., & Safari, A. (2019). Application of Borehole Thermal Energy Storage in Waste Heat Recovery from Diesel Generators in Remote Cold Climate Locations. *Energies* 2019, *12*(4), 656, 1 - 14. DOI : https://doi.org/10.3390/en12040656

6 Giordano, N., Kanzari, I., Miranda, M. M., Dezayes, C., & Raymond, J. (2018). Underground thermal energy storage in subarctic climates: A feasibility study conducted in Kuujjuaq (QC, Canada). Conference proceedings. International Ground Source Heat Pump Association, QC, Canada, n.p. DOI : https://doi.org/10.22488/okstate.18.000024

7 Giordano, N., Riggi, L., Casasso, A., Mandrone, G., Della Valentina, S., & Raymond, J. (2019, August 1). Efficiency evaluation of borehole heat exchangers in Nunavik, Québec, Canada. Conference proceedings. 25th IIR International Congress of Refrigeration., Montréal, Canada, n.p. DOI : https://doi.org/10.18462/iir.icr.2019.0547

8 James, M., Lewkowicz, A. G., Smith, S. L., & Miceli, C. M. (2013a). Multi-decadal degradation and persistence of permafrost in the Alaska Highway corridor, northwest Canada. *Environmental Research Letters, 8*(4), 045013, 1-10. DOI : https://doi.org/10.1088/1748-9326/8/4/045013

9 James, M., Lewkowicz, A. G., Smith, S. L., & Miceli, C. M. (2013b). Multi-decadal degradation and persistence of permafrost in the Alaska Highway corridor, northwest Canada. *Environmental Research Letters, 8*(4), 045013, 1-10. https://doi.org/10.1088/1748-9326/8/4/045013

10 Lochead, David. (10 Aug. 2022). Northern Affairs Minister mum on Baffinland during northern tour. News Article. Nunatsiaq News, Nortext Publishing Corporation (Iqaluit),

Iqaluit, NU, Canada, n.p. URL: https://nunatsiaq.com/stories/article/northern-affairs-minister-mum-on-baffinland-during-northern-tour/

11 Marques, C., Castanier, L. M., & Kovscek, A. R. (2011). Super insulated wells to protect permafrost during thermal oil recovery. *International Journal of Oil, Gas and Coal Technology, 4*(1), 4 - 30. DOI: https://doi.org/10.1504/IJOGCT.2011.037742

12 McMartin, I., Godbout, P.-M., Campbell, J. E., Tremblay, T., & Behnia, P. (2021). A new map of glacigenic features and glacial landsystems in central mainland Nunavut, Canada. *Boreas,* (1), 51–75. DOI : https://doi.org/10.1111/bor.12479

13 Municipality of Baker Lake. (2022). About Baker Lake | Hamlet of Baker Lake | Baker Lake. Web page. Hamlet of Baker Lake, Baker Lake, NU, n.p. URL: https://www.bakerlake.ca/about

14 Nunatsiaq News. (23 Apr. 2021). Fuel spill poses risks to Baker Lake's water supply: Nunavut government. Nunatsiaq News, Nortext Publishing Corporation (Iqaluit), Iqaluit, NU, Canada, n.p. URL: https://nunatsiaq.com/stories/article/fuel-spill-poses-risks-to-baker-lakes-water-supply-nunavut-government/

15 Pei, W., Zhang, M., Li, S., Lai, Y., Jin, L., Zhai, W., Yu, F., & Lu, J. (2017). Geotemperature control performance of two-phase closed thermosyphons in the shady and sunny slopes of an embankment in a permafrost region. *Applied Thermal Engineering, 112*, 986–998. https://doi.org/10.1016/j.applthermaleng.2016.10.143

16 Pinto, H., & Gates, I. D. (2022). Why is it so difficult to replace diesel in Nunavut, Canada? *Renewable and Sustainable Energy Reviews, 157*, 112030, 1-10. https://doi.org/10.1016/j.rser.2021.112030

17 Reid, R. L., Tennant, J. S., & Childs, K. W. (1975). The Modeling of a Thermosyphon Type Permafrost Protection Device. *Journal of Heat Transfer, 97*(3), 382–386. https://doi.org/10.1115/1.3450383

18 Smith, S. L., & Burgess, M. M. (2002). A digital database of permafrost thickness in Canada. Geological Survey of Canada, Ottawa, Ont., Canada, 1 – 28. URL : https://searchworks.stanford.edu/view/6490114

19 Throop, J., Lewkowicz, A. G., & Smith, S. L. (2012). Climate and ground temperature relations at sites across the continuous and discontinuous permafrost zones, northern Canada. *Canadian Journal of Earth Sciences, 49*(8), 865–876. DOI : https://doi.org/10.1139/e11-075

20 Xu, J., & Goering, D. J. (2008). Experimental validation of passive permafrost cooling systems. *Cold Regions Science and Technology, 53*(3), 283–297. DOI: https://doi.org/10.1016/j.coldregions.2007.09.002

21 Zapata, K. (15 Jul. 2021). Arctic oil spill cleanup costs could reach $9.4B over 5 years, says risk analyst CBC News. CBC, Toronto, ON, Canada, n.p. URL: https://www.cbc.ca/news/canada/north/arctic-oil-spill-study-1.6103155

7.2 References - Background

22 Aftret, H & Daleng, V. *Suitability of Thermosyphon as a Ground Freezing Technology in Longyearbyen.* [Internal Master's Thesis, Norwegian University of Science and Technology, Norway]. Personal Communication.

23 Bauer, D., Heidemann, W., Müller-Steinhagen, H., & Diersch, H.-J. G. (2011). Thermal resistance and capacity models for borehole heat exchangers. *International Journal of Energy Research*, *35*(4), 312–320. DOI: https://doi.org/10.1002/er.1689

24 Benge, M., Reyes, J., & Xiao, E. (2016). Lightweight Cement Systems Help Prevent Permafrost Melt. Public report. *SPE Thermal Well Integrity and Design Symposium - Lightweight Cement Systems Help Prevent Permafrost Melt.* Society of Petroleum Engineers, Banff, Alberta, Canada, 1-10. DOI: https://doi.org/10.2118/182524-MS

25 Briquetti, S. (12 May 2021). Security implications of climate change: The case of permafrost thaw. Independent article. Observer Research Foundation, New Delhi, India, n.p. URL: https://www.orfonline.org/expert-speak/security-implications-climate-change-case-permafrost-thaw/

26 Canadrill Limited Geotechnical Division. (22 Feb. 2019). Geotechnical Investigation: QEC Office Building Baker Lake, NU. Internal Final Report. Canadrill Limited Geotechnical Division, Iqaluit, Nunavut, 1 – 25. Personal Communication.

27 Chouinard, C., Fortier, R., & Mareschal, J.-C. (2007). Recent climate variations in the subarctic inferred from three borehole temperature profiles in northern Quebec, Canada. *Earth and Planetary Science Letters*, *263*(3), 355–369. DOI: https://doi.org/10.1016/j.epsl.2007.09.017

28 Cunningham, C. M., & Shilts, W. W. (1977). Surficial geology of the Baker Lake area, District of Keewatin. Conference proceedings. Report of activities part B; Geological Survey of Canada, NU, CA, Paper no. 77-1B, 311-314. URL : https://geoscan.nrcan.gc.ca/starweb/geoscan/servlet.starweb?path=geoscan/fulle.web&search1=R=102802

29 Environment and Climate Change Canada. (25 May 2022). Almanac Averages and Extremes. Wep page. Gouvernement du Canada, CA, n.p. URL : https://climate.weather.gc.ca/climate_data/almanac_e.html?StationID=51417

30 Fatollahzadeh Gheisari, A. (2021). *Long-term efficiency of horizontal closed-loop geothermal heat exchangers for stabilization of permafrost beneath a Subarctic lagoon* (25522). [Master's Thesis, The University of Manitoba]. FGS - Electronic Theses and Practica. URL : https://mspace.lib.umanitoba.ca/xmlui/handle/1993/35668

31 FVB Energy Inc. (1 Feb. 2021). Municipality of Baker Lake District Heat System Business Case study: Baker Lake, Nunavut. Internal report. FVB Energy Inc, Edmonton, Alberta, 1-72.

32 Gascuel, V., Raymond, J., Rivard, C., Marcil, J.-S., & Comeau, F.-A. (2022). Design and optimization of deep coaxial borehole heat exchangers for cold sedimentary basins. *Geothermics*, *105*, 102504, 1-36. DOI : https://doi.org/10.1016/j.geothermics.2022.102504

33 Ghoreishi-Madiseh, S. A., Fahrettin Kuyuk, A., Rodrigues de Brito, M. A., Baidya, D., Torabigoodarzi, Z., & Safari, A. (2019). Application of Borehole Thermal Energy Storage in Waste Heat Recovery from Diesel Generators in Remote Cold Climate Locations. *Energies* 2019, *12*(4), 656, 1 - 14. DOI : https://doi.org/10.3390/en12040656

34 Giordano, N., Kanzari, I., Miranda, M. M., Dezayes, C., & Raymond, J. (2018). Underground thermal energy storage in subarctic climates: A feasibility study conducted in Kuujjuaq (QC, Canada). Conference proceedings. International Ground Source Heat Pump Association, QC, Canada, n.p. DOI : https://doi.org/10.22488/okstate.18.000024

35 Giordano, N., Miranda, M., Kanzari, I., Dezayes, C., & Raymond, J. (21 Nov. 2017). *Shallow geothermal resource assessments for the northern community of Kuujjuaq, Québec, Canada*. Conference proceedings. Santiago de Chile, Republic of Chile, n.p. URL : https://www.researchgate.net/publication/325451055_Shallow_geothermal_resource_assessments_for_the_northern_community_of_Kuujjuaq_Quebec_Canada

36 Giordano, N., Riggi, L., Casasso, A., Mandrone, G., Della Valentina, S., & Raymond, J. (2019, August 1). Efficiency evaluation of borehole heat exchangers in Nunavik, Québec, Canada. Conference proceedings. 25th IIR International Congress of Refrigeration., Montréal, Canada, n.p. DOI : https://doi.org/10.18462/iir.icr.2019.0547

37 Greevenbroek, v. K., & Klein, L. S. (2021). Opportunities for thermal energy storage in Longyearbyen. Public Report. The University Centre in Svalbard – UNIS, Svalbard, Norway, - 13. URL : https://munin.uit.no/handle/10037/22287

38 Gunawan, E., Giordano, N., Jensson, P., Newson, J., & Raymond, J. (2020). Alternative heating systems for northern remote communities: Techno-economic analysis of ground-coupled heat pumps in Kuujjuaq, Nunavik, Canada. *Renewable Energy*, *147*, 1540–1553. DOI : https://doi.org/10.1016/j.renene.2019.09.039

39 Hadlari, T., & Rainbird, R. H. (2011). Retro-arc extension and continental rifting: A model for the Paleoproterozoic Baker Lake Basin, Nunavut [1] Geological Survey of Canada Contribution 20100436. *Canadian Journal of Earth Sciences*, *48*(8), 1232–1258. DOI : https://doi.org/10.1139/e11-002

40 James, M., Lewkowicz, A. G., Smith, S. L., & Miceli, C. M. (2013a). Multi-decadal degradation and persistence of permafrost in the Alaska Highway corridor, northwest Canada. *Environmental Research Letters, 8*(4), 045013, 1-10. DOI : https://doi.org/10.1088/1748-9326/8/4/045013

41 James, M., Lewkowicz, A. G., Smith, S. L., & Miceli, C. M. (2013b). Multi-decadal degradation and persistence of permafrost in the Alaska Highway corridor, northwest Canada. Environmental Research Letters, 8(4), 045013, 1-10. DOI : https://doi.org/10.1088/1748-9326/8/4/045013

42 Javadi, H., Mousavi Ajarostaghi, S. S., Rosen, M. A., & Pourfallah, M. (2019). Performance of ground heat exchangers: A comprehensive review of recent advances. *Energy*, *178*, 207–233. DOI : https://doi.org/10.1016/j.energy.2019.04.094

43 Kanzari, I. (2019). *Évaluation du potentiel des pompes à chaleur géothermique pour la communauté nordique de Kuujjuaq*. [Doctoral dissertation, Université du Québec, Institut national de la recherche scientifique]. EspaceINRS. URL : https://espace.inrs.ca/id/eprint/9063

44 Kleven, M. H. (2018). *An Independent Solar Energy Community in Longyearbyen by use of Borehole Thermal Energy Storage in Permafrost - A feasibility study* (1529). [Master's thesis, Norwegian University of Life Sciences]. NMBU. URL : https://nmbu.brage.unit.no/nmbu-xmlui/handle/11250/2571892

45 Kuang, X., Zheng, C., Jiao, J. J., Cherry, J. A., & Chen, J. (2021). An empirical specific storage-depth model for the Earth's crust. *Journal of Hydrology*, *592*, 125784, 1-10. DOI : https://doi.org/10.1016/j.jhydrol.2020.125784

46 Kurttila, M. P. E. (2021). *Borehole thermal energy storage as a seasonal capacitor in the off-grid Arctic energy supply system* [Master's thesis, Norwegian University of Science and Technology, Faculty of Engineering, Department of Civil and Environmental Engineering]. NTNU. URL: https://ntnuopen.ntnu.no/ntnu-xmlui/handle/11250/2824234

47 LaRocque, A., Leblon, B., Harris, J., Jefferson, C., Tschirhart, V., & Shelat, Y. (2012). Surficial materials mapping in Nunavut, Canada with multibeam RADARSAT-2 dual-polarization C-HH and C-HV, LANDSAT-7 ETM+, and DEM data. *Canadian Journal of Remote Sensing*, *38*(3), 281–305. DOI : https://doi.org/10.5589/m12-020

48 Marques, C., Castanier, L. M., & Kovscek, A. R. (2011). Super insulated wells to protect permafrost during thermal oil recovery. *International Journal of Oil, Gas and Coal Technology*, *4*(1), 4 – 30. DOI: https://doi.org/10.1504/IJOGCT.2011.037742

49 Mendrinos, D., Katsantonis, S., & Karytsas, C. (19 Sep. 2016). Pipe materials for borehole heat exchangers. European Geothermal Congress, Strasbourg, France, 1-8. URL : https://www.researchgate.net/publication/328232447_Pipe_materials_for_borehole_heat_exchangers

50 McMartin, I., Godbout, P.-M., Campbell, J. E., Tremblay, T., & Behnia, P. (2021). A new map of glacigenic features and glacial landsystems in central mainland Nunavut, Canada. *Boreas*, *50*(1), 51–75. https://doi.org/10.1111/bor.12479

51 Milanez, Fernando & Mantelli, Marcia. (2006). Thermal characteristics of a thermosyphon heated enclosure. *International Journal of Thermal Sciences, 45*, 504 – 510. DOI : https://doi.org/10.1016/j.ijthermalsci.2005.08.002

52 Minnick, M., Hickson, C.J., and Shewfelt, D. (2018). Nunavut Geothermal Feasibility Study. Topical Study, RSI 2828. Respec, Saskatoon, SK, 1 – 32. Personal Communication.

53 Miranda, M. M., Giordano, N., Raymond, J., Pereira, A. J. S. C., & Dezayes, C. (2020). Thermophysical properties of surficial rocks: A tool to characterize geothermal resources of remote northern regions. *Geothermal Energy*, *8*(1), 4, 1 – 27. DOI : https://doi.org/10.1186/s40517-020-0159-y

54 Miranda, MM; Raymond, J; Dezayes, C; Wigston, A. (2020 In progress). Field methods to estimate permeability of crystalline rocks in remote northern environments: advantages and limitations. Personal Communication.

55 Miranda, M. M., Velez Márquez, M. I., Raymond, J., & Dezayes, C. (2021). A numerical approach to infer terrestrial heat flux from shallow temperature profiles in remote northern regions. *Geothermics*, *93*, 102064, 1 – 18. DOI : https://doi.org/10.1016/j.geothermics.2021.102064

56 Municipality of Baker Lake. (2022). About Baker Lake | Hamlet of Baker Lake | Baker Lake. Web page. Hamlet of Baker Lake, Baker Lake, NU, n.p. URL: https://www.bakerlake.ca/about

57 M. Ouzzane, P. Eslami-Nejad, M. Badache, Z. Aidoun. (2014). New correlations for the prediction of the undisturbed ground temperature. *Geothermics, 53*, 379 – 384. DOI : https://doi.org/10.1016/j.geothermics.2014.08.001

58 Navrotsky, A. (1995). Thermodynamic Properties of Minerals. In Ahrens, T. J. (Edfs.), *Mineral physics & crystallography: a handbook of physical constants (Vol. 2)* (18-28). American Geophysical Union.

59 Pei, W., Zhang, M., Li, S., Lai, Y., Jin, L., Zhai, W., Yu, F., & Lu, J. (2017). Geotemperature control performance of two-phase closed thermosyphons in the shady and sunny slopes of an embankment in a permafrost region. *Applied Thermal Engineering*, *112*, 986 – 998. DOI : https://doi.org/10.1016/j.applthermaleng.2016.10.143

60 Peterson, T. D., Jefferson, C. W., Anand, A. (2015). Geological setting and geochemistry of the ca. 2.6 Ga Snow island Suite in the central Rae Domain of the Western Churchill Province, Nunavut. Online article. Geological Survey of Canada, Natural Resources Canada, CA, Open File 7841, n.p. DOI : https://doi.org/10.4095/296599

61 Rainbird, R. H., Hadlari, T., Aspler, L. B., Donaldson, J. A., LeCheminant, A. N., & Peterson, T. D. (2003). Sequence stratigraphy and evolution of the Paleoproterozoic intracontinental Baker Lake and Thelon basins, western Churchill Province, Nunavut, Canada. *Precambrian Research*, *125*(1), 21 – 53. DOI : https://doi.org/10.1016/S0301-9268(03)00076-7

62 Regehr, J. D., Milligan, C. A., Montufar, J., & Alfaro, M. (2013). Review of Effectiveness and Costs of Strategies to Improve Roadbed Stability in Permafrost Regions. *Journal of Cold Regions Engineering*, *27*(3), 109 – 131. DOI: https://doi.org/10.1061/(ASCE)CR.1943-5495.0000054

63 Reid, R. L., Tennant, J. S., & Childs, K. W. (1975). The Modeling of a Thermosyphon Type Permafrost Protection Device. *Journal of Heat Transfer*, *97*(3), 382 – 386. DOI : https://doi.org/10.1115/1.3450383

64 Saaly, M., Sinclair, R., Kurz, D., Maghoul, P., Holländer, H., & Gheisari, A. F. (2020). *Assessment of a Closed-Loop Geothermal System for Seasonal Freeze-Back Stabilization of Permafrost*. *Processes 2021, 9*(9), 1636, 1 – 14. DOI : https://doi.org/10.3390/pr9091636

65 Sanner, B., & Hellstroem, G. (1997). Earth Energy Designer, a software for calculating borehole heat exchangers; Earth Energy Designer, eine Software zur Berechnung von Erdwaermesondenanlagen. Conference proceedings. Germany, n.p. URL: https://www.osti.gov/etdeweb/biblio/573620

66 Schön, J. (2011). *Physical properties of rocks: A Workbook (Volume 8)*. Online E-Book Publication. Elseviver, 1 – 494. DOI : https://doi.org/10.1016/S1567-8032(11)08012-8

67 Schulte, D. O., Welsch, B., Boockmeyer, A., Rühaak, W., Bär, K., Bauer, S., & Sass, I. (2016). Modeling insulated borehole heat exchangers. *Environmental Earth Sciences*, *75*(10), 910. DOI: https://doi.org/10.1007/s12665-016-5638-x

68 Śliwa, Tomasz; Kruszewski, Michał; Zare, Alireza; Assadi, Mohsen; Sapińska-Śliwa, Aneta (2018). *Potential application of vacuum insulated tubing for deep borehole heat exchangers. Geothermics, 75*, 58 – 67. DOI : doi:10.1016/j.geothermics.2018.04.001

69 Smith, S. L., & Burgess, M. M. (2002). *A digital database of permafrost thickness in Canada*. Map. Geological Survey of Canada, Open File 4173. https://geoscan.nrcan.gc.ca/starweb/geoscan/servlet.starweb?path=geoscan/fulle.web&search1=R=211804

70 Smith, S. L., Riseborough, D. W., Ednie, M., & Chartrand, J. (2013). A map and summary database of permafrost temperatures in Nunavut, Canada. Public Report. Geological Survey of Canada, Canada, Open File 7393, 1 - 20. DOI: https://doi.org/10.4095/292615

71 Snyder, D. B., Berman, R. G., Kendall, J.-M., & Sanborn-Barrie, M. (2013). Seismic anisotropy and mantle structure of the Rae craton, central Canada, from joint interpretation of SKS splitting and receiver functions. *Precambrian Research*, *232*, 189 – 208. https://doi.org/10.1016/j.precamres.2012.03.003

72 Steven J. Whitmeyer, Karl E. Karlstrom; Tectonic model for the Proterozoic growth of North America. *Geosphere 2007, 3*(4), 220 – 259. DOI: https://doi.org/10.1130/GES00055.1

73 Throop, J., Lewkowicz, A. G., & Smith, S. L. (2012). Climate and ground temperature relations at sites across the continuous and discontinuous permafrost zones, northern Canada. Earth Science Sector (ESS), Contribution 20110128. *Canadian Journal of Earth Sciences*, *49*(8), 865 – 876. DOI : https://doi.org/10.1139/e11-075

74 Waples, D. W., & Waples, J. S. (2004). A review and evaluation of specific heat capacities of rocks, minerals, and subsurface fluids. Part 1: Minerals and nonporous rocks. *Natural resources research*, *13*(2), 97-122. DOI: 10.1023/B:NARR.0000032647.41046.e7

75 Whitmeyer, S. J., & Karlstrom, K. E. (2007). Tectonic model for the Proterozoic growth of North America. *Geosphere*, *3*(4), 220–259. DOI : https://doi.org/10.1130/GES00055.1

76 Woessner, W., & Poeter, E. (2020). Hydraulic Conductivity Values for Earth Materials. In Cherry, J. & Poeter, E. (Edfs.), *Hydrogeologic Properties of Earth Materials and Principles of Groundwater Flow.* The Groundwater Project, Guelph, Ontario, Canada, p. 51. URL: https://books.gw-project.org/hydrogeologic-properties-of-earth-materials-and-principles-of-groundwater-flow/chapter/hydraulic-conductivity-values-for-earth-materials/

77 Xie, Y., Li, J., Lu, Z., Jiang, J., & Niu, Y. (2018). Effects of bentonite slurry on air-void structure and properties of foamed concrete. *Construction and Building Materials*, *179*, 207 – 219. DOI : https://doi.org/10.1016/j.conbuildmat.2018.05.226

78 Xu, J., & Goering, D. J. (2008). Experimental validation of passive permafrost cooling systems. *Cold Regions Science and Technology*, *53*(3), 283 – 297. DOI: https://doi.org/10.1016/j.coldregions.2007.09.002

7.3 References -Methods

79 Aftret, H & Daleng, V. *Suitability of Thermosyphon as a Ground Freezing Technology in Longyearbyen.* [Internal Master's Thesis, Norwegian University of Science and Technology, Norway]. Personal Communication

80 *Baker Lake, Canada — Climate & Monthly weather forecast*. Web page. Weather Atlas, R.Srpska, Bosnia and Herzegovina + United Arab Emirates. URL: https://www.weather-atlas.com/en/canada/baker-lake-climate

81 Canadrill Limited Geotechnical Division. (22 Feb. 2019). Geotechnical Investigation: QEC Office Building Baker Lake, NU. Internal Final Report. Canadrill Limited Geotechnical Division, Iqaluit, Nunavut, 1 – 25. Personal Communication.

82 Clausnitzer, V., & Mirnyy, V. (2016). *Modeling groundwater and heat flow subject to freezing and thawing*. Conference proceedings. *DHI-WASY GmbH, 8*, 12489 Berlin, Germany, 1150 – 1153. URL : https://imwa.info/docs/imwa_2016/IMWA2016_Clausnitzer_261.pdf

83 Diersch, H.-J. G., Bauer, D., Heidemann, W., Rühaak, W., & Schätzl, P. (2011). Finite element modeling of borehole heat exchanger systems: Part 2. Numerical simulation. *Computers & Geosciences*, *37*(8), 1136–1147. https://doi.org/10.1016/j.cageo.2010.08.002

84 Ferguson, G. (2015). Screening for Heat Transport by Groundwater in Closed Geothermal Systems. *Groundwater, 53*(3), 503 – 506. DOI: https://doi.org/10.1111/gwat.12162

85 Gascuel, V., Raymond, J., Rivard, C., Marcil, J.-S., & Comeau, F.-A. (2022). Design and optimization of deep coaxial borehole heat exchangers for cold sedimentary basins. *Geothermics*, *105*, 102504, 1-36. DOI : https://doi.org/10.1016/j.geothermics.2022.102504

86 Geo Slope. (2014). Thermal modeling with temp/w: September 2014 Edition. Public report. GEO-SLOPE International Ltd., Calgary, Alberta, Canada, 1 – 171. URL: http://downloads.geo-slope.com/geostudioresources/books/8/12/temp%20modeling.pdf

87 Giordano, N., Kanzari, I., Miranda, M. M., Dezayes, C., & Raymond, J. (2018). Underground thermal energy storage in subarctic climates: A feasibility study conducted in Kuujjuaq (QC, Canada). Conference proceedings. International Ground Source Heat Pump Association, QC, Canada, n.p. DOI : https://doi.org/10.22488/okstate.18.000024

88 Giordano, N., Miranda, M., Kanzari, I., Dezayes, C., & Raymond, J. (21 Nov. 2017). *Shallow geothermal resource assessments for the northern community of Kuujjuaq, Québec, Canada*. Conference proceedings. Santiago de Chile, Republic of Chile, n.p. URL : https://www.researchgate.net/publication/325451055_Shallow_geothermal_resource_assessments_for_the_northern_community_of_Kuujjuaq_Quebec_Canada

89 Giordano, N., & Raymond, J. (2019). Alternative and sustainable heat production for drinking water needs in a subarctic climate (Nunavik, Canada): Borehole thermal energy storage to reduce fossil fuel dependency in off-grid communities. *Applied Energy*, *252*, 113463, 1 - 20. DOI: https://doi.org/10.1016/j.apenergy.2019.113463

90 Environment and Climate Change Canada. (25 May 2022). Almanac Averages and Extremes. Wep page. Gouvernement du Canada, CA, n.p. URL : https://climate.weather.gc.ca/climate_data/almanac_e.html?StationID=51417

91 Kanzari, I. (2019). *Évaluation du potentiel des pompes à chaleur géothermique pour la communauté nordique de Kuujjuaq*. [Doctoral dissertation, Université du Québec, Institut

national de la recherche scientifique]. EspaceINRS. URL : https://espace.inrs.ca/id/eprint/9063

92 Le Lous, M., Larroque, F., Dupuy, A., & Moignard, A. (2015). Thermal performance of a deep borehole heat exchanger: Insights from a synthetic coupled heat and flow model. *Geothermics*, *57*, 157–172. DOI: https://doi.org/10.1016/j.geothermics.2015.06.014

93 Melinder, Å. (2007). *Thermophysical Properties of Aqueous Solutions Used as Secondary Working Fluids* (07/60). [Doctoral Thesis, Division of Applied Thermodynamics and Refrigeration, Dept. of Energy Technology, School of Industrial Engineering and Management, Royal Institute of Technology, KTH]. ResearchGate. URL : https://www.researchgate.net/publication/267973400_Thermophysical_Properties_of_Aqueous_Solutions_Used_as_Secondary_Working_Fluids_Doctoral_Thesis_By

94 MIKE (2016). piFreeze; A Freeze / Thaw Plug-in for FEFLOW. *User Guide*. *DHI*. Hørsholm, Denmark. URL: https://www.mikepoweredbydhi.com/download/mike-2021/pifreeze-plugin

95 Minnick, M., Hickson, C.J., and Shewfelt, D. (2018). Nunavut Geothermal Feasibility Study. Topical Study, RSI 2828. Respec, Saskatoon, SK, 1 – 32. Personal Communication.

96 Miranda, MM; Raymond, J; Dezayes, C; Wigston, A. (2020 In progress). Field methods to estimate permeability of crystalline rocks in remote northern environments: advantages and limitations. Personal Communication.

97 Miranda, M. M., Velez Márquez, M. I., Raymond, J., & Dezayes, C. (2021). A numerical approach to infer terrestrial heat flux from shallow temperature profiles in remote northern regions. *Geothermics*, *93*, 102064, 1 – 18. DOI : https://doi.org/10.1016/j.geothermics.2021.102064

98 Mokon. (2022). HEAT TRANSFER FLUID - PROPYLENE GLYCOL. Technical & Engineering Data, Buffalo, NY. URL: https://www.mokon.com/products/fluids/glycol-solutions/pdf/Propylene-Glycol-Technical-Data.pdf

99 Mu, Y., Li, G., Yu, Q., Ma, W., Wang, D., & Wang, F. (2016). Numerical study of long-term cooling effects of thermosyphons around tower footings in permafrost regions along the Qinghai-Tibet Power Transmission Line. *Cold Regions Science and Technology*, *121*, 237–249. DOI: https://doi.org/10.1016/j.coldregions.2015.06.005

100 Nguyen, A., Pasquier, P., & Marcotte, D. (2017). Borehole thermal energy storage systems under the influence of groundwater flow and time-varying surface temperature. *Geothermics*, *66*, 110–118. DOI: https://doi.org/10.1016/j.geothermics.2016.11.002

101 Ouzzane, P. Eslami-Nejad, M. Badache, Z. Aidoun. (2014). New correlations for the prediction of the undisturbed ground temperature. *Geothermics,* 53 (2015), 379 – 384. DOI : 10.1016/j.geothermics.2014.08.001

102 Ramires, M. L. V., Nieto de Castro, C. A., Nagasaka, Y., Nagashima, A., Assael, M. J., & Wakeham, W. A. (1995). Standard Reference Data for the Thermal Conductivity of Water. *Journal of Physical and Chemical Reference Data*, *24*(3), 1377–1381. DOI: https://doi.org/10.1063/1.555963

103 Sanner, B., & Hellstroem, G. (1997). Earth Energy Designer, a software for calculating borehole heat exchangers; Earth Energy Designer, eine Software zur Berechnung von Erdwaermesondenanlagen. Conference proceedings. Germany, n.p. URL: https://www.osti.gov/etdeweb/biblio/573620

104 Wang, J. (2014). Comparative Heat Transfer Efficiency Study of Coaxial and U-loop Boreholes. *GSTF Journal of Engineering Technology*, *2*(4), 1 – 13. DOI: https://doi.org/10.5176/2251-3701_2.4.92

7.4 References - Discussion

105Aftret, H & Daleng, V. *Suitability of Thermosyphon as a Ground Freezing Technology in Longyearbyen.* [Internal Master's Thesis, Norwegian University of Science and Technology, Norway]. Personal Communication

106Diersch, H.-J. G. (2014). FEFLOW: Finite Element Modeling of Flow, Mass and Heat Transport in Porous and Fractured Media. *Springer Science & Business Media.* DOI: https: //doi.org/10.1007/978-3-642-38739-5

107Eppelbaum, L. Kutasov, I. (2019). Well drilling in permafrost regions – dynamics of the thawed zone. *Polar Research, 38*. DOI: 10.33265/polar.v38.335

108Gascuel, V., Raymond, J., Rivard, C., Marcil, J.-S., & Comeau, F.-A. (2022). Design and optimization of deep coaxial borehole heat exchangers for cold sedimentary basins. *Geothermics*, *105*, 102504, 1-36. DOI : https://doi.org/10.1016/ j.geothermics.2022.102504

109Google Earth. (2022). Baker Lake, Nunavut. URL:https://earth.google.com/web/search/ Baker+Lake, +Nunavut,+Canada/ @64.31549694,-96.00306599,21.31018424a,32244.50057204d,35y,0h,0t,0r/ data=CoYBGlwSVgolMHg1MjFhOWI5YjhmMzA0OTVmOjB4ZmZiYjY2Y2Q0NjY 5NjhlMxkLRbqfUxRQQCGs3uF2aAFYwCobQmFrZXIgTGFrZSwgTnVuYXZ1dCwg Q2FuYWRhGAIgASImCiQJZfX4E2x-MkARZfX4E2x-MsAZedY_lpGlQEAhMhR8WotoUMA

110Government du Canada. (2022.) Alcohols Group - information sheet. *Chemical Safety.* URL: https://www.canada.ca/en/health-canada/services/chemical-substances/fact-sheets/chemicals-glance/alcohols-group.html

111Hadlari, T., Rainbird, R. H., & Donaldson, J. A. (2006). Alluvial, eolian and lacustrine sedimentology of a Paleoproterozoic half-graben, Baker Lake Basin, Nunavut, Canada. *Sedimentary Geology, 190*(1), 47–70. DOI: https://doi.org/10.1016/j.sedgeo.2006.05.005

112Hannus, M. (2016). *Skredfarekartlegging utvalgte områder på Svalbard.* [Report by NVE: NVE.]

113Holmberg, H. Acuña, J. Næss, E. Sønju, O.K. (2016.) Thermal evaluation of coaxial deep borehole heat exchangers. *Renewable Energy, 97*, 65-76. DOI: https://doi.org/10.1016/ j.renene.2016.05.048.

114Kanzari, I. (2019). *Évaluation du potentiel des pompes à chaleur géothermique pour la communauté nordique de Kuujjuaq*. [Doctoral dissertation, Université du Québec, Institut national de la recherche scientifique]. EspaceINRS. URL : https://espace.inrs.ca/ id/eprint/9063

115Kleven, M. H. (2018). An Independent Solar Energy Community in Longyearbyen by use of Borehole Thermal Energy Storage in Permafrost - A feasibility study. [Master's thesis, Norwegian University of Life Sciences. NMBU.]

116Regehr, J. D., Milligan, C. A., Montufar, J., & Alfaro, M. (2013). Review of Effectiveness and Costs of Strategies to Improve Roadbed Stability in Permafrost Regions. *Journal of Cold Regions Engineering, 27*(3), 109–131. DOI: https:// doi.org/10.1061/(ASCE)CR.1943-5495.0000054

117Robak, C. W., Bergman, T. L., & Faghri, A. (2011). Economic evaluation of latent heat thermal energy storage using embedded thermosyphons for concentrating solar power applications. *Solar Energy*, *85*(10), 2461–2473. DOI : https://doi.org/10.1016/j.solener.2011.07.006

APPENDIX I – BACKGROUND

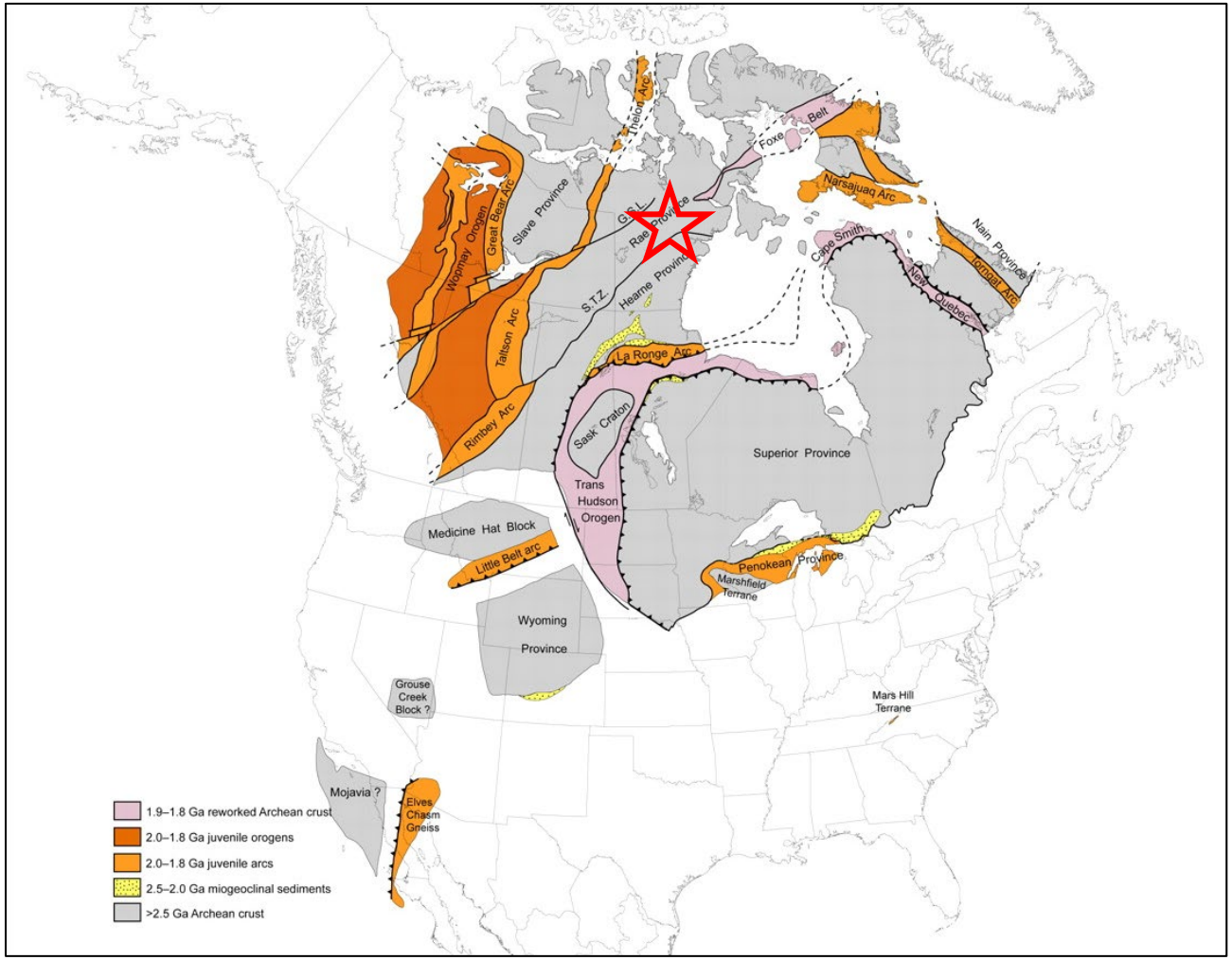

Figure 8.1. Rae Hearne shortening with the collision of the Superior craton (pictured as the Superior Province) 1.84–1.82 Ga. Adapted from Whitmeyer & Karlstrom 2007. Hollow red star indicates the Baker Lake Community's location between the Rae and Hearne provinces.

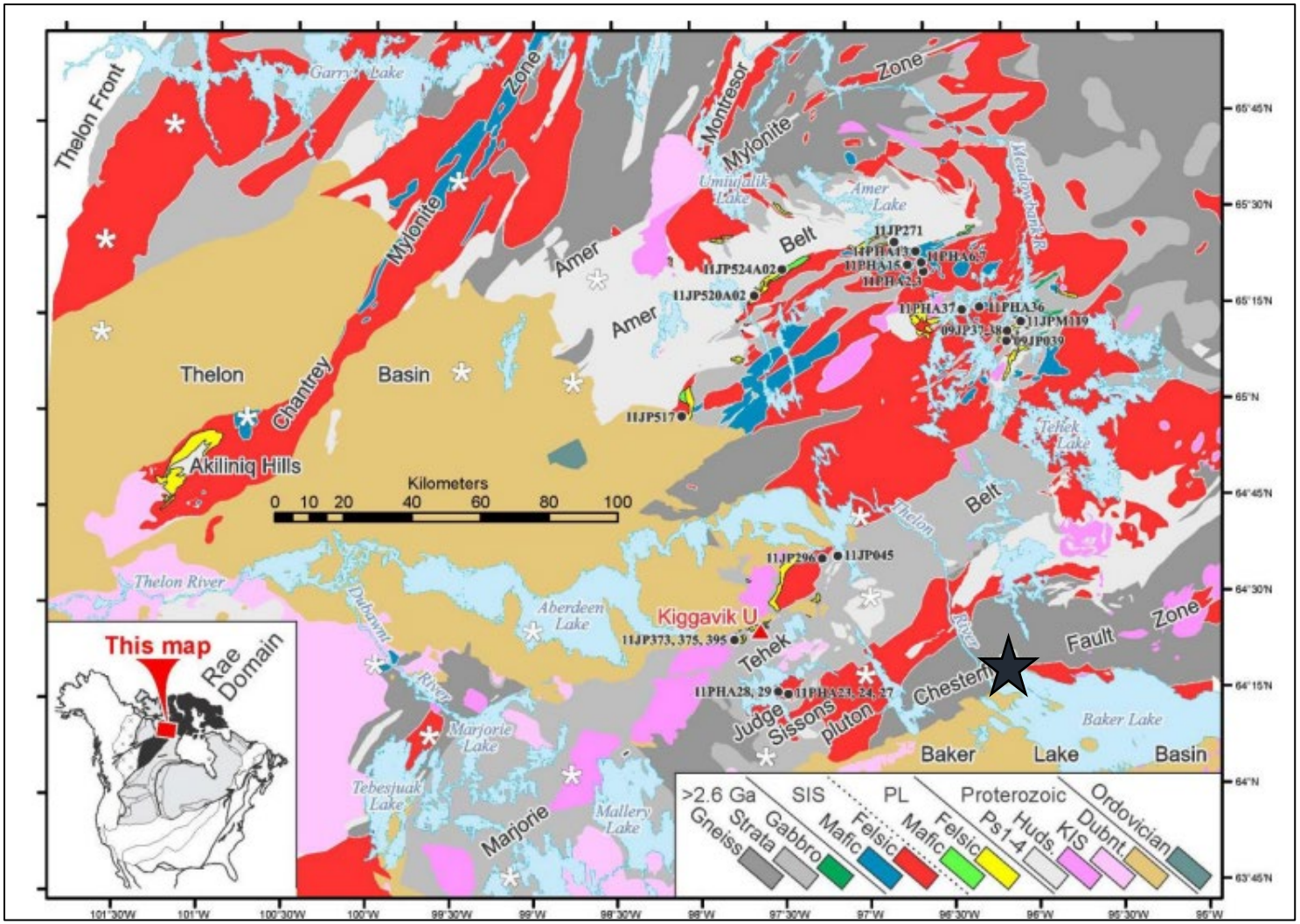

Figure 8.2. Map of modern structural and bedrock composition of the Baker Lake area. The black star indicates the location of the Baker Lake community. Map adapted from Peterson et al. 2015.

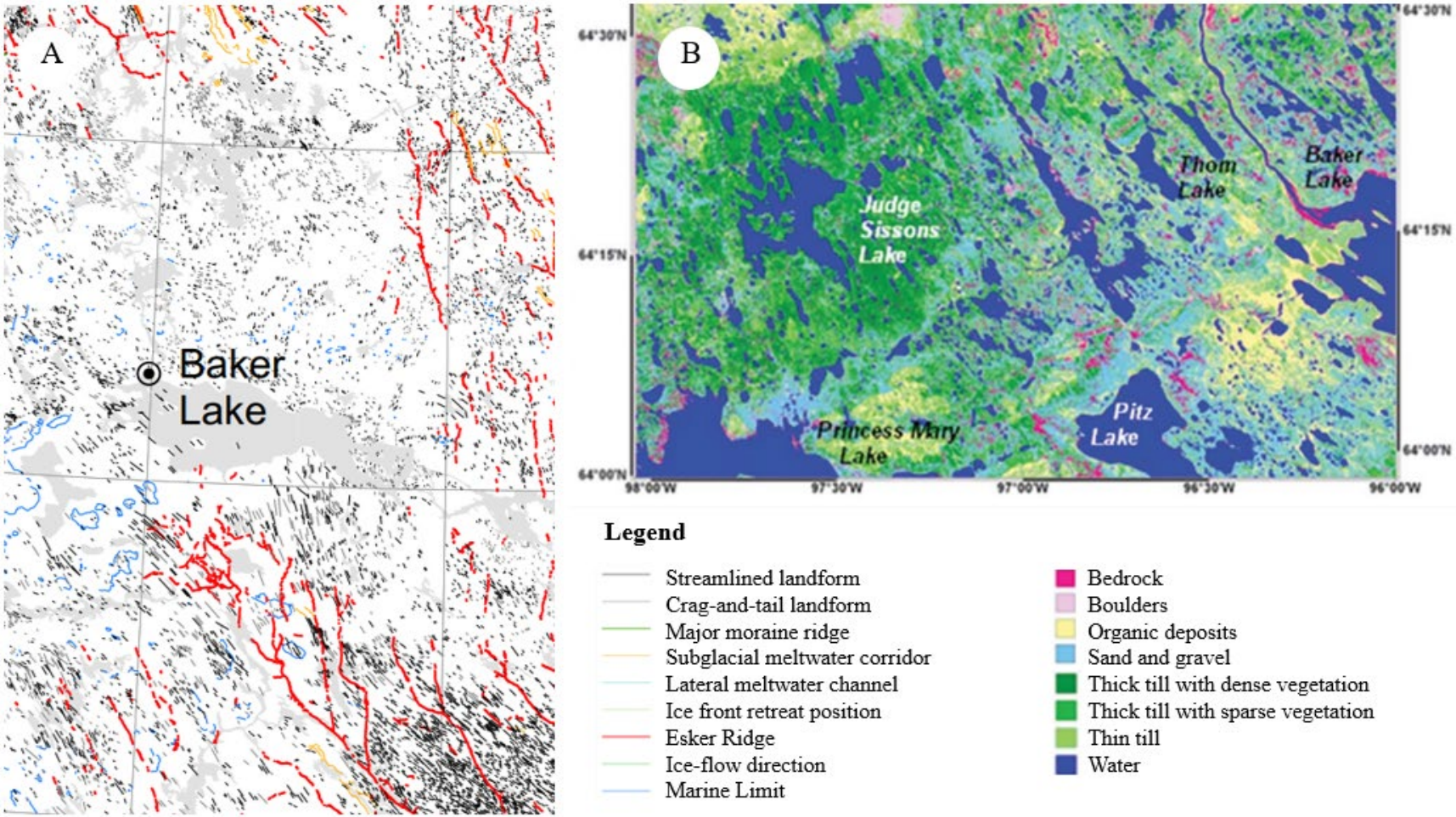

Figure 8.3. A) Glacial structural map of the Baker Lake Area adapted from McMartin et al. 2021. B) Classified image of the Schultz Lake test area using the RADARSAT-2 C-HH and C-HV images together with the 6 optical bands of LANDSAT-7 ETM and the DEM adapted from Larocque et al. 2012.

Table 8.1. Borehole termination depths adapted from Canadrill Limited Geotechnical Division 2019.

Pile	Depth to bedrock (m)	Pile	Depth to bedrock (m)	Pile	Depth to bedrock (m)	Pile	Depth to bedrock (m)	Pile	Depth to bedrock (m)
4	4	53	3.5	28	3.4	58	3.2	60	3
1	3.5	75	2.7	47	3.1	33	2.9	31	3.1
2	2.6	23	3	55	3.7	49	3.4	64	2.7
6	3.7	51	3.2	78	3.7	48	3.3	66	2.7
8	3.4	52	3.5	80	3.5	74	3.1	88	2.7
10	3.4	26	3.8	92	3.1	72	3.4	67	2.7
12	2.7	24	2.74	81	3.5	73	3.4	65	2.7
14	2.5	76	3.4	93	2.9	83	3.2	63	2.7
21	3.5	86	3	79	3.1	84	3.4		
46	2.7	7	3.7	57	3.7	87	2.7		
3	2.4	29	3.51	9	3.1	32	2.9		
5	3.4	27	3.4	11	3.2	59	3.1		
22	3.4	54	3.5	56	3.6	61	2.7		
50	3.9	77	3.7	13	2.3	85	3.1		
25	3.5	30	3.7	82	3.2	62	2.7		
Average Depth to Bedrock (m)							3.2		
Minimum Depth to Bedrock (m)							2.3		
Maximum Depth to Bedrock (m)							4		

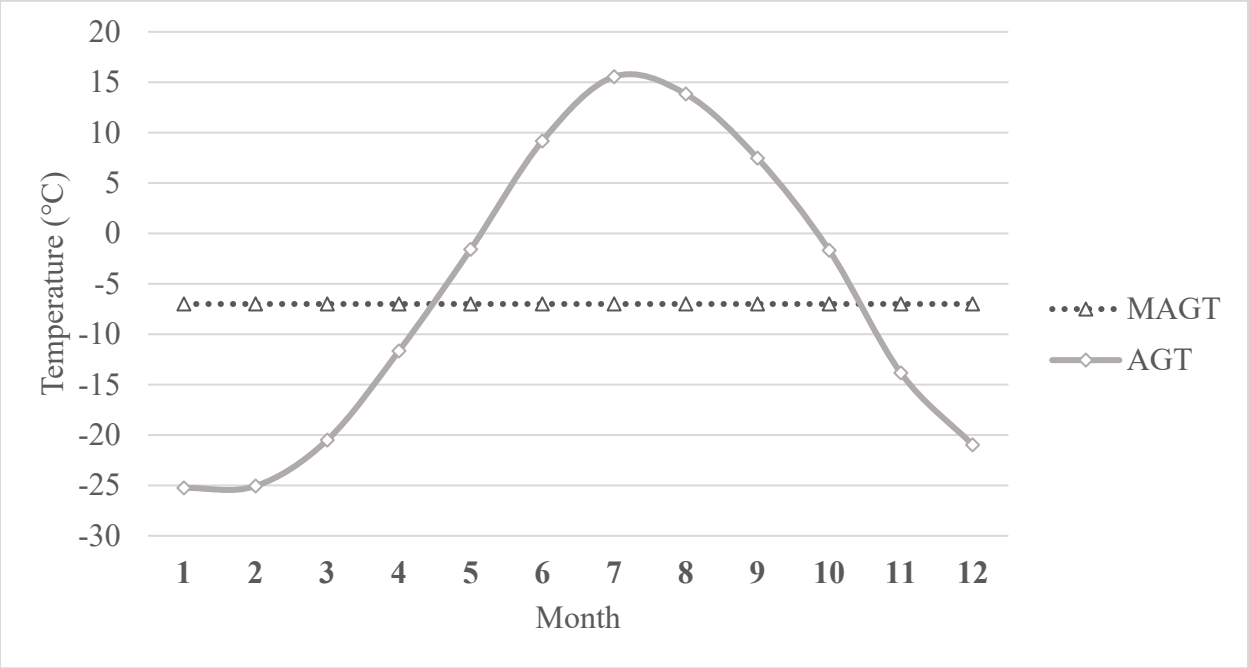

Figure 8.4. Monthly temperature data from the Baker Lake Airport (Environment and Climate Change Canada 2022). Included is Tetra-Tech's determined MAGT of -7 °C (Canadrill Limited Geotechnical Division 2019).

Figure 8.5. District heating customer clusters. Adapted from FVB Energy 2021

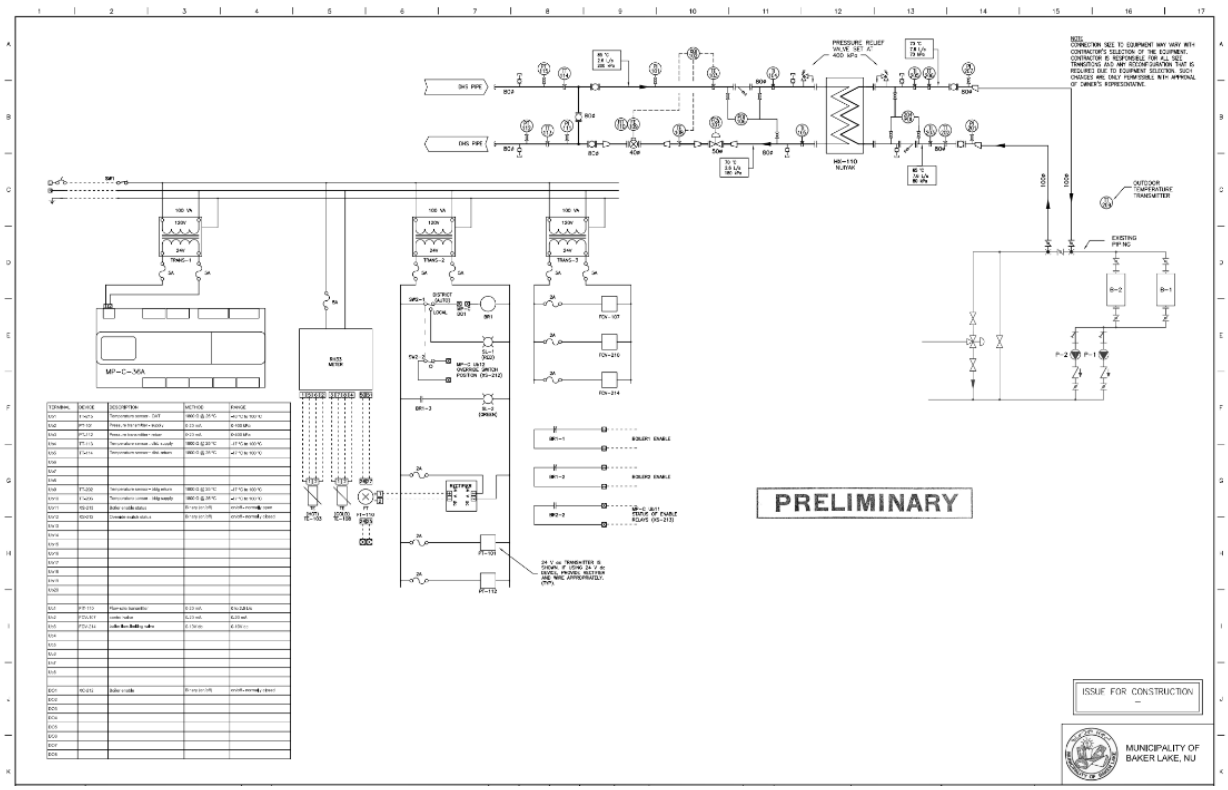

Figure 8.6. Preliminary design of the district heating system energy transfer station flow schematic in Baker Lake, Nunavut. Adapted from FVB Energy 2021.

APPENDIX II – METHODS

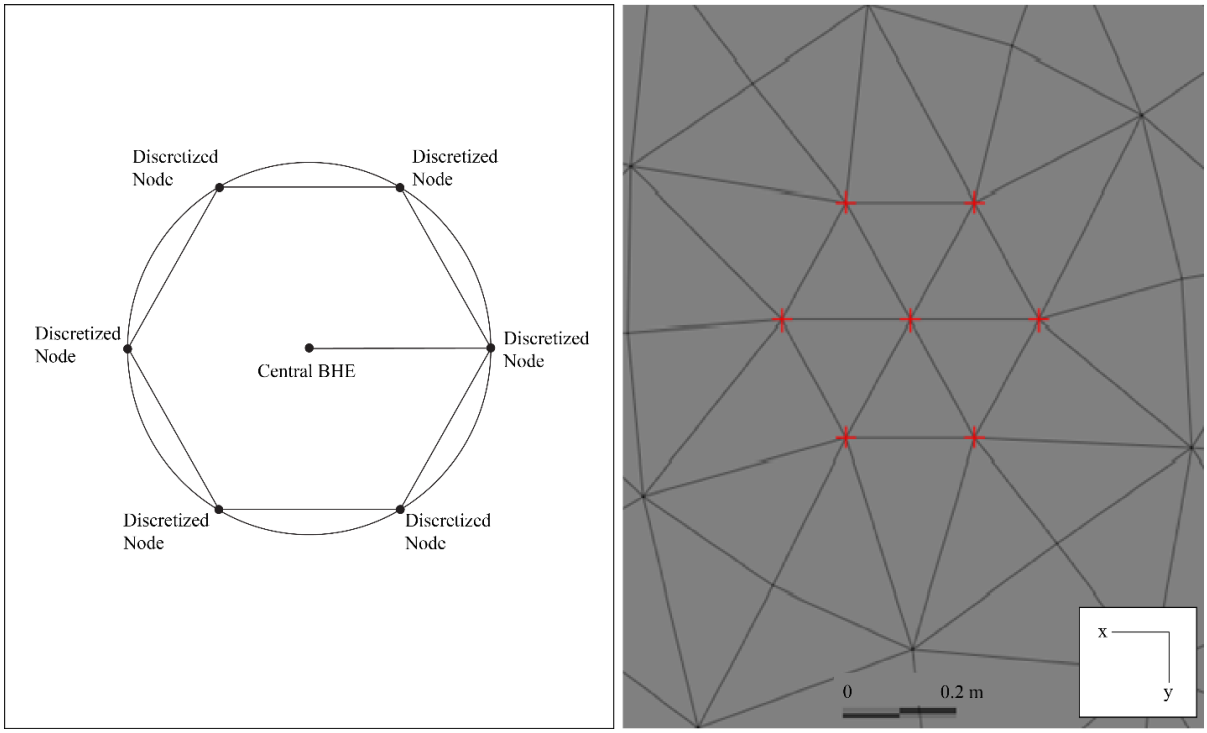

Figure 9.1 Discretion of 6 BHE nodes around central BHE node.

APPENDIX III - RESULTS

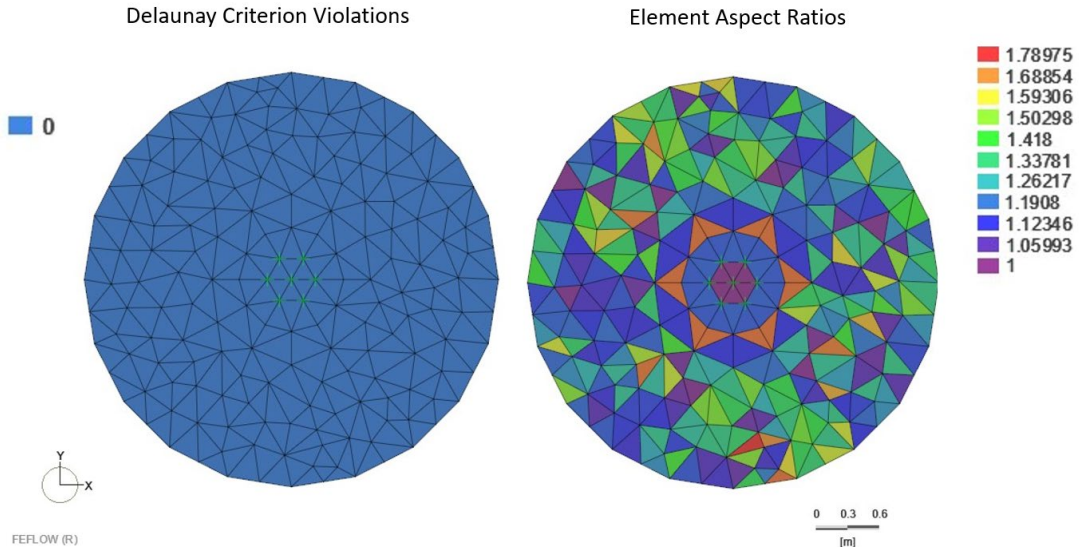

Figure 10.1 Delaunay criteria violations and element aspect ratios for a model within the accepted ranges (Delaunay: x = 0; aspect ratios 1 < x < 3) of values for a proper mesh.

Table 10.1 ΔT and relative percent difference between S1 & S3.

Bentonite 10%, in Water + HDPE (S1 + S3)			
Distance from BHE	**Depth**	**Δ T**	**Difference**
Point	*m*		*%*
L	0.8	4.09	105.6%
M	0.8	2.70	87.0%
N	0.8	2.14	76.8%
O	0.8	1.87	71.1%
P	0.8	6.78	28.2%
L	2	14.49	67.8%
M	2	9.06	49.7%
N	2	7.57	43.6%
O	2	6.86	40.5%
P	2	6.34	38.1%
L	4	8.86	28.6%
M	4	6.03	20.8%
N	4	5.50	19.4%
O	4	5.25	18.7%
P	4	5.07	18.3%

APPENDIX IV - DISCUSSION

Table 11.1 Comparison of % differences between scenarios for mean annual ground temperature (MAGT) 0.23 m from the central BHE.

Comparison	**% Diff. MAGT 0.23 m to BHE**
HDPE + Air	**Year 3**
0.8 m	1485.39
2	155.45
4	2.79
Air + VIT	**Year 3**
0.8 m	38.83
2 m	80.00
4 m	10.72
Air + Thermosyphon	**Year 3**
0.8 m	189.12
2 m	427.85
4 m	96.64
Air + Thermosyphon & VIT	**Year 3**
0.8 m	125.57
2 m	220.10
4 m	210.86

Table 11.2. Comparison of the natural ground's MAGT (NMAGT) to the air insulation's MAGT (AMAGT) with percent difference included. Minimum ground temperatures for the natural ground (NMiGT) and the air insulation scenario (AMiGT) as well as maximums for the natural ground (NMaGT) and air insulation scenario (AMaGT) are provided.

Year	**NMAGT**	**AMAGT**	**% Diff.**	**AMiGT**	**NMiGT**	**AMaGT**	**NMaGT**
0.8 m							
'24 to '25	-4.23	-6.04	35.2	-12.77	-17.61	12.48	7.27
'25 to '26	-5.55	-3.46	46.4	-11.90	-12.65	15.17	2.04
'26 to '27	-5.55	-2.86	64.0	-8.21	-8.12	30.67	-2.48
2 m							
'24 to '25	-4.18	-4.36	4.2	-12.27	-17.77	13.45	6.59
'25 to '26	-5.76	0.28	220.4	-5.46	-12.89	16.46	1.19
'26 to '27	-5.83	0.9	273.0	-1.11	-8.41	31.58	-3.19
4 m							
'24 to '25	-4.71	4.62	20733.3	-12.25	-17.81	13.57	6.52
'25 to '26	-5.87	9.51	845.1	-5.21	-12.94	16.58	1.08
'26 to '27	-6.02	10.59	726.9	-0.90	-8.59	31.76	-3.32